Modeling Two-Phase Flow in the Downcomer of a Once-Through Steam Generator using RELAP5/MOD2

Randy Raymond Clark, Jr.

Thesis submitted to the faculty of Virginia Polytechnic Institute and State University in partial fulfillment of the requirements for the degree of

Master of Science

in

Mechanical Engineering

Alan A. Kornhauser, Chair
Mark A. Pierson
Danesh K. Tafti

December 7, 2011
Blacksburg, Virginia

Keywords: Two-Phase Flow, Thermohydraulics, Steam Generator, RELAP

Modeling Two-Phase Flow in the Downcomer of a Once-Through Steam Generator Using RELAP5/MOD2

Randy Raymond Clark, Jr.

ABSTRACT

The purpose of this study is to develop an accurate model of the downcomer of the once-through steam generator (OTSG) developed by Babcock & Wilcox, using RELAP5/MOD2. While the physical model can be easily developed, several parameters are left to be adjusted to optimally model the downcomer and match data that was retrieved in a first-of-a-kind (FOAK) study conducted at Oconee Unit I in Oconee, South Carolina. Once the best-fit set of parameters has been determined, then the model must be tested for power levels exceeding that for which the steam generator was originally designed, so as to determine the power level at which a phenomenon known as flood-back becomes a concern.

All known previous studies that have been conducted using RELAP5/MOD2 have shown that RELAP over-predicts interphase friction. However, all of those studies focused on heated two-phase upflow, whereas the downcomer is modeled as adiabatic two-phase downflow. In this study, it is found that the original slug drag model for RELAP5/MOD2 developed by Idaho National Engineering Laboratory (INEL) under-predicts the interphase friction between the liquid and vapor phase within the downcomer. Using a modified version of the original slug drag model created by Babcock & Wilcox (B&W), an optimum multiplier is found for each power level. An increase of 1181% in interphase friction over the INEL slug drag model, which equals an increase of 4347% for the default B&W model provides the most accurate results for all power levels studied.

Emphasis is also placed on modeling the orifice plate of the OTSG downcomer which has been added to stabilize pressure fluctuations between the downcomer and tube bundle of the

OTSG. While several different schemes are explored for modeling the orifice plate, a branch connection with an inlet area 14.22% of that of the downcomer is used to model the orifice plate along with the volume that transitions the two-phase downflow to horizontal flow into the tube nest of the OTSG.

Power levels exceeding that for which the steam generator was designed are tested in RELAP using the slug drag multiplier to determine at which power level a liquid level would occur and would flood-back become a concern. In this study, it is determined that a liquid level would form at 135% power and that at any higher power level, flood-back would be of concern for any user of the steam generator.

Acknowledgements

I would like to give special thanks to several individuals who provided technical and financial support throughout this study. First and foremost, I would like to thank Dr. Al Kornhauser who provided great insight into two-phase flow and challenged and encouraged me to strive to gain better understanding of RELAP5/MOD2 throughout this study. I would also like to thank Dr. Mark Pierson and Dr. Danesh Tafti for their assistance in helping me write and perfect this thesis, and Dr. Bob Masterson for providing his insight with work related to RELAP5/MOD2. This project would not have been possible without Areva, Inc. who provided their in-house version of RELAP5/MOD2 and their data for the once-through steam generator downcomer. Specifically, I would like to acknowledge the expertise that was provided by the individuals that I worked with at the Areva, Inc. office in Lynchburg, Virginia, namely John Klingenfus, Cris Schamp, John Adams, Jeff Seals and Bret Boman. In terms of financial support, I would like to thank the Center for Advanced Engineering Research (CAER) for funding this project, and Dr. Pierson again, who helped me earn a fellowship with the Nuclear Regulatory Commission, without which, this program may not have been allowed to continue.

Table of Contents

Table of Figures

Table of Tables

Nomenclature

Variables

A	Cross-Sectional Area
a	Interfacial Area per Unit Volume
B	Body Force, or Coefficient used in EPRI Drift Velocity Model
C	Coefficient of Virtual Mass, Drag, or Drift Velocity
D	Diameter
$DISS$	Energy Dissipation Function
f	Interphase Friction Factor
FI	Interphase Friction Force per Unit Volume
FIF	Interphase Drag Coefficient on the Liquid
FIG	Interphase Drag Coefficient on the Vapor
FWF	Wall Friction Drag Coefficient on the Liquid
FWG	Wall Friction Drag Coefficient on the Vapor
g	Acceleration Due to Gravity
G	Mass Flux
h	Specific Enthalpy
j	Superficial Velocity, Volumetric Flux
K	Coefficient Used in EPRI Drift Velocity Model, Kinetic Energy Coefficient
L	Function of Vapor Void Fraction and Pressure, or Length
P	Pressure
Q	Volume Flow Rate or Heat Transfer
Re	Reynolds Number
u	Specific Internal Energy
v	Velocity
V	Specific Volume
We	Weber Number
x	Quality
α	Void Fraction
δ	Film Thickness
δ^*	Deryagin Number
ε	Ratio
Γ	Vapor Generation
ν	Kinematic Viscosity
ρ	Density
σ	Surface Tension

Subscripts

ann	Annular
avg	Average over a Given Interval
b	Bubble
c	Continuous
$crit$	Critical Value
d	Drift Difference

D	Drag
f	Liquid Phase
fI	Liquid Interface
g	Vapor Phase
gf	Vapor to Liquid
gI	Vapor Interface
gj	Vapor to Total Superficial
H	Hydraulic
if	Interface to Liquid
ig	Interface to Vapor
k	k-th Phase
L	Loss
m	Mixture
r	Relative
ref	Reference
sb	Small Bubble
st	Static
T	Taylor Bubble
wf	Wall to Liquid
wg	Wall to Vapor

Superscripts

s	Saturation

Acronyms

B&W	Babcock & Wilcox
CAER	Center for Advanced Engineering Research
CHF	Critical Heat Flux
FOAK	First of a Kind
INEL	Idaho National Engineering Laboratory
LTS	Lower Tube Sheet
NSS	Nuclear Steam System
OTSG	Once-Through Steam Generator
PWR	Pressurized Water Reactor
RELAP	Reactor Excursion and Leak Analysis Program
RELAPSE	Reactor Leak and Power Safety Excursion
TRAC	Transient Reactor Analysis Code
TRACE	TRAC/RELAP Advanced Computational Engine

I. Introduction

1.1: Overview

The once-through steam generator (OTSG) was designed by the Babcock & Wilcox Company (B&W) in the late 1960s to transfer heat from the moderating liquid water in a pressurized water reactor (PWR) nuclear power plant to the secondary loop, converting liquid water to steam that would be used to power turbines, generating electricity. As the water entering the steam generator would be subcooled, the OTSG was designed with steam aspirator ports, allowing saturated steam to mix with the subcooled water. The intention was that the liquid water and saturated steam would mix while flowing through an exterior downcomer to the bottom of the OTSG. At the bottom of the OTSG, the intended result was for the steam to have fully condensed, while bringing the temperature of the liquid water to saturation, and ready to be boiled to saturated steam as it rose through the interior tube bundle of the OTSG. Observed data suggested that when the feedwater approached the bottom of the OTSG, the steam was not fully condensed, and steam carry-under was entering into the tube bundle. There has been no indication that this carry-under has adversely affected performance or safety of the OTSG. As Areva, Inc., the successor to the nuclear power division of B&W, works to develop the next generation Enhanced-OTSG (EOTSG) and power plants operate at power levels that exceed the original design conditions of the OTSG, it is expected that the amount of carry-under will be reduced, raising concern over a phenomenon known as flood-back. Flood-back occurs when the liquid level within the downcomer of the OTSG rises to same level as the feedwater nozzles, preventing feedwater from entering the steam generator.

In the nuclear power industry, there are several computer codes used to model nuclear power plants. One of the first was a program released in 1966 known as RELAPSE (REactor

Leak And Power Safety Excursion), with updated versions taking the shortened name RELAP (Reactor Excursion and Leak Analysis Program), developed by Idaho National Engineering Laboratory (INEL). RELAP5/MOD2 is used in this study and was originally developed in 1985 by INEL. The program allows the user to input initial and boundary conditions for the steam/water, along with the dimensions of the parts of a plant to develop a thermohydraulic model of either an entire nuclear power plant, or just a particular component.

As is the case with any computer modeling program, there are certain conditions that RELAP models very accurately, while RELAP can be very inaccurate under other conditions, such as the steam-water flow that is present in the downcomer of the OTSG. The purpose of this project was to use RELAP5/MOD2 to model the downcomer of the OTSG, and vary different input parameters such that the output best matched first-of-a-kind (FOAK) data taken from the OTSG installed at Oconee Nuclear Station in Oconee, South Carolina. Using the findings from the study of the OTSG, the parameters are to be applied in modeling the EOTSG by Areva, Inc. to determine if flood-back would be an issue for the downcomer when the power level was raised beyond the original design of the downcomer.

1.2: Proprietary Data and Non-Dimensionalization

Much of the data that has been provided in this study by Areva, Inc. is proprietary, and thus cannot be openly published. Great care has been taken in non-dimensionalizing the proprietary data, so that the results can be published without divulging any trade secrets of Areva, Inc. For the sake of preserving Areva's Inc.'s property rights, data relating to the dimensions of the OTSG downcomer and thermohydraulic data from the FOAK study that has not previous been published has been non-dimensionalized. This includes data retrieved from

RELAP model runs that is being compared against FOAK data. The non-dimensionalization scheme for the OTSG downcomer dimensions is described in Section 2.1, while the non-dimensionalization scheme for the FOAK data is described in Section 2.2.

II. Background

2.1: The Once-Through Steam Generator (OTSG)

The Babcock & Wilcox Company (B&W) developed the OTSG in the late 1960s as part of their pressurized water reactor nuclear steam system (NSS) [11]. The diagram in Figure 1 shows, the feedwater enters the OTSG through 32 spray heads that encircle the OTSG (node 1 in Figure 1), while steam "bleeds" from the interior tube bundle through aspirator ports (node 6) into the downcomer of the OTSG (node 2). In the downcomer, the steam mixes with the feedwater, causing the steam to condense while the feedwater temperature is raised to saturation. The saturated liquid then continues to flow through the downcomer, through an orifice plate (node 4) which has been added to the bottom of the OTSG. The purpose of the orifice plate is to stabilize pressure fluctuations between the downcomer and the tube bundle, and can be adjusted manually during shut down. Below the orifice plate, the feedwater enters the shell side of the tube bundle, also known as the tube nest, through the ports shown (node 5), where it contacts the tubes that are heated by water coming from the reactor core (node 6). The incoming feedwater is heated by the tubes, causing the steam to rise through the tube nest, to be either bled off back in to the downcomer, or superheated in the upper portion of the OTSG, where it is used to power the turbines that are used to generate electrical power.

As discussed in Section 1.2, the dimensions of the OTSG downcomer are considered to be proprietary. All lengths have been non-dimensionalized with respect to the total length of the OTSG downcomer, and areas have been non-dimensionalized with respect to the cross-sectional area of the downcomer. For example, a length of 0.35 represents a length that is 35% of the total length of the downcomer, while an area of 0.7 would be 70% of the cross-sectional area of the downcomer.

From the aspirator ports to the lower tube sheet (LTS), the downcomer has a length of 1.000. The downcomer is in the shape of an annulus, with the diameter of the inner shell at 0.300 and the diameter of the outer shell is 0.345. As a result, the downcomer has a cross-sectional area of 1.000 and a hydraulic diameter of 0.450. These dimensions were obtained from blueprints for the OTSG that were provided by Areva, Inc.

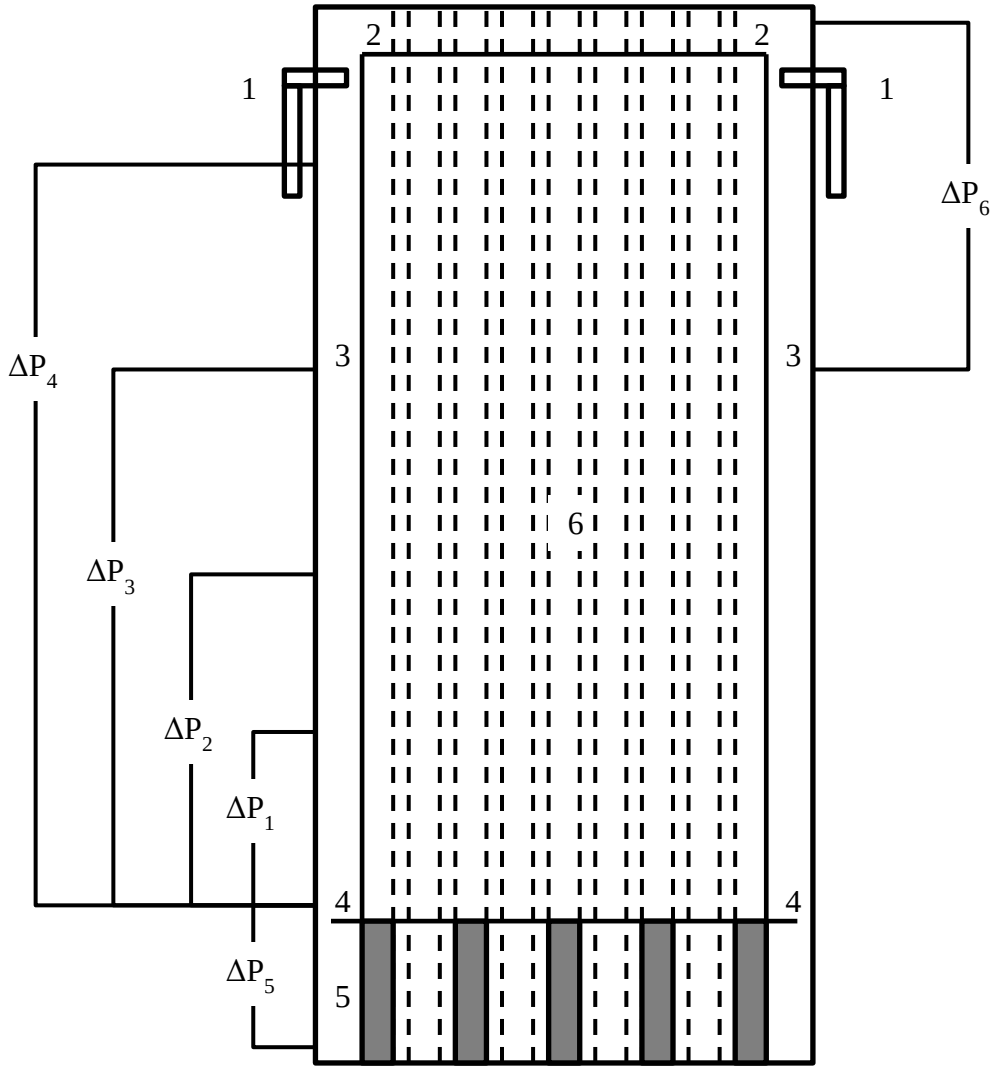

Figure 1: Schematic of The Babcock & Wilcox Once-Through Steam Generator

One of the greatest concerns with a two-phase system like the OTSG is the stability of the two-phase flow. A laboratory study of a reduced scale OTSG showed that it was prone to fluctuations in pressure between the downcomer and the tube nest, which would cause flow

reversals and swells in the liquid level. These tests also showed that if the resistance of the inlet to the tube bundle were increased, the pressure fluctuations could be stabilized by increasing. This resulted in the installation of an orifice plate assembly near the bottom of the downcomer, with two plates, one that was fixed and the other adjustable. [11] The cross-sectional area of the orifice plate assembly when fully open is 0.310, while it is 0.0887 when fully closed, as there is still a gap between the outer edge of the orifice plate and the outer wall of the downcomer. For the FOAK study, as well as throughout this study, the orifice plate is set to 25% open, with a cross-sectional area of 0.144.

As a result of the laboratory testing, when the OTSG was installed at Oconee Unit I it was able to meet or exceed its design specifications. As a result of the orifice plate, no oscillations in pressure affected either the performance of the OTSG or its control systems occurred during the power escalation process. This allowed the OTSG to be more tolerant of fouling-induced increases of pressure drops in the tube bundle. Instrumentation of the OTSG at Oconee Unit I showed that the subcooled feedwater that was sprayed from the feedwater nozzles achieved saturation within 0.0150 of the nozzles, as it mixed with the saturated steam from the aspirator ports. Other design parameters of the secondary side of the OTSG, along with the measured results at Oconee Unit I are provided in Table 1. [11]

Table 1: Conditions of the Secondary Side of the OTSG at Oconee Unit I [15]

	Design	Measured
Flow (10^6 lb_m/hr)	5.30	5.16
Feedwater Temperature (°F)	455	455
Steam Pressure (psia)	925	925
Steam Temperature (°F)	570	594
Steam Superheat (°F)	35	59
Total Heat Transferred (10^9 Btu/hr)	4.21	4.21

2.2: First of a Kind (FOAK) Study at Oconee Unit I

In order to better understand the performance of the OTSG, B&W and Duke Power Company conducted a FOAK study of the OTSG installed at Unit I of Oconee Nuclear Station. The OTSG was instrumented with pressure taps to measure pressures at selected locations throughout the OTSG, as shown in Figure 1. The lengths of each of the intervals are provided in Table 2. The common pressure tap for ΔP_1, ΔP_2, ΔP_3, ΔP_4, and ΔP_5 is located at a height 0.0125 above the orifice plate, while the bottom pressure tap for the interval ΔP_5 is located at a height 0.0150 above the bottom of the LTS. [5,12]

Table 2: Lengths between Pressure Taps [5]

Interval	Length (in)
ΔP_1	0.1506
ΔP_2	0.3406
ΔP_3	0.5892
ΔP_4	0.7706
ΔP_9	0.0894
ΔP_{10}	0.1250

Given this information, the pressure can be determined at seven locations, which are at heights of 1.000, 0.875, 0.694, 0.445, 0.255, 0.1044 and 0.0150 above the LTS. Pressure readings were taken from the pressure taps and were recorded during a power escalation at power levels of 45%, 55%, 65%, 75%, 85% and 95%. The pressure readings were averaged with respect to time, and were taken for power levels as low as 15%. However, for these lower power levels, the variation in pressure readings with respect to time were significant in comparison to the time averaged value, and thus have been considered to be impractical for study. This instability in the data was noted at power levels up to and including 45% power.

As discussed in Section 1.2, all of the FOAK data, as well as RELAP data that is compared against FOAK data has been non-dimensionalized to protect Areva, Inc.'s property

rights. The pressures that are reported from both the FOAK data and from the RELAP model runs are represented as ratios to the summation of ΔP_3, ΔP_5, and ΔP_6 at 95% power, regardless of the power level. For example, a pressure value of 0.85, which may be given at any power level, is 85% of the summation of ΔP_3, ΔP_5, and ΔP_6 at 95% power. The time averaged, non-dimensionalized pressure readings for each interval are provided in Table 3. [12]

Table 3: Time Averaged Pressure Readings [12]

Power Level	45%	55%	65%	75%	85%	95%
ΔP_1	0.0757	0.1110	0.1437	0.1671	0.1930	0.2082
ΔP_2	0.1582	0.2203	0.2735	0.3286	0.3777	0.4315
ΔP_3	0.2188	0.3150	0.3980	0.4868	0.5723	0.6813
ΔP_4	0.2862	0.4015	0.5027	0.6175	0.7335	0.8818
ΔP_5	0.0911	0.0911	0.0814	0.0698	0.0568	0.0372
ΔP_6	0.0686	0.1041	0.1407	0.1774	0.2013	0.2816

2.2.1: Relative Pressure

Using the pressure data retrieved from the power escalation of Oconee Unit I, and neglecting wall friction and cross-sectional velocity variation, engineers at B&W were able to calculate relative pressure, density, static quality and void fraction profiles throughout the downcomer, among other parameters. The relative pressure profile is determined with respect to the pressure at the aspirator ports. In other words, the relative pressure at the steam aspirator ports is 0.00. From there, the pressure relative to that point is calculated as a sum and/or difference of the pressures measured in the downcomer, as shown in Equation (1). [5]

$$Relative\ Pressure = \begin{cases} 0 & \text{Height = 1.0000} \\ \Delta P_6 + \Delta P_3 - \Delta P_4 & \text{Height = 0.8750} \\ \Delta P_6 & \text{Height = 0.6936} \\ \Delta P_6 + \Delta P_3 - \Delta P_2 & \text{Height = 0.4450} \\ \Delta P_6 + \Delta P_3 - \Delta P_1 & \text{Height = 0.2550} \\ \Delta P_6 + \Delta P_3 & \text{Height = 0.1044} \\ \Delta P_6 + \Delta P_3 + \Delta P_5 & \text{Height = 0.0150} \end{cases} \quad (1)$$

The relative pressures at each point are given in Table 4. Figure 2 shows the relative pressure profiles for each power level, as well as the estimated effect that cross-sectional velocity variation has on the feedwater when exiting the feedwater nozzles at 95% power, which was calculated and provided by Areva, Inc.

Table 4: Relative Pressures with Respect to Height at Each Power Level [5]

Height	45%	55%	65%	75%	85%	95%
1.0000	0.0000	0.0000	0.0000	0.0000	0.0000	0.0000
0.8750	0.0012	0.0176	0.0360	0.0466	0.0401	0.0810
0.6936	0.0686	0.1041	0.1407	0.1774	0.2013	0.2816
0.4450	0.1292	0.1988	0.2652	0.3356	0.3959	0.5314
0.2550	0.2117	0.3081	0.3950	0.4970	0.5806	0.7547
0.1044	0.2874	0.4191	0.5387	0.6641	0.7736	0.9628
0.0150	0.3785	0.5102	0.6202	0.7339	0.8304	1.0000

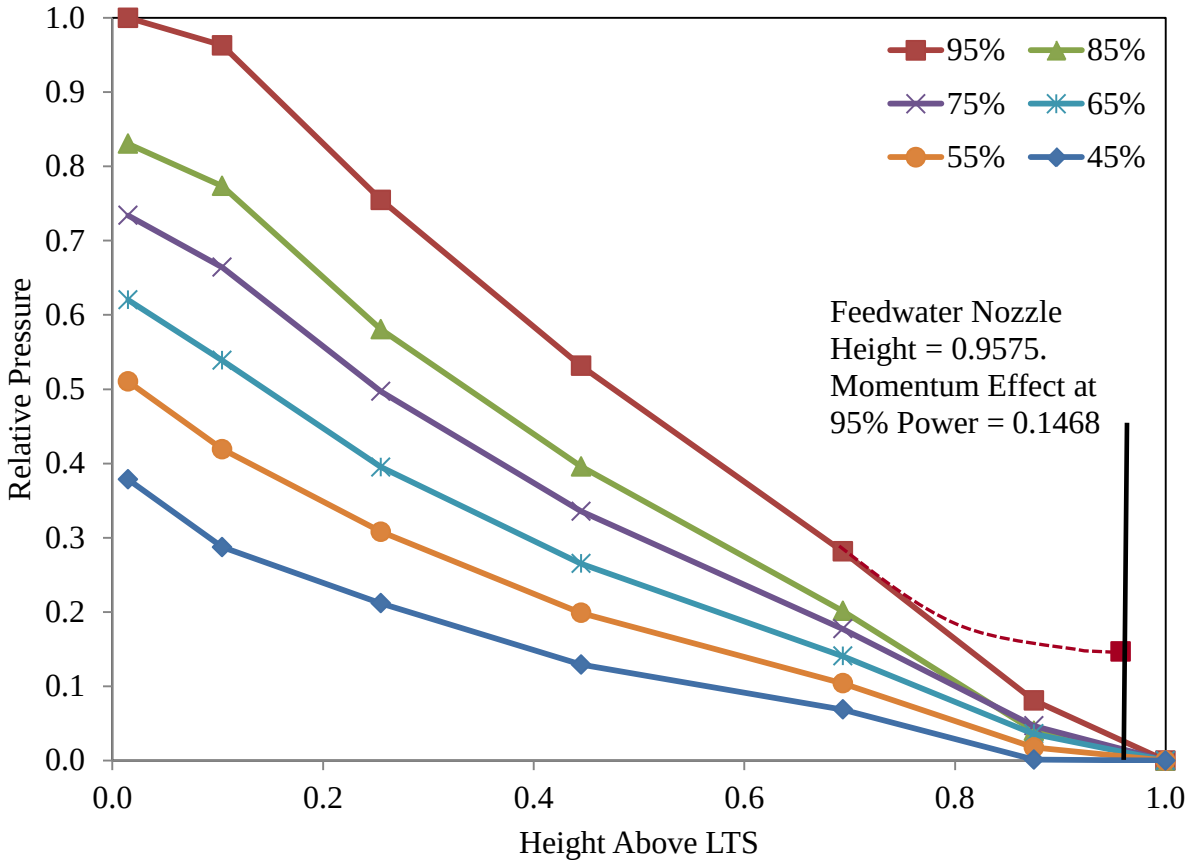

Figure 2: Relative Pressure Profiles for Various Power Levels [5]

2.2.2: Density

From the pressure, the average density of the flow was calculated, assuming that the pressure change was primarily hydrostatic. Thus, the average density over the intervals ΔP_1, ΔP_2, ΔP_3, and ΔP_4 were calculated using Equation (2).

$$\rho_{avg} = \frac{\Delta P}{g \Delta z} \tag{2}$$

Density at the orifice plate has been linearly extrapolated from the densities calculated for the bottom two intervals, and the average densities are shown in Table 5. Average density profiles for the downcomer for various power levels are shown in Figure 3. The height given corresponds with the central height of the interval for which the density was calculated, except in the case of height equals 0.0919, the height of the orifice plate. Below the orifice plate, the density cannot be calculated because there is only one pressure tap. Density values have been non-dimensionalized with respect to the orifice plate density for each power level. Thus the density ratio provided is always 1.0 at the orifice plate for each power level, and all other values are a percentage of the orifice plate density. [5]

Table 5: Average Density Ratio of the Fluid in the Downcomer at Varying Power Levels [5]

Height	45%	55%	65%	75%	85%	95%
0.7843	0.6906	0.5805	0.5298	0.5795	0.6168	0.7429
0.5693	0.4536	0.4644	0.4568	0.5117	0.5431	0.6750
0.3500	0.8076	0.7003	0.6249	0.6833	0.6746	0.7895
0.1797	0.9345	0.8980	0.8724	0.8922	0.8893	0.9284
0.0919	1.0000	1.0000	1.0000	1.0000	1.0000	1.0000

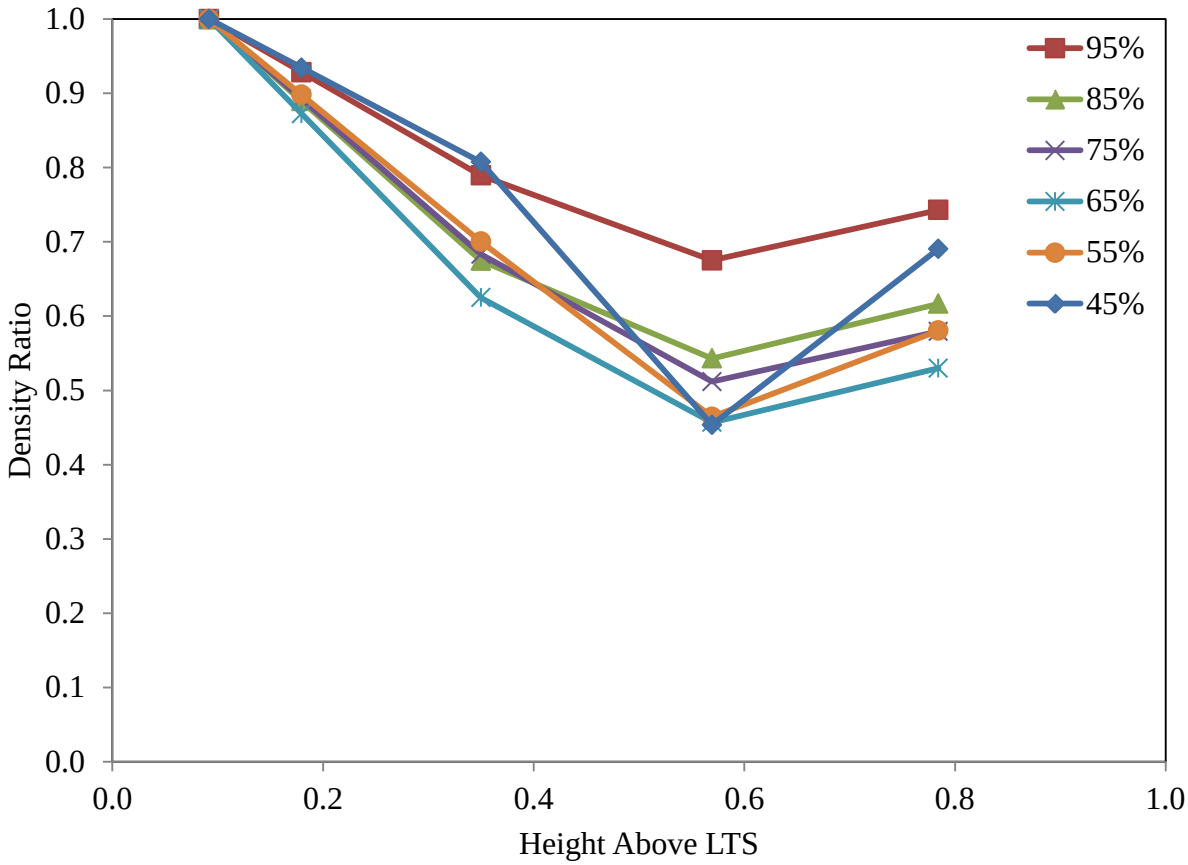

Figure 3: Average Density Ratio Profiles for Various Power Levels [5]

2.2.3: Static Quality

Using the pressure data found for each node, the average saturation specific volume for liquid and vapor of each interval can be found, and along with average density, can be used to calculate the average steam static quality over the interval, using Equation (3). [5]

$$x_{st} = \frac{\frac{1}{\rho_{avg}} - v_f}{v_g - v_f} \tag{3}$$

As is the case with the density profile, the static quality cannot be calculated below the orifice plate due to the lack of a second pressure tap. The static quality calculated for each interval throughout the downcomer is provided in Table 6, while the profiles are depicted in Figure 4.

Static quality values have been non-dimensionalized with respect to the orifice plate static quality for each power level. [5]

Table 6: Average Static Quality Ratio in the Downcomer

Height	45%	55%	65%	75%	85%	95%
0.7843	1.5822	2.1250	2.6800	2.5789	2.6667	2.0000
0.5693	2.5685	2.8000	3.2600	3.0789	3.2593	2.4167
0.3500	1.3082	1.6750	2.1400	2.0000	2.2963	1.7917
0.1797	1.0890	1.1750	1.2600	1.2632	1.3333	1.2500
0.0919	1.0000	1.0000	1.0000	1.0000	1.0000	1.0000

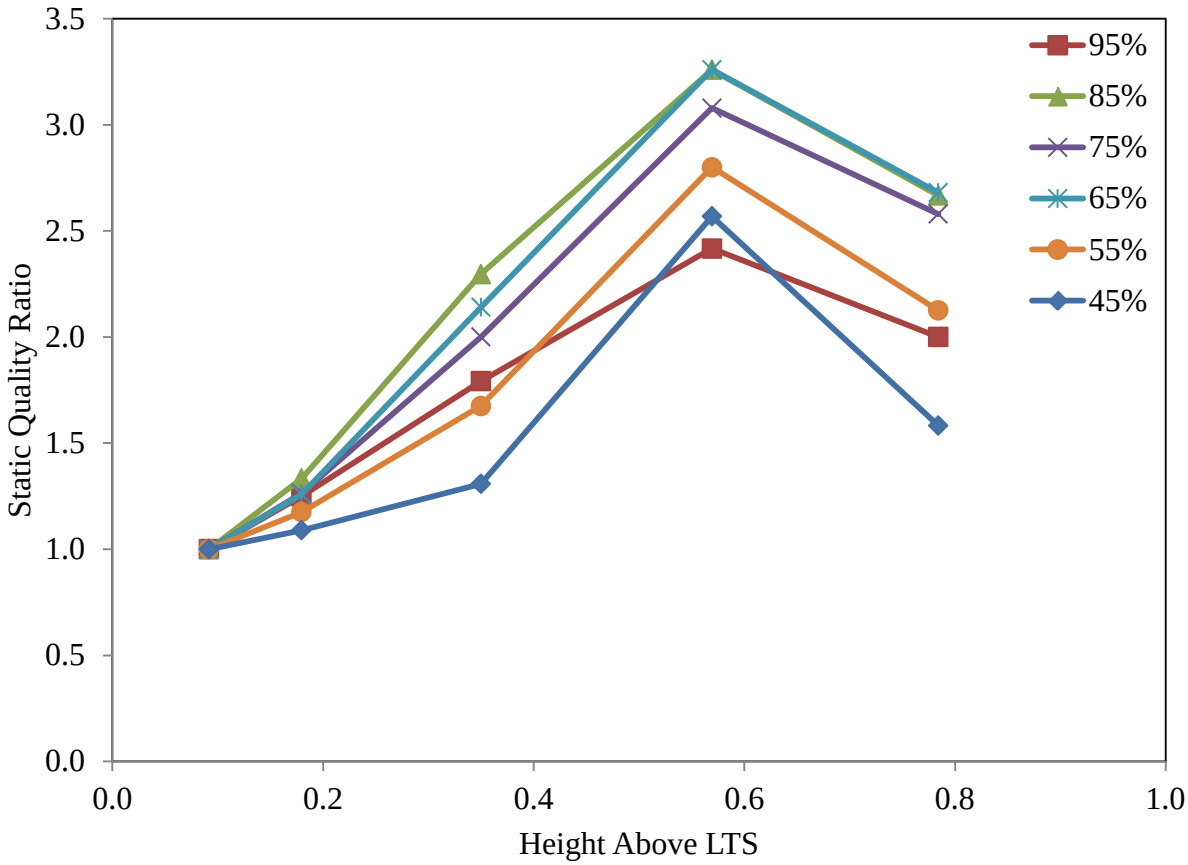

Figure 4: Static Quality Ratio Profiles in the Downcomer for Various Power Levels [5]

2.2.4: Void Fraction

In turn, the vapor void fraction can be calculated using Equation (4)

$$\alpha = \frac{x v_g}{x v_g + (1 - x) v_f} \tag{4}$$

Similar to the static quality and the density, the vapor void fraction cannot be calculated below the orifice plate. The vapor void fraction calculated for each interval is given in Table 7, and is graphically displayed in Figure 5. Void fraction values have been non-dimensionalized with respect to the orifice plate void fraction for each power level. [5]

Table 7: Average Void Fraction Ratios in the Downcomer [5]

Height	45%	55%	65%	75%	85%	95%
0.7843	1.0951	1.2362	1.4338	1.5021	1.6615	1.4862
0.5693	1.1677	1.3019	1.5018	1.5840	1.7865	1.6160
0.3500	1.0588	1.1689	1.3456	1.3782	1.5599	1.3978
0.1797	1.0200	1.0583	1.1176	1.1282	1.1901	1.1354
0.0919	1.0000	1.0000	1.0000	1.0000	1.0000	1.0000

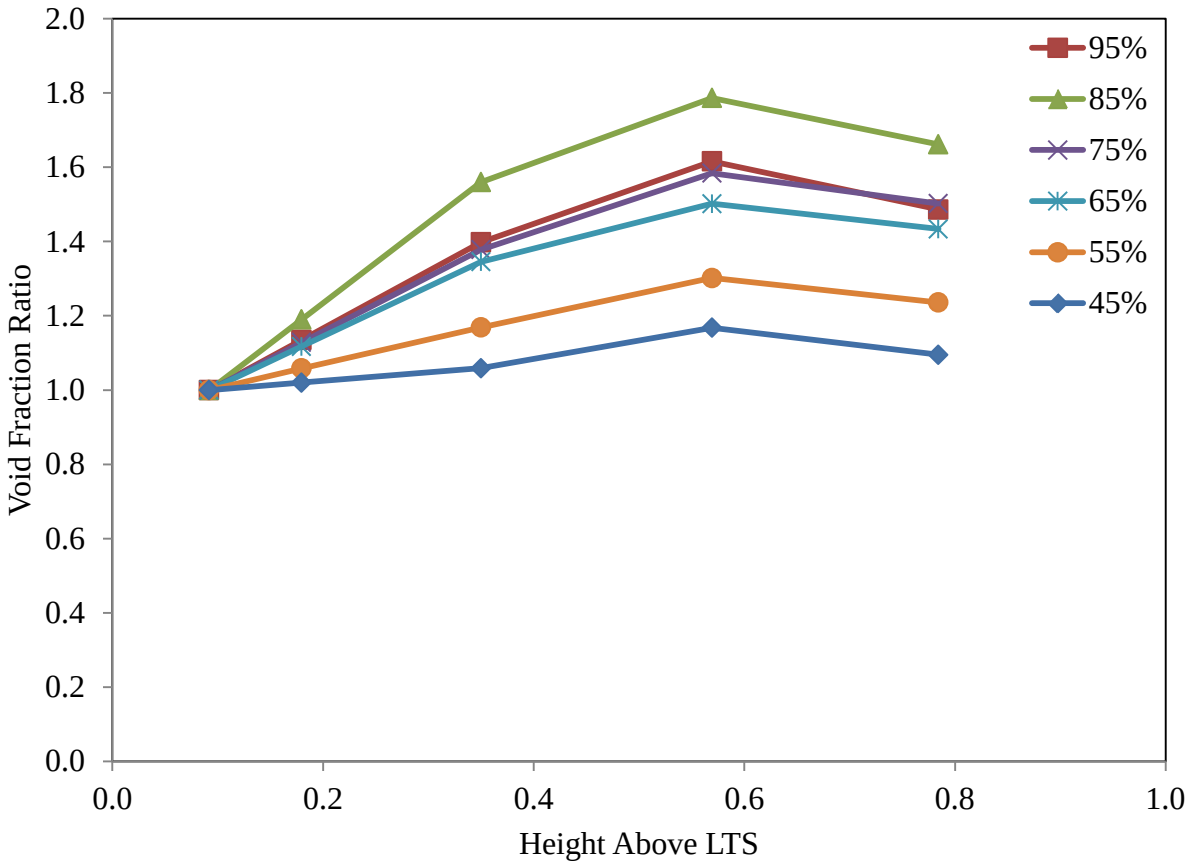

Figure 5: Void Fraction Ratio Profiles in the Downcomer for Various Power Levels [5]

2.3: Two-Phase Flow

As the flow into the downcomer contains steam and water, an understanding of two-phase flow is pivotal to understanding the physics of this problem. There exists three primary ways that a one-dimensional two-phase flow problem may be analyzed. The simplest method was the homogeneous model, where the phases are considered to be mixed into a single fluid and all properties are weighted averages for each of the two phases. By contrast, the separated flow model assumes that the phases flow alongside each other, thus requiring separate equations for continuity, momentum and energy for each phase, along with terms that account for mass, momentum and energy transfer between the phases. A third model, known as the drift flux model, is similar to the separated flow model, however, is based on the difference in motion between the two phases, as opposed to the separated flow model's emphasis on each phases' motion. [23]

RELAP5 was the first version of RELAP to feature a two-fluid model that was for both non-homogeneous and non-equilibrium situations. However, in RELAP5/MOD1, the liquid and vapor were modeled with five equations, forcing a saturation phase, while RELAP5/MOD2 contains six primary equations, lifting the saturation constraint. However, RELAP5/MOD2 does contain homogeneous and equilibrium options that when activated, revert to the earlier versions of RELAP, and are primarily intended to be used for comparison to results from those earlier versions of RELAP. [19]

The six equations used by RELAP5/MOD2 used to model the two-phase flow consist of equations for continuity, momentum and energy for each phase. The continuity equations for the vapor and liquid phases respectively are: [19]

$$\frac{\partial}{\partial t}(\alpha_g \rho_g) + \frac{1}{A}\frac{\partial}{\partial x}(\alpha_g \rho_g v_g A) = \Gamma_g \tag{5}$$

$$\frac{\partial}{\partial t}(\alpha_f \rho_f) + \frac{1}{A}\frac{\partial}{\partial x}(\alpha_f \rho_f v_f A) = -\Gamma_g \tag{6}$$

The momentum equations for the vapor and liquid phases are: [19]

$$\begin{aligned}\alpha_g \rho_g A \frac{\partial v_g}{\partial t} + \frac{1}{2}\alpha_g \rho_g A \frac{\partial {v_g}^2}{\partial x} \\ = -\alpha_g A \frac{\partial P}{\partial x} + \alpha_g \rho_g B_x A - (\alpha_g \rho_g A) FWG v_g + \Gamma_g A (v_{gI} - v_g) \\ - (\alpha_g \rho_g A) FIG (v_g - v_f) \\ - C \alpha_g \alpha_f \rho A \left[\frac{\partial (v_g - v_f)}{\partial t} + v_f \frac{\partial v_g}{\partial x} - v_g \frac{\partial v_f}{\partial x}\right]\end{aligned} \tag{7}$$

$$\begin{aligned}\alpha_f \rho_f A \frac{\partial v_f}{\partial t} + \frac{1}{2}\alpha_f \rho_f A \frac{\partial {v_f}^2}{\partial x} \\ = -\alpha_f A \frac{\partial P}{\partial x} + \alpha_f \rho_f B_x A - (\alpha_f \rho_f A) FWF v_f - \Gamma_g A (v_{fI} - v_f) \\ - (\alpha_f \rho_f A) FIF (v_f - v_g) \\ - C \alpha_f \alpha_g \rho A \left[\frac{\partial (v_g - v_f)}{\partial t} - v_f \frac{\partial v_g}{\partial x} + v_g \frac{\partial v_f}{\partial x}\right]\end{aligned} \tag{8}$$

It should be noted that the values for interphase friction, *FIF* and *FIG* are equal for any given volume in RELAP5/MOD2. Further discussion of the interphase friction and its relevance to this study are discussed in Section 2.5, where *FIF* and *FIG* are calculated as FI_{gf}. [19]

The energy equations for each phase are:

$$\begin{aligned}\frac{\partial}{\partial t}(\alpha_g \rho_g u_g) + \frac{1}{A}\frac{\partial}{\partial x}(\alpha_g \rho_g u_g v_g A) \\ = -P \frac{\partial \alpha_g}{\partial t} - \frac{P}{A}\frac{\partial}{\partial x}(\alpha_g v_g A) + Q_{wg} + Q_{ig} + \Gamma_{ig} h_g^* + \Gamma_w h_g^s \\ + DISS_g\end{aligned} \tag{9}$$

$$\begin{aligned}\frac{\partial}{\partial t}(\alpha_f \rho_f u_f) + \frac{1}{A}\frac{\partial}{\partial x}(\alpha_f \rho_f u_f v_f A) \\ = -P \frac{\partial \alpha_f}{\partial t} - \frac{P}{A}\frac{\partial}{\partial x}(\alpha_f v_f A) + Q_{wf} + Q_{if} - \Gamma_{ig} h_f^* - \Gamma_w h_f^s \\ + DISS_f\end{aligned} \tag{10}$$

If the system is experiencing phase change, h_g^* is the specific enthalpy of the saturated vapor and h_f^*, is the saturation enthalpy of the saturated liquid. The energy dissipation function for each phase that is caused by wall friction is defined as [19]

$$DISS_g = \alpha_g \rho_g FWG v_g{}^2 \tag{11}$$

$$DISS_f = \alpha_f \rho_f FWF v_f{}^2 \tag{12}$$

A key to understanding the interaction between the liquid and vapor phases in two-phase flow is the shape which the two phases take within a given flow channel, otherwise known as the flow regime. The flow regime that a two-phase system is experiencing can be observed visually in an experiment with a transparent channel, but in real-world situations such as the OTSG downcomer, observation is not possible. As a result, flow regime maps have been developed that are used to predict the flow regime occurring in a channel, based on other known properties such as phase-specific flow rates and/or thermodynamic properties. Flow regime maps are discussed further in the next segment on vertical downflow.

2.4: Two-Phase Vertical Downflow

There have been many studies over the years with regards to two-phase vertical flow. However, only a small handful of those studies have researched two-phase downflow. The studies that have researched two-phase vertical flow have largely involved water and air at or near atmospheric conditions, as opposed to steam/water at the conditions of the OTSG downcomer. Each of these studies has sought to develop a flow regime map for the conditions that the experiment was conducted. While each study varies in its categorization of flow regimes, there are three flow regimes that are common amongst all maps, and these are the three vertical flow regimes identified by RELAP: bubbly flow, slug flow and annular flow.

Bubbly flow, as the name suggests, is distinguished by separate bubbles that are suspended within liquid flow that is continuous. However, by this definition, bubbly flow can range from a single bubble flowing in the liquid to a frothy flow where liquid film is all that separates the bubbles from each other. It is rare for a flow to reach stable equilibrium as bubbly flow either because the smaller bubbles will combine into larger bubbles or because the bubbles represent a phase change in evaporation or condensation. [23]

Often times, as the void fraction increases, the bubbles in a bubbly flow will collide into each other and merge until they form large bubbles that are roughly the same diameter as the pipe, forming what is known as slug flow. This transition can occur over a range of void fractions, with a special sensitivity to the purity level of the fluid. For example, with pure liquids, a rule of thumb states that the transition from bubbly to slug flow occurs at a void fraction of 0.10. However, bubbly flow has also been known to exist in tap water at a void fraction of 0.60, and with foam flows, the void fraction can reach almost 1.00. [23]

With increasing void fraction, the elongated gas bubbles in slug flow become even longer, eventually to the point that the bubbles are infinitely long in a flow regime known as annular flow. As the name suggests, the liquid film flows along the sides of the duct, forming an annulus through which vapor travels in its core. The vapor core may contain liquid droplets in what is known as drop-annular flow. [23]

2.4.1: Previous Research in Two-Phase Downflow

The earliest known study of two-phase vertical downflow was by Golan and Stenning [7], who sought to develop the first documented two-phase vertical downflow flow regime map. In their flow regime map comparing the superficial velocities of air and water in a 1.5 in. diameter tube, they identified three flow regimes: slug and bubble flow, oscillatory flow and annular-mist

and annular flow. The oscillatory flow regime describes an intermediate flow regime between slug and annular flow where Golan and Stenning observed a buildup of foam within the vertical downcomer, and linked it to the presence of U-tube bends placed at each end.

Other work with vertical downflow includes Oshinowo and Charles [16], Barnea et. al. [2] and Crawford et. al. [6]. Oshinowo and Charles studied air/water and air/glycerol solution flows in a downcomer, and created a map comparing the ratio of vapor volume flow to liquid volume flow to the two-phase Froude number. While Oshinowo and Charles were able to compare the chart created for upflow favorably to data from other studies, no results were available for downflow. It was assumed that the flow regime map would compare favorably, based on the comparisons with the upflow map. [16] Barnea et. al. develop a vertical downflow map that is largely based on the vertical upflow research of Taitel et. al, that divides downflow into three regimes: annular, slug and bubbly flow. [2,21] Crawford et. al. examined two-phase downflow with refrigerant 113 and found that when correlating the superficial velocities with a non-dimensionalized parameter based on the flow's thermodynamic and hydraulic qualities, the resulting flow regime map worked for both upflow and downflow. [6]

2.4.2: Two-Phase Downflow in RELAP5/MOD2

Despite evidence that showed the difference between upflow and downflow affects flow regime transitions, RELAP determines the flow regimes for upflow and downflow using the same flow regime map. Three conditions are used by RELAP to determine the flow regime: the critical heat flux (CHF), the void fraction and the mass flux. In Figure 6, the vertical flow regime map that RELAP uses to determine the flow regime of two-phase vertical flow is shown, for both pre-CHF and post-CHF at varying vapor void fraction, while Figure 7 shows the pre-

CHF flow regime map for varying void fraction with respect to the mass flux, using Equations (14) through (17), and the conditions for the OTSG downcomer. [19]

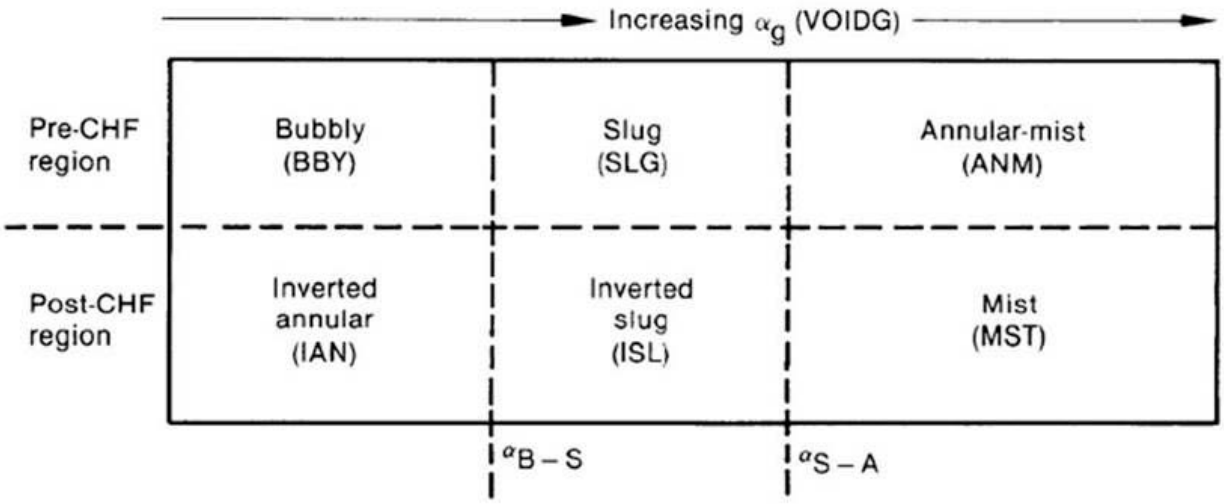

Figure 6: Vertical Flow Regime Map for Pre-CHF and Post-CHF in RELAP5/MOD2 (Reproduced from Ransom, V.H. et.al., 2011 [19])

The CHF refers to the amount of heat that is being added through the walls at which the liquid at the wall ceases to boil and is completely vaporized. In RELAP, two-phase flow can be described as either pre-CHF, where the liquid phase is in contact with the wall, or post-CHF, where the vapor phase is in contact with the wall. For the OTSG downcomer, as well as any other flow where no heat is being added, the flow is considered to be pre-CHF. CHF is determined using the modified Zuber correlation that is given in Equation (13)

$$q_{CHF} = 0.131(1-\alpha_g)h_{fg}\sqrt{\frac{\rho_g\rho_f}{\rho_f+\rho_g}}\sqrt[4]{\sigma g(\rho_f-\rho_g)}\left\{\max\left[1,\sqrt[3]{\frac{G}{G_{ref}}}\right]\right\} \quad (13)$$

where G_{ref} is considered to be a reference mass flux that is equal to 67.8 kg/m^{2}s. [19]

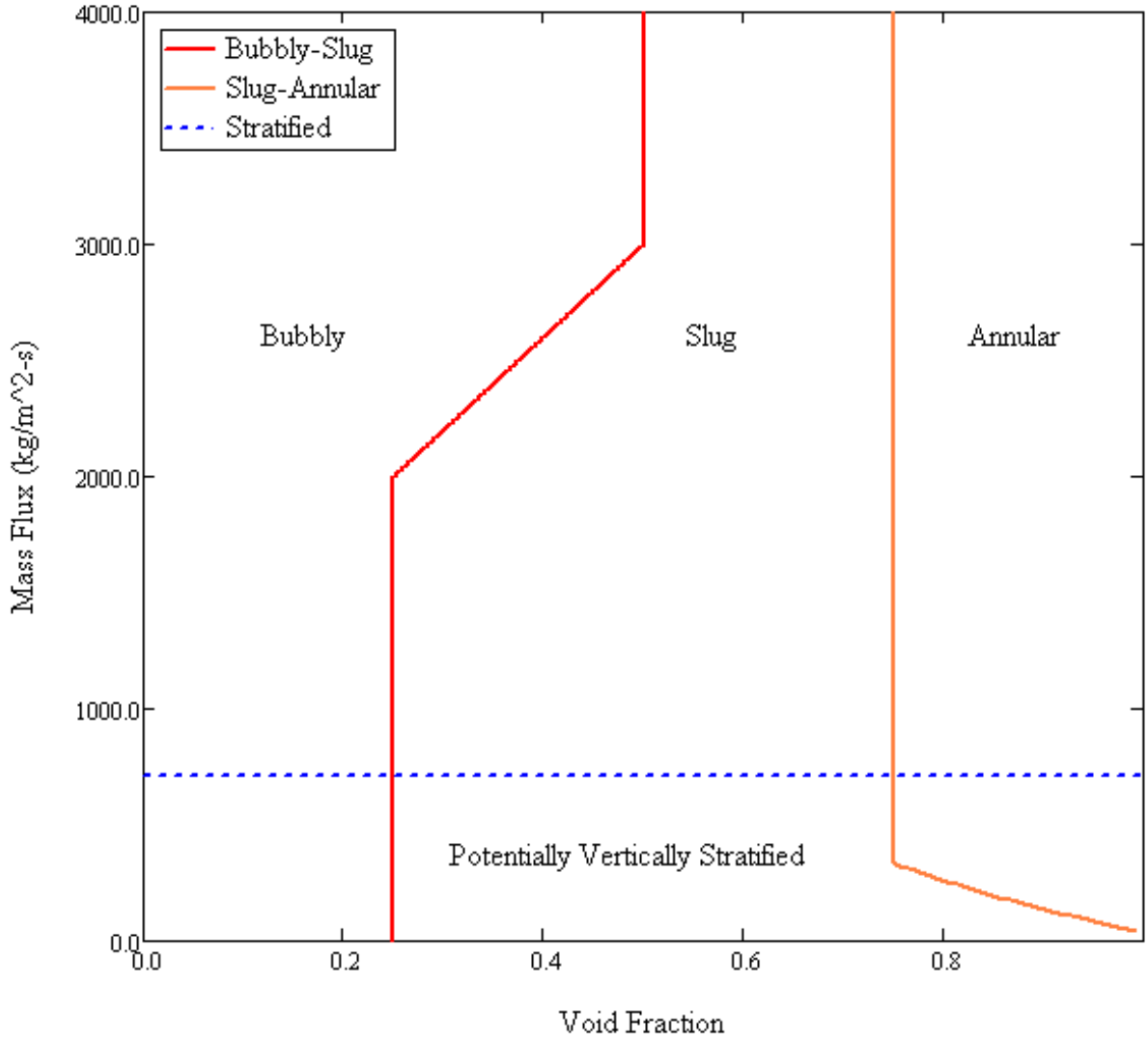

Figure 7: RELAP5/MOD2 Vertical Flow Regime Map [19]

In both figures, $\alpha_{B\text{-}S}$ represents the void fraction at which bubbly flow transitions to slug flow, and $\alpha_{S\text{-}A}$ is the void fraction at which slug flow transitions to annular-mist flow. The transition from bubbly flow to slug flow is determined using Equation (14)

$$\alpha_{B-S} = \begin{cases} \alpha_L & G \le 2000 \text{ kg/m}^2\text{s} \\ \alpha_L + 0.001(G - 2000)(0.5 - \alpha_L) & 2000 \text{ kg/m}^2\text{s} \le G \le 3000 \text{ kg/m}^2\text{s} \\ 0.5 & G \ge 3000 \text{ kg/m}^2\text{s} \end{cases} \quad (14)$$

where α_L is determined using Equation (15)

$$\alpha_L = 0.25 \min\left[1.0, \left(\frac{D\sqrt{\frac{g(\rho_f - \rho_g)}{\sigma}}}{19}\right)^8\right] \tag{15}$$

For the transition from slug to annular flow, $\alpha_{S\text{-}A}$, there is no dependence on the mass flux, and it is determined using Equation (16). [19]

$$\alpha_{S-A} = \max\left\{0.75, \frac{1.4\sqrt[4]{\sigma g(\rho_f - \rho_g)}}{v_g\sqrt{\rho_g}}\right\} \tag{16}$$

Aside from the bubbly flow-slug flow transition void fraction, $\alpha_{B\text{-}S}$, mass flux is used to determine whether the vertical flow regime is stratified rather than bubbly, slug or annular mist. For the flow regime to be stratified, two conditions must be satisfied. First, the difference in void fraction between two vertically aligned, adjacent volumes must be greater than 0.5. Second, the mass flux must be less than that of a Taylor bubble, which is determined using Equation (17). [19]

$$|G| < 0.35\rho_g\sqrt{gD(\rho_f - \rho_g)\rho_f} \tag{17}$$

The flow regime maps used in RELAP5/MOD2 are based on the work of several sources. Taitel et. al. [21] developed a flow regime map that is based on superficial velocities for liquid and vapor, similar to that seen in Figure 9. Figure 9 serves as the basis for the pre-CHF vertical two-phase flow regime map that is used in RELAP. In addition to the three flow regimes used in RELAP, Taitel et. al. include a finely dispersed bubble flow regime and a churn flow regime. Finely dispersed bubble flow is self-explanatory. Churn flow, sometimes called churn-turbulent

flow, differs from slug flow in that the Taylor bubbles take on odder, elongated shapes between poorer-defined liquid slugs, like those shown in Figure 8.

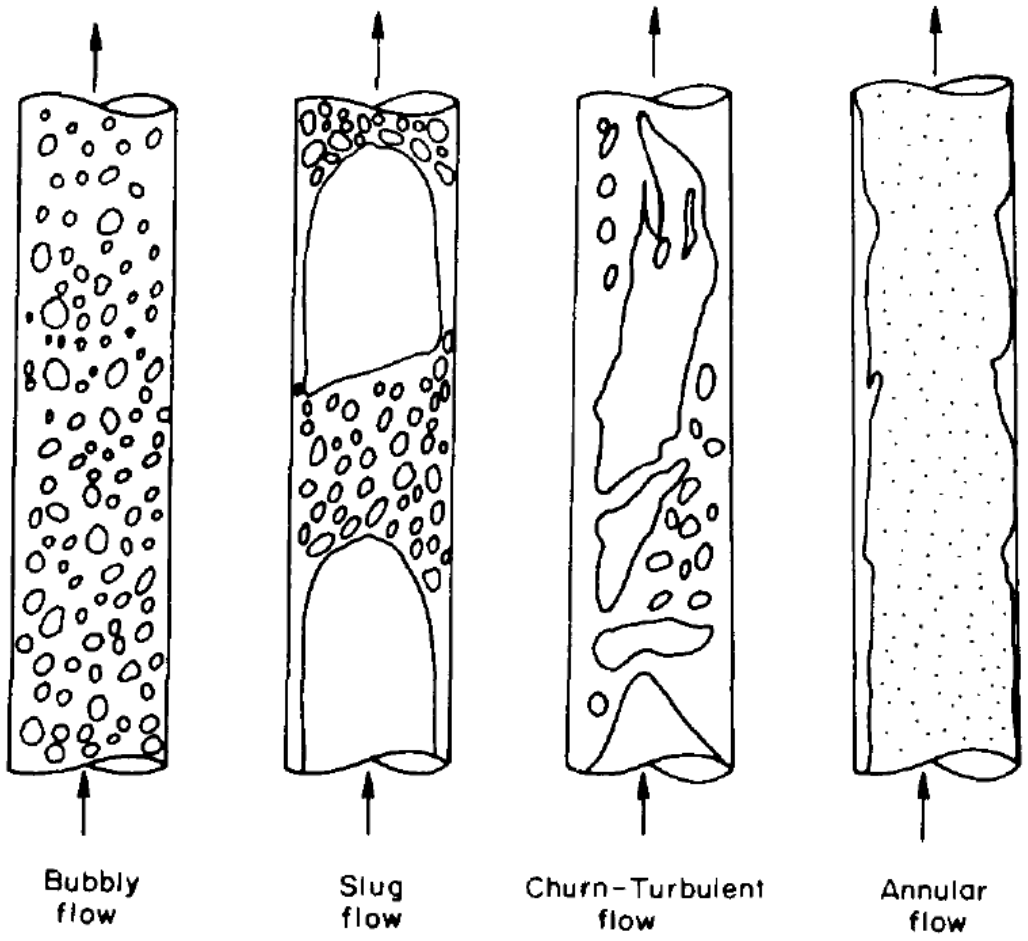

Figure 8: Vertical Flow Regimes (Used with Permission from Elsevier, 2011[1]) [22]

[1] – Reprinted from the International Journal of Multiphase Flow, Volume 8, Vince, M.A. and Lahey, R.T., "On the Development of an Objective Flow Regime Indicator," pp. 93-124, 1982, with permission from Elsevier.

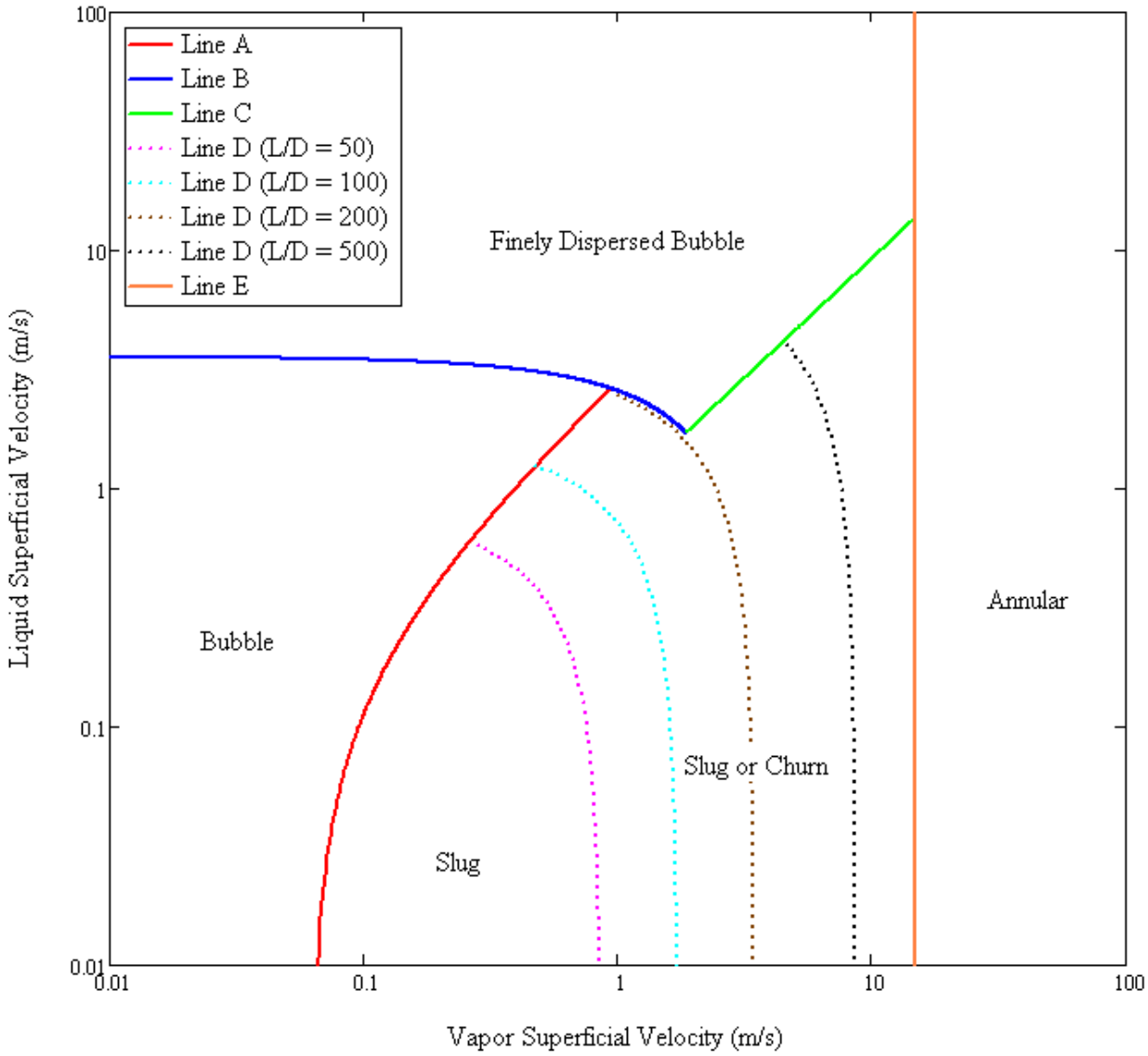

Figure 9: Vertical Flow Pattern Map for a 5 cm Diameter Pipe, with an Air-Water Mixture at T = 25°C and P = 10 N/cm^2 [8,21]

Using the superficial velocities and thermodynamic properties provided by Taitel et. al, an equivalent flow regime map has been created in Figure 10, showing the relationship between mass flux and void fraction. A comparison between the flow regime map presented in the RELAP manual (Figure 7) and the Taitel et. al. flow regime map (Figure 10) reveals that while there are a few similarities between the two flow regime maps, there are also several differences.

The most noticeable similarity is that the bubbly-slug flow transition void fraction is roughly 0.25 for lower mass fluxes, and is 0.5 for higher mass fluxes. Also, the slug/churn-

annular flow transition mirrors Equation D given by the RELAP manual, although Taitel et. al. use a coefficient of 3.1 instead of 1.4 in Equation (16) for the calculation of the slug-annular flow regime transition void fraction when greater than 0.75. The coefficient of 1.4 was first used by Wallis and proved to be a better match in RELAP5/MOD2 testing. [19,23]

The differences are primarily the result of simplifications that were made to the RELAP flow regime map that allowed for smoother calculations and easier programming. [19] The most notable difference is the absence of churn flow in the RELAP flow regime map. Also among the differences is the transition zone for the bubbly-slug flow void fraction, that is linearly interpolated in RELAP, but is not the case with Taitel et. al.

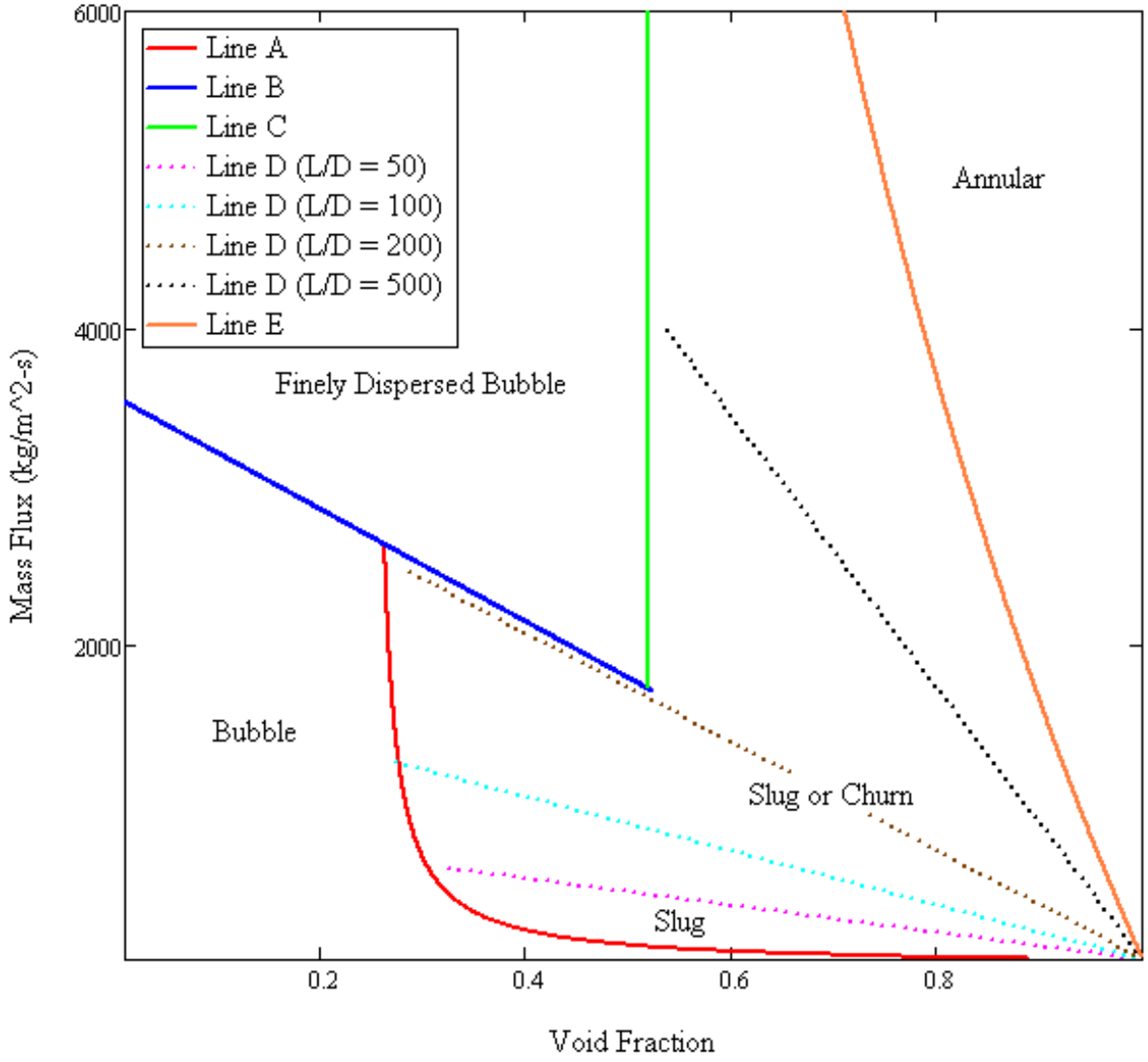

Figure 10: Vertical Flow Regime Map on a Mass Flux - Void Fraction Basis for a 5 cm Diameter Pipe, with an Air-Water Mixture at T= 25°C and P = 10N/cm^2 [21]

A simplified version of the Taitel et. al. flow regime map, similar to that used by Vince and Lahey [22], is shown in Figure 11, with the mass flux-void fraction equivalent map shown in Figure 12. [21] Where Taitel et. all used an air-water mixture at a pressure of 10N/cm^2 and temperature of 25°C, flowing in a 5 cm pipe, the flow regime maps shown in Figure 11 and Figure 12 are based on the conditions of the downcomer, with steam-water at a pressure of 925 psi and temperature of 535°F flowing in a channel with a hydraulic diameter of 0.0450. The

annular flow regime transition void fraction is calculated using the coefficient of 1.4, as is used in RELAP, instead of 3.1 as used in Taitel et. al. [21]

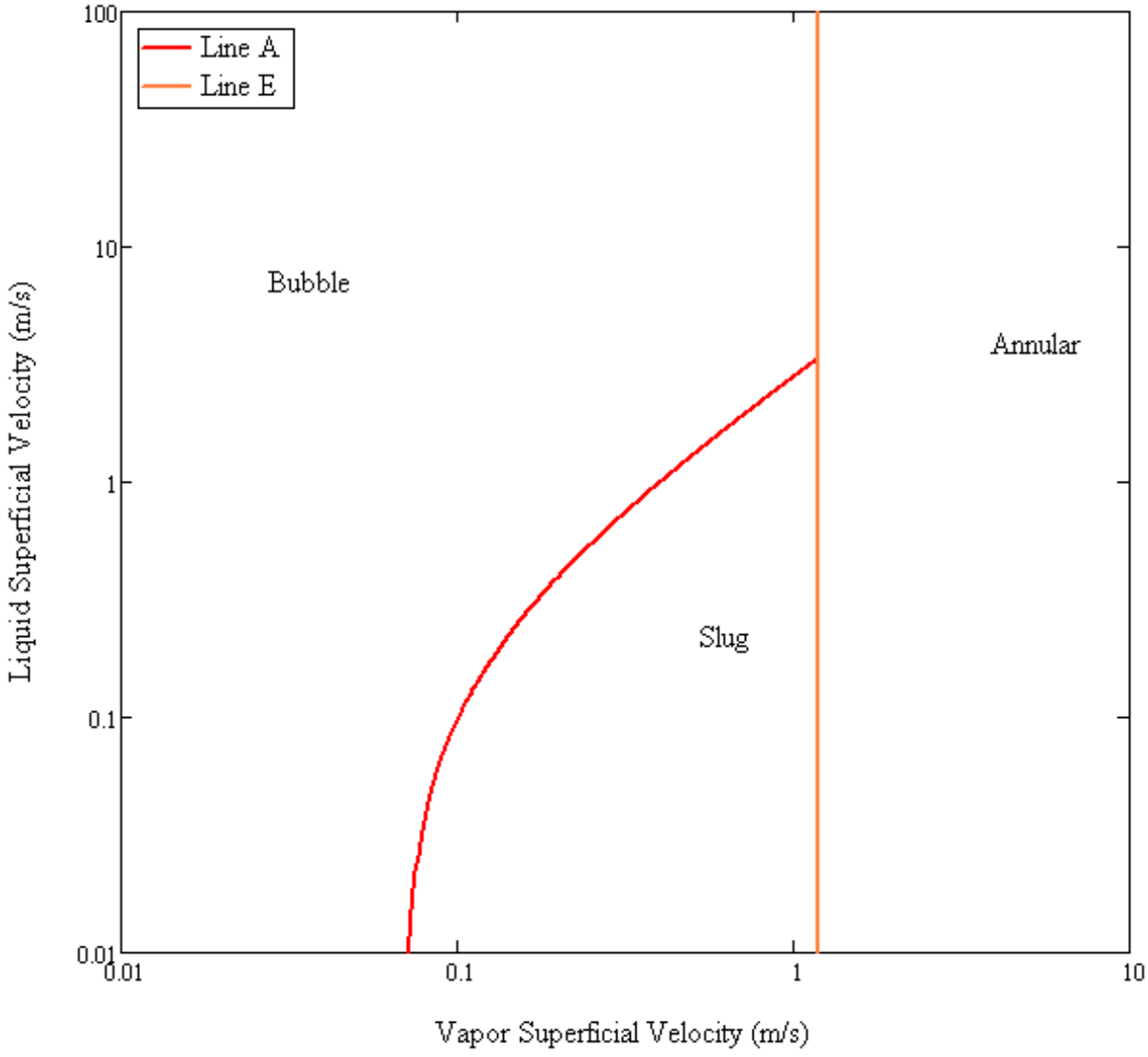

Figure 11: Simplified Taitel et. al. Flow Regime Map for Steam-Water at P = 925 psi, T = 535°F and a Hydraulic Diameter of 0.0450 [21]

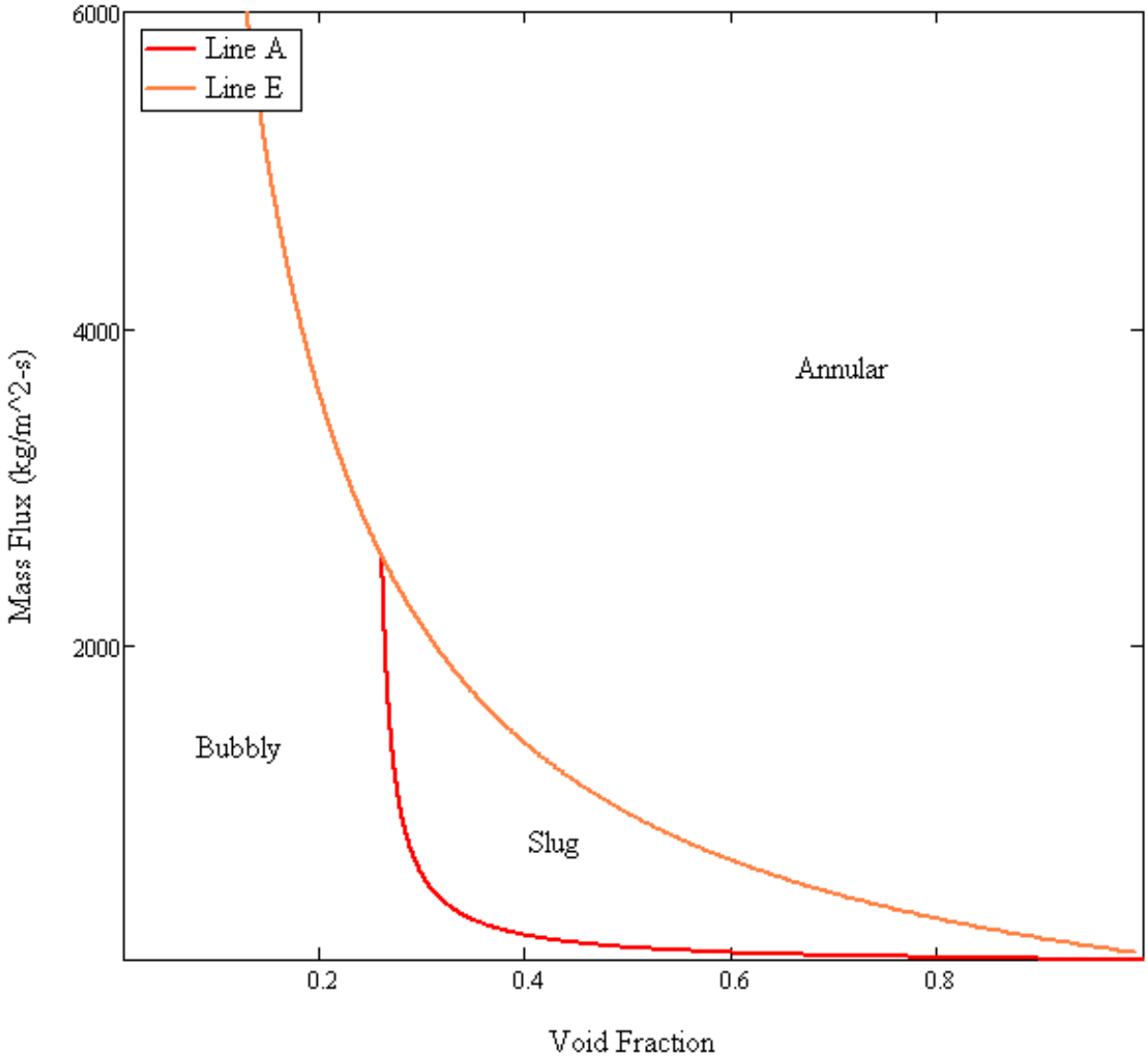

Figure 12: Mass Flux-Void Fraction Flow Regime Map for Steam-Water at P = 925 psi, T = 535°F and a Hydraulic Diameter of 0.0450 Based on Simplified Taitel et. al. Flow Regime Map [21]

Shown in Figure 13, a comparison of the Taitel et. al. map shown in Figure 12 to the RELAP5/MOD2 flow regime map shown in Figure 7. A comparison at 95% power, not shown in Figure 13 out of consideration to Areva Inc.'s proprietary rights, revealed that the slug-annular flow regime transition occurs at the same void fraction in both the Taitel et. al. and RELAP5/MOD2 flow regime maps. However, the bubbly-slug flow regime occurs at a void

fraction of 0.25 in the RELAP5/MOD2 flow regime map, while in Taitel et. al., it occurs at a void fraction of 0.332 at 95% power.

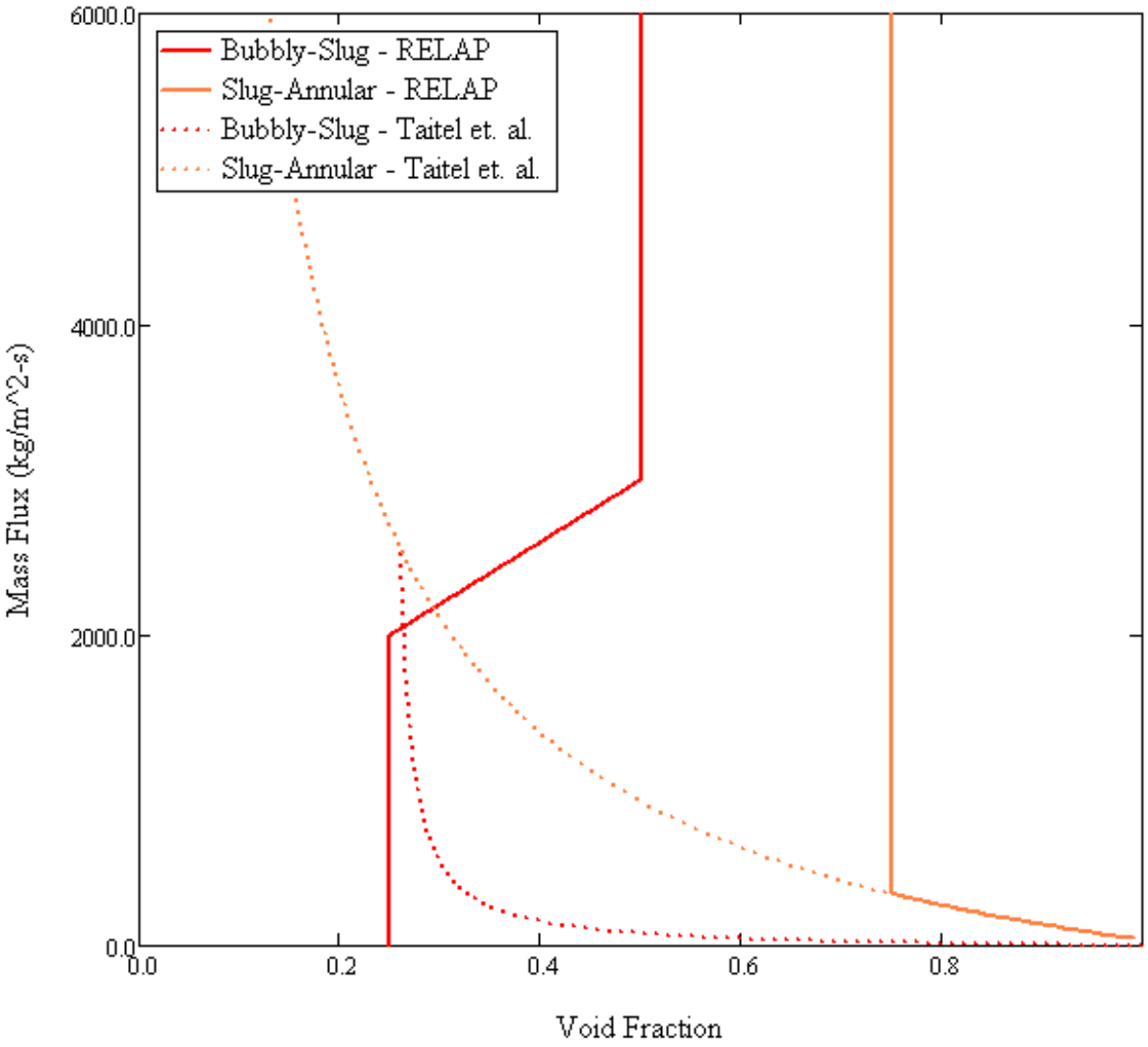

Figure 13: Comparison of RELAP5/MOD2 Flow Regime Map [19] to Taitel et. al. [21] Map for P = 925 psi, T = 535F and a Hydraulic Diameter of 0.0450

2.5: Interphase Friction in RELAP5/MOD2

One of the most important parameters to be evaluated is the interphase drag between the liquid and vapor in the downcomer since the wall friction is comparatively small. The interphase drag force per unit volume is used in the momentum equations (7) and (8), where it is known as *FIF* and *FIG*, is calculated in RELAP5/MOD2 by Equation (18). [19]

$$FI_{gf} = -f_{gf}|v_g - v_f|(v_g - v_f) \tag{18}$$

The interphase friction factor, f_{gf}, is determined using Equation (19).

$$f_{gf} = \frac{1}{8}[\rho_c S_f a_{gf} C_D] \tag{19}$$

The shape factor, S_f, is assumed equal to 1.0 for all cases, while all other factors are dependent on the flow regime. The continuous density, ρ_c, is assumed to be the density of liquid for the bubbly and slug flow regimes. For the annular-mist flow regime, the continuous phase is liquid for the liquid film along the wall, and vapor for the interior column. [19]

2.5.1: Bubbly Flow Interphase Friction

For bubbly flow regime, the interfacial area of the bubbles is determined using Equation (20)

$$a_{gf} = \frac{3.6\alpha_g}{d_o} \tag{20}$$

where the average bubble diameter, d_o, is assumed to be half of the maximum bubble diameter, d_{max}, which is derived from the critical Weber number, *We*, that is calculated using Equation (21)

$$We = d_{max}\rho_f \frac{(v_g - v_f)^2}{\alpha_g} \tag{21}$$

In the original version of RELAP5/MOD2, the critical Weber number for bubbles is 10, where as in the Areva, Inc. version, the value is 5. [15,19] The bubble drag coefficient is calculated using Equation (22). [19]

$$C_D = \frac{24\left(1 + 0.1{Re_b}^{0.75}\right)}{Re_b} \tag{22}$$

The Reynolds number of the bubbles, Re_b, is calculated using Equation (23). [19]

$$Re_b = \frac{\left|v_g - v_f\right| d_o \rho_f \alpha_f}{\mu_f} \tag{23}$$

2.5.2: Slug Flow Interphase Friction

In the slug flow regime, RELAP5/MOD2 must account for the interphase drag that is produced by both the large Taylor bubbles and by the smaller bubbles within the liquid slugs between them. Since RELAP assumes that the diameter of a Taylor bubble is roughly equal to that of the pipe in which it is flowing, the film that separates the Taylor bubbles from the wall is considered to be negligible. The total interphase drag can be found as a sum of the interphase drag of each of the parts, as shown in Equation (24). [15]

$$f_{gf} = f_{gf,sb} + f_{gf,T} \tag{24}$$

The interphase friction factor for the small bubbles within the liquid is calculated similarly to the case with bubbly flow, with the added consideration that the flow occurs within a smaller share of the overall flow. This is accomplished by determining the average void fraction in the liquid film and slug region, α_{gs}, and the void fraction of a single Taylor bubble, α_b, using Equations (25) and (26). [19]

$$\alpha_{gs} = \alpha_{B-S} e^{\frac{-10\left(\alpha_g - \alpha_{B-S}\right)}{\alpha_{S-A} - \alpha_{B-S}}} \tag{25}$$

$$\alpha_b = \frac{\alpha_g - \alpha_{gs}}{1 - \alpha_{gs}} \tag{26}$$

where $\alpha_{B\text{-}S}$ is the bubbly-slug flow transition void fraction (typically 0.25) and $\alpha_{S\text{-}A}$ is the slug-annular-mist flow transition void fraction (typically 0.95). Thus, the small bubble interphase friction is calculated using Equation (27).

$$f_{gf,sb} = \frac{1}{8}\left(\rho_f \frac{3.6\alpha_{gs}}{d_o} C_{D,b}(1-\alpha_b)\right) \tag{27}$$

For Taylor bubbles, the interfacial area and drag coefficients are calculated using Equations (28) and (29), respectively

$$a_{gf,T} = \frac{4.5 C_t \alpha_{gs}}{D} \tag{28}$$

$$C_{D,T} = 9.8(1-\alpha_b)^3 \tag{29}$$

where C_t is a roughness parameter assumed to equal 1. [19]

2.5.3: Previous Research on Slug Flow Interphase Friction

Several studies were conducted on the accuracy of RELAP5/MOD2 during the late 1980s, after it had been released in 1985. Many of these studies examined deficiencies that RELAP5/MOD2 had and explored solutions for both MOD2, as well as RELAP5/MOD3. Once MOD3 was released in the early 1990s, research with MOD2 was largely abandoned in favor of MOD3. While no studies have been published using Areva's version or RELAP5/MOD2, or for the OTSG downcomer, there have been several studies examining the interphase friction with RELAP5/MOD2.

Of the available published studies that are discussed below, all examined two-phase vertical upflow rather than downflow, and focused largely on bubbly flow. The general consensus of these studies was that RELAP5/MOD2 over-predicted interphase drag, causing excessive liquid to be carried over in vertical two-phase upflow. The solution proposed in all of

these studies involves substituting the velocity difference used to calculate the interphase friction force in Equation (18) with the relative velocity, first proposed in Zuber and Findlay [25].

Zuber and Findlay [25] developed what they called the weighted mean drift velocity, that for vapor is defined in Equations (30) through (33). A similar weighted mean drift velocity can be calculated for liquid, with which the difference can be substituted into Equation (18).

$$\overline{v_g} = C_0\langle j\rangle + \frac{\langle \alpha_g v_{gj}\rangle}{\langle \alpha_g\rangle} \tag{30}$$

where, for a given cross-sectional area A

$$C_0 = \frac{\langle \alpha j\rangle}{\langle \alpha\rangle\langle j\rangle} = \frac{\frac{1}{A}\int_0^A \alpha j\, dA}{\left(\frac{1}{A}\int_0^A \alpha\, dA\right)\left(\frac{1}{A}\int_0^A j\, dA\right)} \tag{31}$$

$$j = j_f + j_g = \frac{Q_f}{A} + \frac{Q_g}{A} \tag{32}$$

$$v_{gj} = v_g - j \tag{33}$$

Zuber and Findlay state that the distribution parameter, C_o, refers to the distribution of vapor with respect to liquid in the two-phase flow, and can be described using the void fraction at the wall, α_w, and the void fraction in the center of a channel, α_c, using Equation (34).

$$C_0 \begin{cases} < 1 & \alpha_c < \alpha_w \\ = 1 & \alpha_c = \alpha_w \\ > 1 & \alpha_c > \alpha_w \end{cases} \tag{34}$$

When $\alpha_c < \alpha_w$, it implies that the system is experiencing film boiling, and is post-CHF. A centerline void fraction equal to the wall void fraction implies that the heat flux is at CHF, and when the wall void fraction is less than the centerline void fraction, the flow is implied to be pre-CHF, the flow within the OTSG downcomer.

Putney and Preece [18] tested RELAP5/MOD2 against data from the Westinghouse U-tube steam generator at Wolf Creek PWR near Burlington, Kansas. The study focused mainly on

the performance of RELAP5/MOD2 in the tube bundle of the steam generator, although the downcomer is also modeled so as to provide information on the liquid level inventory. With regards to interphase drag, the study only discussed two-phase upflow in the tube bundle on the secondary side, and found that RELAP over-predicted the interphase drag for bubbly flow. As a result, excess liquid is carried up through the tube bundle, and the amount of liquid in the downcomer is under-predicted. Putney and Preece also noted that in the circular channel above the tube bundle, which has a diameter of 3.6 m, RELAP sometimes predicted the flow regime turning to slug flow. A Taylor bubble of such girth would likely break apart under real world conditions, leading Putney and Preece to conclude an under-prediction in interphase friction for that section of the steam generator, and partially correcting for the over-prediction of interphase friction in the tube bundle. Putney and Preece also noted that in several cases, annular flow was the predicted flow regime, rendering slug drag inapplicable. Putney and Preece cite improvements made to RELAP5/MOD3 that address the interphase friction in the tube bundle that are summarized in Putney [17].

Putney [17] used RELAP5/MOD2 to model several experiments regarding both vertical upflow and depressurization of pools to develop a new interphase friction model for bubbly and slug vertical flows. A model using drift flux velocity is proposed, with correlations by Zuber and Findlay [25], Kataoka and Ishii [10] and EPRI [3,4] tested for different situations. Although no tests examined vertical downflow, Putney suggests that the EPRI drift velocity model described in Equations (35) through (39) should be used for modeling two-phase vertical downflow when the mass flow rate exceeds 100 kg/m^2s, as is the case in the OTSG downcomer. The variable, C_0, is the EPRI equivalent to the drift velocity coefficient described in Zuber and Findlay [25].

$$C_0 = \frac{L(\alpha_g, P)}{K_o + (1 - K_o){\alpha_g}^r} \tag{35}$$

$$L(\alpha_g, P) = \frac{1 - e^{-C_1 \alpha_g}}{1 - e^{-C_1}} \tag{36}$$

$$C_1 = \frac{4{P_{crit}}^2}{P(P_{crit} - P)} \tag{37}$$

$$K_o = B_1 + (1 - B_1)\left(\frac{\rho_g}{\rho_f}\right)^{\frac{1}{4}} \tag{38}$$

$$r = \frac{1 + 1.57\left(\frac{\rho_g}{\rho_f}\right)}{1 - B_1} \tag{39}$$

B_1 is defined as a function of the superficial Reynolds number of the liquid, Re_f, and vapor, Re_g, phases, that is solved using Equations (40) through (44).

$$B_1 = \min(0.8, A_1) \tag{40}$$

$$A_1 = \frac{1}{1 + e^{\frac{-Re}{60000}}} \tag{41}$$

$$Re = \begin{cases} Re_g & \text{if } Re_g > Re_f \text{ or } Re_g < 0.0 \\ Re_f & \text{if } Re_g \leq Re_f \end{cases} \tag{42}$$

$$Re_f = \frac{We_f D_H}{\mu_f A} \tag{43}$$

$$Re_g = \frac{We_g D_H}{\mu_g A} \tag{44}$$

The drift velocity that is used by Putney is given in Equation (45). While Putney [17] states that the liquid void fraction, 1- α_g, should be exponentiated to a value K_1, Chexal et. al. [4] state that the value should be exponentiated to B_1 that is discussed above. The coefficients, C_2, C_3 and C_4 are determined using properties of the liquid and vapor flow, including the density, hydraulic diameter and Reynolds number of the liquid flow. [4,17]

$$v_{gj} = 1.41\sqrt[4]{\frac{(\rho_f - \rho_g)\sigma_f}{{\rho_f}^2}}\left(1-\alpha_g\right)^{B_1} C_2 C_3 C_4 \tag{45}$$

Analytis [1] used data from the NEPTUN heated rod bundle to model low flooding rate reflood experiments and boil off experiments. Similar to work Analytis had conducted with TRAC-BD1, RELAP over-predicted the liquid carry-over in the tube bundle due to excessive bubbly/slug flow interphase shear. The drift flux velocity calculated using Equation (46) was substituted into RELAP to calculate the velocity difference in Equation (18) for calculating the interphase drag, and resulted in an improved modeling of the liquid carry-over.

$$v_d = 0.124\sqrt{\frac{g(\rho_f - \rho_g)D_H}{\rho_g}} \tag{46}$$

Hassan [9] also modified RELAP5/MOD2 using a drift flux model to reduce the interphase drag in the tube bundle by substituting the velocity difference in Equation (18) with the relative velocity calculated using Equation (47). The drift flux coefficient C_0 is calculated for bubbly/slug turbulent flow using Equation (48).

$$v_d = \frac{\left(1 - C_o\alpha_g\right)v_g}{\left(1-\alpha_g\right)} - C_0 v_f \tag{47}$$

$$C_0 = 1.2 - 0.2\sqrt{\frac{\rho_g}{\rho_f}} \tag{48}$$

2.5.4: Areva's Slug Flow Interphase Friction Modifications

Within the Areva, Inc. version of RELAP5/MOD2 that was provided, there are three different options provided to determine the interphase friction factor, the default INEL model, the B&W modified slug drag model and the Wilson model. The default INEL model is the original version produced for RELAP5/MOD2 that is calculated as described above. The B&W

modified and Wilson slug drag models were added to RELAP5/MOD2 by Areva, Inc, and include coefficients that can be set at each volume within a given system. [15]

To overcome shortfalls with the INEL model, Babcock & Wilcox developed their own version of an interphase drag model. The B&W modified model continues to use the same formulae for determining $f_{gf,sb}$ and $f_{gf,T}$, but added multipliers to the equation to adjust the interphase friction parameters. The B&W modified formulation for interphase friction is [15]

$$f_{gf} = M_{st}\left(f_{gf,sb} + M_s f_{gf,T}\right) \tag{49}$$

where

$$M_{st} = xslg * P_{vol} + cxslg \tag{50}$$

$$M_s = \begin{cases} 1.0 & \text{if } \alpha_g \leq \alpha_{sl} \\ 1.0 - M_m(1 - xsg) & \text{if } \alpha_{sl} \leq \alpha_g \leq \alpha_{sh} \\ xsg \; if \; \alpha_g \geq \alpha_{sh} & \text{if } \alpha_{sh} \geq \alpha_g \end{cases} \tag{51}$$

$$M_m = \frac{\alpha_{sl} - \alpha_g}{\alpha_{sl} - \alpha_{sh}} \tag{52}$$

For the B&W modified slug drag model, *xslg* is the slope of the pressure term, and has a default value of 2.52223x10^{-8} Pa^{-1}, *cxslg* is the x-intercept of the pressure term, with a default value of 0.1109, α_{sl} and α_{sh} are the low and high end adjustments for the void fraction, respectively, and have default values of 0.2 and 0.95, and *xsg* is the high void fraction slug drag coefficient, with a default value of 0.1. Assuming that the volume pressure, P_{vol}, is 925 psi, the interphase friction model coefficient, M_{st}, has a default value of 0.2718. The Areva, Inc. version of RELAP5/MOD2 allows for the parameters *xslg*, *cxslg*, α_{sl}, α_{sh} and *xsg* to be set for each volume by adding a line with the desired values to the input file. [15]

The Wilson model features a different approach to the modeling of the slugs, along with its own set of multipliers for the Taylor bubbles. While the formula for the interphase friction

factor of the small bubbles is the same as in the INEL model, the interphase friction factor for the Taylor bubbles is given in Equation (53). [15]

$$f_{gf,T} = \frac{C_{WSL}(\rho_f - \rho_g)g(1-\alpha_b)\alpha_b}{(C_{WB}\Delta v)^2} \tag{53}$$

with C_{WSL} and C_{WB} being user-defined multipliers and Δv representing the difference in velocity that is calculated using a correlation that was developed by Wilson et al. [15,24]

2.5.5: Annular-Mist Interphase Friction

For the annular-mist regime, RELAP5/MOD2 calculates the interphase friction factor similarly to slug flow, by dividing the factor into two parts, one for the interphase friction between the liquid film along the walls and the vapor core, and one for the friction between the vapor core and the liquid droplets within the core. For the interaction between the liquid film and the vapor core, the interfacial area, $a_{gf,ann}$, is calculated as shown in Equation (54).

$$a_{gf,ann} = \frac{4C_{ann}}{D}\sqrt{1-\alpha_{ff}} \tag{54}$$

where C_{ann} is a parameter used to account for roughness created by waves in the liquid film and α_{ff} is the liquid void fraction of the film that is calculated using Equation (55) for vertical flow.

$$\alpha_{ff} = {\alpha_f}^2 \rho_f v_f \frac{D}{\mu_f} e^{-7.5\times10^{-5}\left(\frac{v_g}{v_{gL}}\right)^6} \times 10^{-4} \tag{55}$$

An interfacial friction coefficient, f_i, is substituted in place of the drag coefficient, C_D, for the interaction between the vapor core and liquid film, and is calculated using Equations (56) through (59). [19]

$$f_i = 4[0.005 + A(\delta^*)^B] \tag{56}$$

$$A = 10^{\left(-0.56+\frac{9.07}{D^*}\right)} \tag{57}$$

$$B = 1.63 + \frac{4.74}{D^*} \tag{58}$$

$$\delta^* = \delta \sqrt{\frac{(\rho_f - \rho_g)g}{\sigma}} \tag{59}$$

The interphase friction factor for the droplets with the vapor core is calculated similarly to the interphase friction factor for bubbles, however, certain values are changed in order to apply the same method to droplets instead of bubbles. The interfacial area for the droplets in the vapor core is calculated using Equation (60).

$$a_{gf,d} = \frac{3.6\alpha_{fd}}{d_o}(1 - \alpha_{ff}) \tag{60}$$

where α_{fd} is the average liquid void fraction within the vapor core and is calculated using Equation (61).

$$\alpha_{fd} = \frac{\alpha_f - \alpha_{ff}}{1 - \alpha_{ff}} \tag{61}$$

The drag coefficient for droplets is calculated in the same manner as is for bubbles, with the most significant difference being the critical Weber number, which for droplets is 3. [19]

2.6: Components in RELAP5/MOD2

In RELAP, the different parts of a plant are made up as an assemblage of different components that RELAP is designed to model. The three major categories of components are volumes, junctions and branches. Volumes are components that have a defined cross-sectional area and length, while the fluid is characterized by its thermodynamic properties. Junctions are solely defined by their cross-sectional area, as they are considered to have zero length. The fluid in a junction is characterized by it velocity or mass flow rate. Branches are a combination of volumes and junctions, with a defined length and cross-sectional area, but the fluid is described

by its flow at the branch inlets and outlets, and by its thermodynamic properties within the branch. [19]

2.6.1: Volumes in RELAP5/MOD2

Examples of volumes used in this study include time dependent volumes, single volumes and pipes/annuli, while volumes such as pumps, turbines and accumulators are not used. Time dependent volumes and single volumes generally serve as boundaries for a fluid system. The user sets the thermodynamic properties throughout the model run for a time dependent volume, and only change when the user specifies such a change. In this study, the thermodynamic properties for a time dependent junction were held constant throughout the model run. With a single volume, the user specifies the thermodynamic properties as an initial condition, but change accordingly as model run progresses. The input for pipes and annuli only dictate the initial thermodynamic properties as well. In pipes and annuli, the direction of flow cannot change, meaning vertical flow cannot become horizontal within a pipe or annulus, and vice versa. Annuli are modeled as pipes with the appropriate hydraulic diameter, and can only be oriented vertically in RELAP5/MOD2. [19]

2.6.2: Junctions in RELAP5/MOD2

Junctions serve to connect volumes together, with time dependent junctions and single junctions being examples used in this study, while valves were not used in this study. The flow rate through a time dependent junction is explicitly stated in the RELAP input file by the user, and only changes as the user dictates in a given model run. Meanwhile, the flow rate for a single junction that is input by the user only serves as an initial condition, and RELAP adjusts the flow rate accordingly to the conditions in the model run. RELAP determines the flow rate through all single junctions for the remainder of the model run. In addition to the cross-sectional area, a

junction may also be described as either having an abrupt area change or smooth area change, with an energy loss factor. The difference between the two is discussed further at length in Section 2.7. [19]

2.6.3: Branches in RELAP5/MOD2

Branches are combinations of volumes and junctions, and may be modeled with either multiple inlets, multiple outlets or as a cross flow branch. The main volume of a branch has a defined length and cross-sectional area, with the fluid being described by its thermodynamic properties. The junctions connected to the branch volume at its inlets and outlets are defined by their cross-sectional areas and the abrupt/smooth area change. The advantages to using a branch connection over a pipe or annulus is that flow may be merged or diverged, and the flow direction can be changed in a branch connection. To calculate the velocity of the two-phase mixture in the branch, RELAP5/MOD2 divides the sum of the volume flow rates into the branch by the cross sectional area of the branch connection, conserving mass but failing to conserve momentum. As an alternative, the jet mixer was developed specifically for mixing two fluids, while conserving both mass and momentum. Jet mixers are a special type of branch with two inlets and one outlet, where one fluid is entering at a significantly higher speed than the other fluid. The upstream volume with high-speed fluid is called the drive volume and the upstream volume low-speed fluid is called the suction volume. A schematic of a jet mixer is provided in Figure 14, showing a smooth area change for the drive junction and an abrupt area change for the suction junction. One other type of branch connection that is not used in this study is a separator. [19]

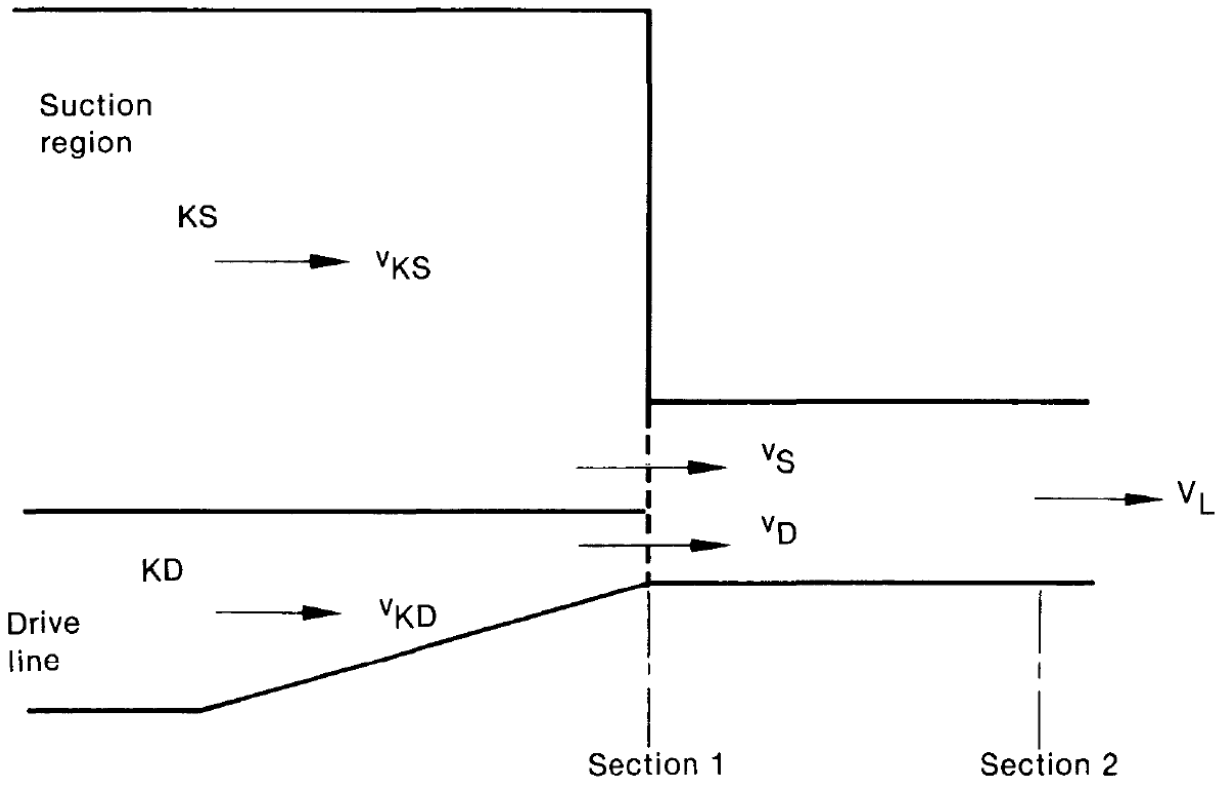

Figure 14: Schematic Diagram of a Jet Mixer (Reproduced from Ransom, V.H. et. al., 2011 [19])

2.7: Abrupt and Smooth Area Change Junctions in RELAP5/MOD2

In RELAP5/MOD2, the maximum cross-sectional area that a junction may have is the smaller cross-sectional area of the two volumes that it connects. Junctions are assumed to have the lesser cross-sectional area of the two adjoining volumes, unless the user specifies a smaller cross-sectional area. In the event that the junction is used to contract or expand the flow from one volume to the next, there exists two options for modeling losses through that junction, the abrupt area change and the smooth area change. The smooth area change assumes that the change in area at a junction occurs over a gradual length of the flow and requires the user to provide the kinetic energy loss factor, K_L, for both forward and reverse flow to accurately model the losses through the junction. [19] Munson et. al. [14] define the kinetic energy loss factor in Equation (63).

$$K_L = \frac{2\Delta P}{\rho v^2} \tag{62}$$

The abrupt area change assumes that while flows upstream and downstream of the junction are transient, the flow at the junction is quasi-steady, neglecting changes in inertia, mass and energy. The assumption is validated by the fact that the volume of the fluid, and by extension the inertia, mass and energy, are zero in the junction. As one would expect, the most common case of using the abrupt area change would be in the event of an orifice plate, like that shown in Figure 15. In the single phase case, losses that are caused by contracting flow upstream of the vena-contracta (point c), are considered negligible by RELAP, while the dynamic pressure loss downstream of the vena-contracta that is caused by expansion of the flow is calculated using Equation (63). [19]

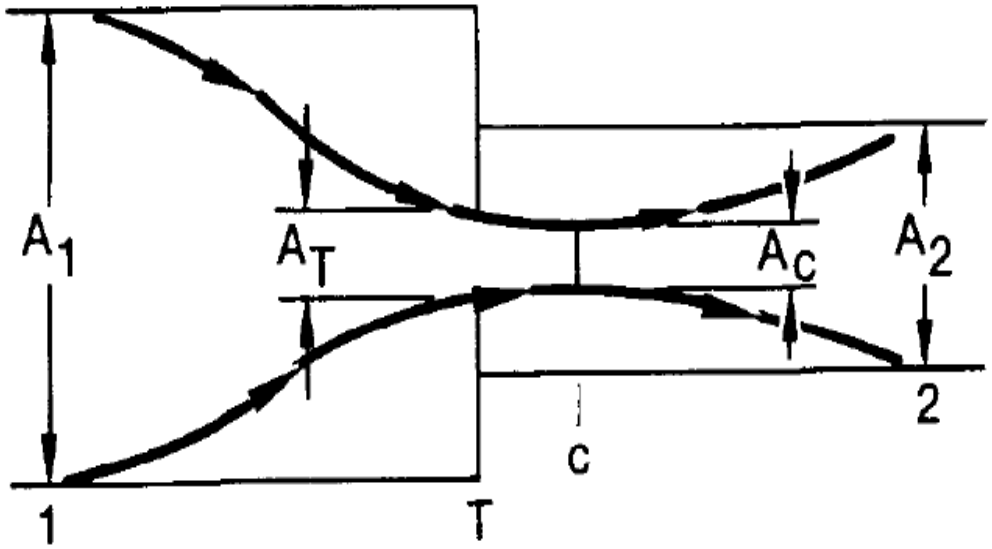

Figure 15: Orifice at Abrupt Area Change (Reproduced from Ransom, V.H. et. al., 2011 [19])

$$\Delta P = \frac{1}{2}\rho\left(1 - \frac{A_c}{A_2}\right)^2 {v_c}^2 \tag{63}$$

The area of minimum contraction, A_c, is determined using Equation (65). [20]

$$A_c = A_T\left[0.62 + 0.38\left(\frac{A_T}{A_1}\right)^3\right] \tag{64}$$

Equation (63) can also be written as Equation (65), where ε_C is the ratio between the area of the vena-contracta to the minimum physical area, ε_T is the ratio of the minimum physical area to the area upstream of the orifice and ε is the ratio of the downstream area to the upstream area. The ratios ε_C, ε_T and ε are calculated using Equations (66), (67) and (68), respectively. Continuity allows v_2 to be determined from v_C, using Equation (69). [19]

$$\Delta P = \frac{1}{2}\rho\left(1 - \frac{\varepsilon}{\varepsilon_C \varepsilon_T}\right)^2 {v_2}^2 \tag{65}$$

$$\varepsilon_C = \frac{A_C}{A_T} \tag{66}$$

$$\varepsilon_T = \frac{A_T}{A_1} \tag{67}$$

$$\varepsilon = \frac{A_2}{A_1} \tag{68}$$

$$v_C = \frac{A_T v_T}{A_C} = \frac{v_T}{\varepsilon_C} = \frac{A_2 v_2}{A_T\, \varepsilon_C} = \frac{\varepsilon}{\varepsilon_T \varepsilon_C} v_2 \tag{69}$$

In the case of two-phase flow through an abrupt area change, RELAP models each phase similarly to the single phase, with additional considerations for the phase-specific flow area and the interphase friction. As depicted in Figure 16, the cross-sectional areas for the upstream volume, orifice, vena-contracta and downstream volume are divided between each phase by calculating for the phase volume fraction at each point. While wall friction, gravity and mass transfer are considered negligible through an abrupt area change orifice plate, the interphase drag cannot be neglected because the velocity difference gradient between the phases may be large at the orifice. Thus, the liquid and vapor velocity phases are governed by the phasic momentum equations provided in Equations (70) and (71) [19]

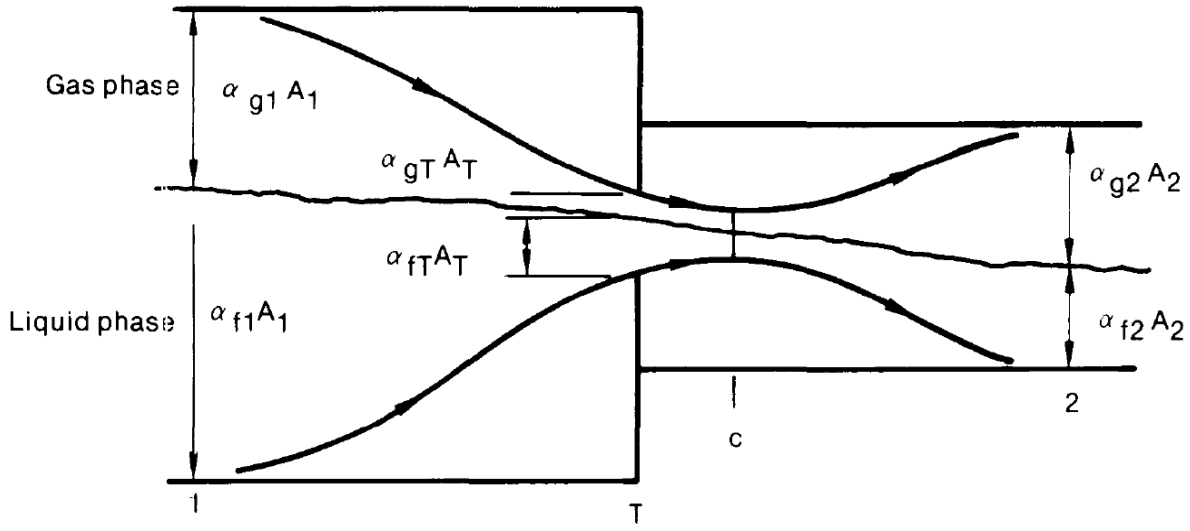

Figure 16: Schematic of Two-Phase Flow through an Abrupt Area Change (Reproduced from Ransom, V.H. et. al., 2011 [19])

$$\left(\frac{1}{2}\rho_f {v_f}^2 + P\right)_1 = \left(\frac{1}{2}\rho_f {v_f}^2 + P\right)_2 + \frac{1}{2}\rho_f \left(1 - \frac{\alpha_{f2}\varepsilon}{\alpha_{fT}\varepsilon_{fC}\varepsilon_T}\right)^2 {v_{f2}}^2 + \left(\frac{FI'}{\alpha_f}\right)_2 (v_{f1} - v_{g1})L_1 + \left(\frac{FI'}{\alpha_f}\right)_2 (v_{f2} - v_{g2})L_2 \quad (70)$$

$$\left(\frac{1}{2}\rho_g {v_g}^2 + P\right)_1 = \left(\frac{1}{2}\rho_g {v_g}^2 + P\right)_2 + \frac{1}{2}\rho_g \left(1 - \frac{\alpha_{f2}\varepsilon}{\alpha_{gT}\varepsilon_{gC}\varepsilon_T}\right)^2 {v_{g2}}^2 + \left(\frac{FI'}{\alpha_g}\right)_2 (v_{g1} - v_{f1})L_1 + \left(\frac{FI'}{\alpha_g}\right)_2 (v_{g2} - v_{f2})L_2 \quad (71)$$

where L_1 and L_2 are the lengths from points 1 and 2 to the orifice.

The interphase drag, *FI'*, is calculated from the interphase friction force per unit volume using Equations (72) and (73) [20], for the upstream and downstream volumes. Also, the ratio between the ratio of the minimum physical area to the area upstream of the orifice for the liquid and vapor phases is calculated using Equations (74) and (75), respectively. [19]

$$FI' = \alpha_f \alpha_g \rho_f \rho_g FI \quad (72)$$

$$FI = \frac{FIF + FIG}{\rho_m} \tag{73}$$

$$\varepsilon_{fT} = \frac{\alpha_{fT}}{\alpha_{f1}} \varepsilon_T \tag{74}$$

$$\varepsilon_{gT} = \frac{\alpha_{gT}}{\alpha_{g1}} \varepsilon_T \tag{75}$$

III. Model Development and Parametric Analysis

The first challenge of this project was to understand how RELAP5/MOD2 worked, which was accomplished by developing a basic model of the OTSG downcomer, with which individual model runs could be conducted and the model output could be analyzed. Once a basic model was developed, a FORTRAN shell program was developed that enabled the user to conduct parametric analysis of the OTSG downcomer model.

3.1: RELAP OTSG Downcomer Model Development

In understanding how RELAP5/MOD2 worked, individual runs modeling the OTSG downcomer were conducted, using a single, individually made input file. These individual runs were developed using data retrieved from the Oconee I FOAK report, along with OTSG downcomer dimensions that were found on blueprints that had been provided by Areva, Inc. As the majority of operation of the downcomer takes place at 95% power, the model was developed primarily with that power level in mind, and most model runs were conducted at that power level.

With several different options available for modeling different components of the OTSG downcomer, the first step was to develop a basic model of the downcomer that could be used to test the different slug drag parameters. A schematic of the basic model is provided in Figure 17, detailing the cross sectional area and lengths of the relevant volumes to the model. The volumes that are only 0.00750 long correspond to points in the downcomer where pressure taps had been placed in the FOAK report, and are used to analyze for the pressure profile produced by RELAP5.

Per the RELAP5/MOD2 Manual, a time dependent volume is necessary to establish the boundary conditions of any system. Thus, the inlet conditions of the aspirating steam and

feedwater, along with the exit conditions of the mixture were set by the conditions of the time dependent volumes at those points. For the steam source, the pressure was set to the corresponding pressure determined in the Oconee FOAK Report for the given power level, with an assumed quality of 1. The feedwater source had a default pressure of 925 psi in all cases while the temperature was set to the temperature measured at each power level in the FOAK data. For the time dependent volume that represents the tube nest, the pressure was set to the exit pressure determined by the FOAK data, with a correction for hydrostatic pressure difference between its center height and the pressure tap 6 inches above the LTS. The quality was set to 0, and adjusted through an iteration of model runs until the difference in static quality between two consecutive runs was less than 0.1%.

In RELAP5/MOD2, the velocity or mass flow rate is set at the junctions between volumes. Since the FOAK report only contained flow rate data and no velocity data to benchmark the OTSG downcomer model, flow rates were provided to establish flow conditions. A time dependent junction was used to regulate the flow of feedwater into the feedwater nozzle. At 95% power, the liquid flow rate was set to 1433.33 lb_m/s, and proportionally decreased for lower power levels, while the vapor flow rate was set to 0 lb_m/s. A single junction was used for the aspirating steam, with an initial mass flow rate equal to the amount of saturated steam that when mixed with the subcooled feedwater, would produce saturated liquid water, and was adjusted for each power level. As a single junction, RELAP could adjust the steam flow rate according to its calculations of the downcomer. The combined mass flow rate of the steam and feedwater was used to determine the mass flow rate into the tube nest, initially assuming that the total mass flow rate was saturated liquid. When the static quality of the tube nest time dependent volume was adjusted, the mass flow rate for the liquid and vapor was adjusted accordingly.

The pipe of the feedwater nozzle was set to a arbitrary length of 0.5 ft, while the area of 0.391 was selected based on the total area of the nozzle plates of the 32 feedwater nozzles entering the downcomer. The area for the feedwater inlet into the downcomer mixing section was set to 0.0200, in accordance with the total area of the all feedwater nozzle holes entering the downcomer. FOAK data showed that at 95% power, the pressure buildup in the feedwater nozzles was 5.24. A parametric study with RELAP showed that the junction for the feedwater entering the mixing section had an equivalent energy loss factor of 0.7.

There were many options for modeling the mixing section of the downcomer. The length of the mixing section was set by the distance between the feedwater nozzles and the first pressure tap in the FOAK data. Based on the information provided in the RELAP5/MOD2 manuals, the jet mixer was assumed to be the more appropriate component for the mixing section, as the jet mixer was designed to model the merging of two flows, where one inlet would have fluid entering at a much higher velocity than the other. However, in practice with RELAP, this proved not to be the case.

In the FOAK report, it is concluded that the liquid-vapor mixture achieved thermodynamic equilibrium within 6 feet of the feedwater nozzle. Within RELAP there exists an option that allows equilibrium to be forced upon the steam/water if the user chooses. Model runs with equilibrium off showed that the water that reached the exited the downcomer was below its saturation temperature by at least 30°F. Thus, in order to correctly model the downcomer, the forced equilibrium option was turned on.

There were no issues with the jet mixer when equilibrium was not forced, but in model runs where the equilibrium was forced and the jet mixer was used to model the mixing section, RELAP usually became unstable. Water property errors, where RELAP determines the pressure

in a given volume is such that RELAP cannot determine the other thermodynamic properties, would occur and cause the model run to fail before completing a full model run. The one-dimensional branch connection proved to be a more stable component under those conditions, and was chosen over the jet mixer for that reason.

The main body of the downcomer was modeled as an annulus with volumes of varying lengths. The volumes that are only 0.0075 long shown in Figure 17 are centered at the FOAK pressure tap points, while the volumes of varying length represent the distances between each point, with 0.00375 taken from each side to account for the volumes at the pressure taps. As part of the parametric analysis of the downcomer model, the volumes between the pressure taps were broken up into smaller parts, as part of a study on the spatial resolution of the downcomer model, which is further discussed in Section 4.3.

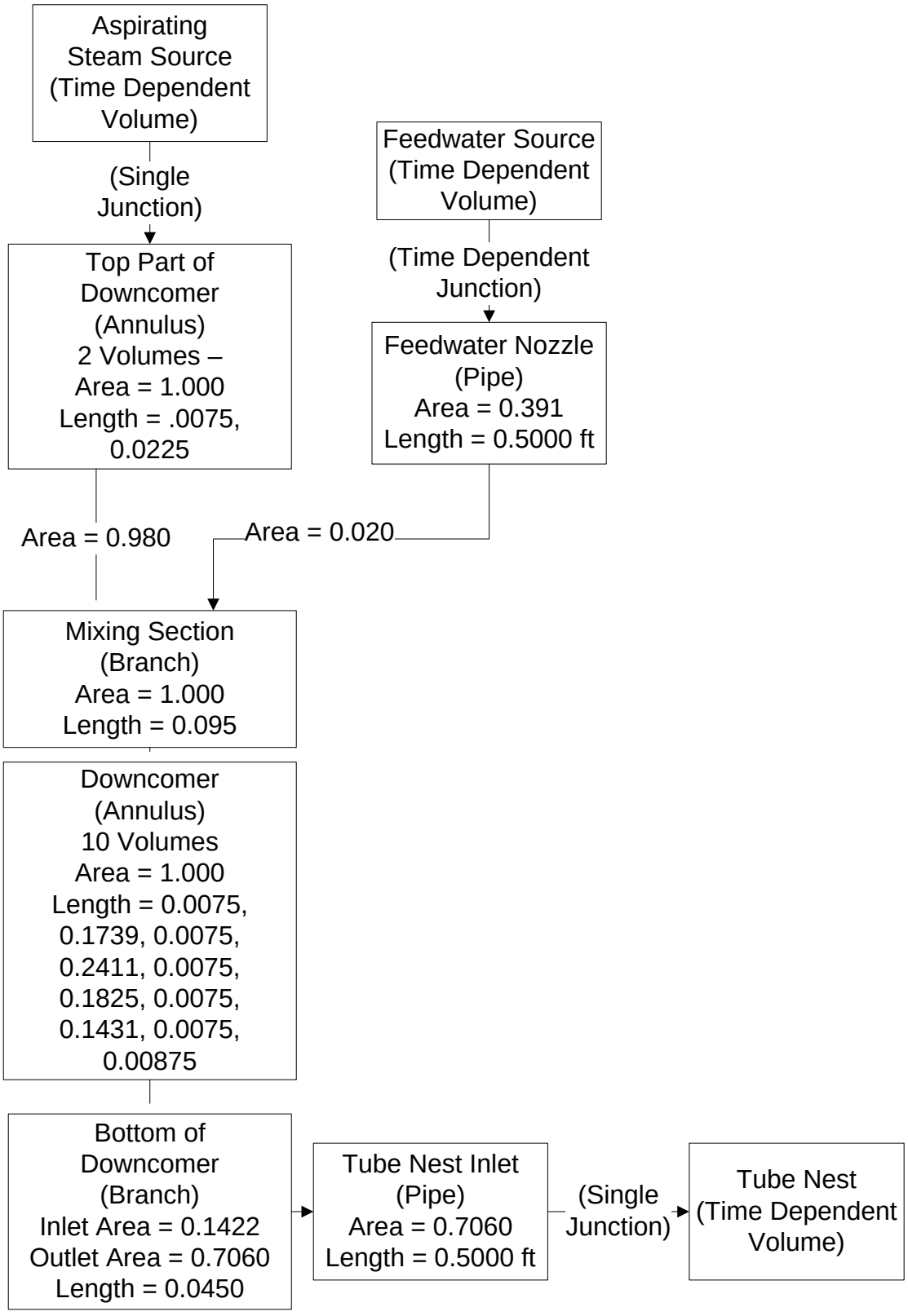

Figure 17: Schematic of the Basic RELAP5/MOD2 Downcomer Model

Several challenges were presented with modeling the orifice plate, along with the bottom portion of the downcomer. Early in the development of the downcomer model, the orifice plate was modeled as a simple single junction, with the appropriate cross sectional area, followed by the continuation of the annulus to the LTS. Early experiments assumed the orifice was an abrupt area change, with later model runs focusing on a smooth area change and different energy loss factors. In reality, the orifice plate is not a simple thin plate, but rather a system of three components that restrict the flow to an area less than that of the downcomer annulus. A finite volume design for the orifice plate that varied the cross-sectional area for each component was developed. With the correct energy loss factors, both models were able to match the pressure change caused by the orifice plate in the FOAK report.

As RELAP is a one-dimensional program, flow into the tube nest provided an additional complication to modeling the region below the orifice plate. In order to turn the flow from downward to horizontal, a branch connection needed to be used instead of a pipe or annulus. Flow out of the branch connection could not be split into several paths and then re-entered into a solitary tube nest volume easily, so the section below the orifice plate was modeled as a single branch connection. This is important because the pressure within a volume is determined at its central height, and the pressure rise below the orifice plate is greater than the pressure decrease caused by the orifice plate.

Since a volume could not be placed with its center at 0.0150 above the LTS, the pressure at that height had to be derived from a pipe placed between the branch and the tube nest time dependent volume, with a center height of 0.0469 above the LTS. Using the flow regime and density for the pipe, a density profile was determined allowing for the hydrostatic pressure difference between 0.0469 and 0.0150 above the LTS to be added to the pipe's pressure. In all

cases, the flow regime in the pipe was either slug or bubbly flow, and the density was assumed to be uniform throughout the pipe, however there was consideration in the calculated given in the event the flow regime was stratified.

The final design for the bottom of the downcomer called for a branch connection with the inlet junction serving as the orifice plate and the outlet junction normal to the vertical plane, allowing for horizontal flow into the tube nest. The pressure in the RELAP model data to be compared to the pressure tap 0.0150 above the LTS was calculated using the centerline pressure in the tube nest inlet pipe, along with the flow regime and the density data within the pipe.

3.2: FORTRAN Shell Program

To determine which parameters produced the most accurate representation of the downcomer, a FORTRAN program was written that could automatically write input files for RELAP and then run the RELAP executable file. As the study progressed, several capabilities were developed for the shell program, beginning with the ability to read data from chosen files, write RELAP input files, run RELAP model runs and perform basic analysis on those model runs. With further modifications, additional capabilities were added to the program, such as the ability to recognize whether a water property error had occurred in a model run, identifying the set of input parameters at which the system achieved a desired state, and re-running the model until that desired state was achieved. A schematic diagram of the shell program has been provided in Figure 18.

With the version of RELAP5/MOD2 made available by Areva, Inc., RELAP model runs outputted minor edit data to tables in text files. Using this output, a subroutine was developed that would be able to read the minor edit output files, allowing for automated analysis of many

key parameters. For example, the minor edit file that included pressure data for selected nodes within the downcomer was used to determine whether the model had achieved steady state, at what point in the model run that steady state was achieved and how well the pressure profile matched that of the FOAK data, which was summarized using a least squares difference between the FOAK data and the corresponding model data. Other parameters, such as flow regime, static quality, void fraction, liquid and vapor density, and liquid and vapor velocity were also analyzed, providing insight to the phenomena that RELAP modeled.

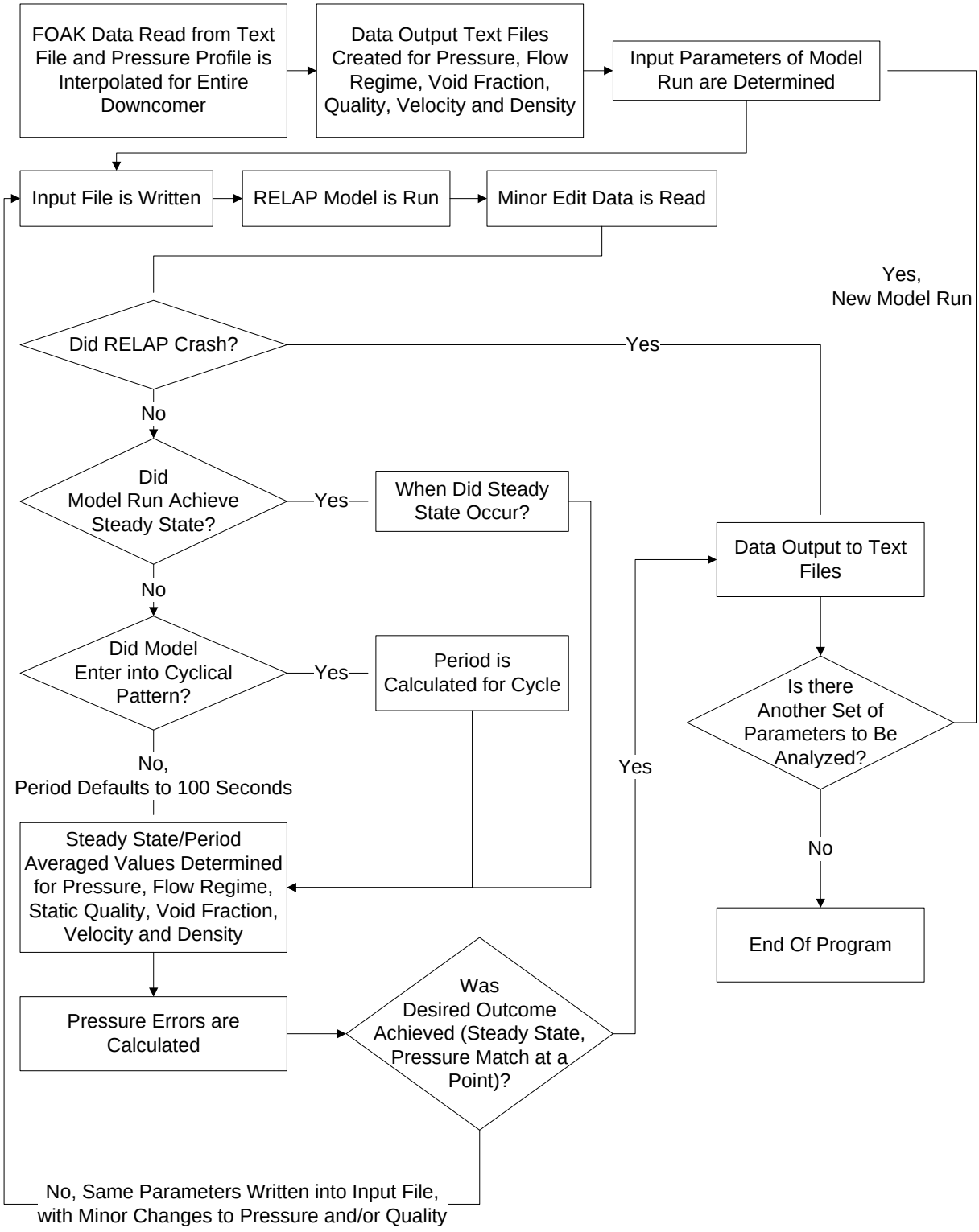

Figure 18: Schematic Diagram of FORTRAN Shell Program

In the input file, the pressure was specified at the inlet of the feedwater and the aspirating steam, as well as at the outlet of the downcomer, which would represent entrance into the tube bundle of the OTSG. However, as the majority of data made available for the downcomer was above the orifice plate, it was considered most important that the pressure above the orifice plate in the model data matched that of the FOAK data. Since the pressure above the orifice plate could not be specified, pressure at the outlet had to be assumed and corrected so that the pressure at the orifice plate would match the FOAK data. This was done by running an initial model run with assumed values for pressure based on FOAK data, and then running subsequent runs with "corrected" pressure input data from the previous run to achieve a pressure match at the orifice plate.

Only when the model had achieved the desired pressure at the orifice plate, was the data from the model run recorded to several text files, which then could be imported into a spreadsheet for analysis. Afterwards, the program would move on to the next value of a given parameter to be tested, repeating the process of writing a new input file, running the RELAP executable for the input file, reading the output, re-writing a corrected input file based on the output before writing the final data to a text file.

In order to find results for individual model runs, the program was modified to run for a single set of parameters, and to match the pressure at the orifice plate with what had been observed in the FOAK data. For analysis of the individual runs, the data was taken at the model time of 900 seconds, regardless of whether the pressure profile in the model had achieved steady state (pressures at all nodes were constant for at least 5 seconds) or not. In most cases, pressure fluctuations within the downcomer were varying by only ± 0.011% for a given node when the model reached a run time of 900 seconds.

3.3: Parametric Analysis

In studying the different parameters, the first set of comparisons drawn was comparing the INEL model to the default B&W modified slug drag model and the default Wilson slug drag model. As the INEL model does not provide any options for modifying the model, no further study was conducted with the INEL model after this point, while numerous parametric studies could be set up with the B&W and Wilson models. The B&W model was emphasized over the Wilson model due to easier comparison with the INEL model and the interphase drag could be modeled in relation to a single factor.

Research with the B&W slug drag model focused on the interphase friction model coefficient, M_{st}, which as Equations (49) through (52) would suggest, is the most sensitive parameter of the B&W slug drag model. Adjustments to M_{st} were made by adjusting the slope factor, *xslg*, while the x-intercept value, *cxslg*, is held constant at its default value of 0.1109. Values of M_{st} are given with an assumed volume pressure, P_{vol}, of 925 psi.

Initial parametric studies for the M_{st} values were run assuming an orifice plate energy loss factor of 0.90. The best-fit M_{st} was determined by finding a least squares pressure error for the pressure taps above the orifice plate compared to the FOAK data, using Equation (76), where RP is the relative pressure, and the relative pressure for the pressure taps at 0.8750, 0.6936, 0.4450, 0.2550 and 0.1044 above the LTS are used.

$$Error = \sqrt{\sum (RP_{RELAP} - RP_{FOAK})^2} \tag{76}$$

Once the best-fit M_{st} value was determined for each power level, a parametric study was conducted to determine the best orifice plate loss factor, K_L, for each power level, given the previously determined M_{st} values. From this series of model runs, a best fit orifice plate energy loss factor was determined for all power levels, and a second parametric study of the M_{st} values

was run to determine the best M_{st} value for each power level. This second parametric study of M_{st} also determined the best M_{st} value for all power levels and developed a function that may help predict the best M_{st} value for power levels exceeding 95% power. The reason for not conducting a simultaneous parametric study of both was because M_{st} helps determine the pressure gradient and void fraction above the orifice plate, affecting the pressure change across the orifice plate. The second parametric study for M_{st} was to ensure that the usage of a best-fit orifice plate energy loss factor did not significantly impact the optimal M_{st} values,

As the model for the downcomer that was depicted in Figure 17 provided what was considered to be a very coarse spatial resolution of the downcomer, a parametric analysis of the spatial resolution was needed to ensure that the results at the presented resolution would not significantly change if the size of the volumes between the pressure tap volumes changed. Thus, the large volumes of the downcomer were broken into 8 volumes to determine the effects of resolution on the downcomer model, using the optimum M_{st} and orifice plate loss factors.

Once the integrity of the spatial resolution of the model had been determined, a parametric study was conducted varying the pressure rise between the aspirator port and the LTS, and compared to the void fraction at the orifice plate and at FOAK data point above the orifice plate (0.1797 above the LTS). This study was conducted to help understand the interaction between the downcomer and the tube nest on the interior of the OTSG, which was otherwise neglected for the sake of simplicity in this study.

Finally, in an effort to predict what may happen at power levels exceeding 95%, a parametric study was conducted ranging for power levels ranging from 105% to 145%, which would be useful towards the development of the EOTSG model. Similar to the previously mentioned study, the overall pressure rise was varied, and compared to the void fraction at both

the orifice plate and at 0.1797 above the LTS. While the FOAK report does not include any data with which these results could be compared, the pressure rise over the downcomer was extrapolated to the higher power levels to provide estimates of what pressure difference would be between the aspirator ports and the LTS.

IV. Results

Results from each of the parametric studies are presented in the following sections. Unless otherwise stated, the results are taken from the data output text files that have been created using the minor edit data provided by RELAP. If the model run did not achieve steady state, the shell program calculated the mean average value over the final 100 seconds of the model run, along with the high and low values over that time period. Thus, for data points that did not converge to steady state, the mean average value is shown with error bars showing the range over the final 100 seconds. For pressure profiles, error data for the point at 0.0150 above the LTS was not calculated, as the pressure is fixed by the shell program.

4.1: Comparing the Default Slug Drag Models

The INEL slug drag model is the default model in RELAP5/MOD2, and is the original model for calculating slug drag that was programmed into RELAP by INEL. Using the downcomer model with the INEL slug drag calculation provides an initial benchmark with which the B&W Modified Slug Drag Model and the Wilson Slug Drag Model can be compared. For all model runs showing the B&W Modified Slug Drag Model, all parameters are set to their default value given in Section 2.5.4 (i.e. M_{st} = 0.2718). The default value for all Wilson Slug Drag Model multipliers is 1.

4.1.1: 95% Power

In Figure 19, the relative pressure profile at 95% power for each model run is compared to the FOAK data for Oconee Unit I, while Figure 20 shows the corresponding void fraction ratio profiles. None of the three models converged to a steady state, and the range that the values varied over the last 100 seconds of the model run has been depicted. Even in the last 100

seconds of a 900 second model run, there appears to be a wide fluctuation in the pressure profile, particularly at the nodes closer to the top of the downcomer, where the momentum of the feedwater ejecting from the nozzles may be playing a role in the pressure profile. None of the model runs accurately predicted the pressure profile, as all model runs under-predicted the pressure rise in the higher sections of the downcomer. As the void fraction ratio profile shows, RELAP over-predicted the amount of vapor in the higher regions of the downcomer, before a sharp drop off occurred, and RELAP under-predicted the void fraction ratio in the lower downcomer. According to RELAP, the flow regime is mist flow at 1.000 above the LTS, and slug flow in the upper sections. At 0.445 above the LTS, the INEL and Wilson models are in the slug flow regime, while the B&W model has switched to bubbly flow, which all models show to be the flow regime in the lower sections. It appears that RELAP is predicting a liquid level at 0.445 above the LTS, but almost a quarter of the volume below the liquid level is vapor rather than liquid. While this may be the case in some real-world scenarios, it is clearly not the case with the OTSG downcomer, based on comparisons to the FOAK data.

The abundance of vapor in the upper regions of the downcomer, and lack thereof in the lower regions indicates that vapor is being insufficiently dragged downward by RELAP in all three models. As discussed in Section 2.5.3, all previously known studies with RELAP5/MOD2 indicated RELAP over-predicted, not under-predicted, interphase friction. However, the OTSG downcomer model is an adiabatic model, and Putney and Preece [18] indicated that in the unheated region of the riser of the steam generator the INEL slug drag model under-predicted interphase friction because RELAP expected the Taylor bubbles to attain an unstable diameter equal to that of the circular channel. In the downcomer annulus, RELAP would model a Taylor bubble as if it were in a pipe of equivalent hydraulic diameter. In reality, there are more likely to

be several Taylor bubbles around the downcomer, with a diameter closer to the distance between the inner and outer walls of the downcomer, with a greater interfacial area than RELAP would predict.

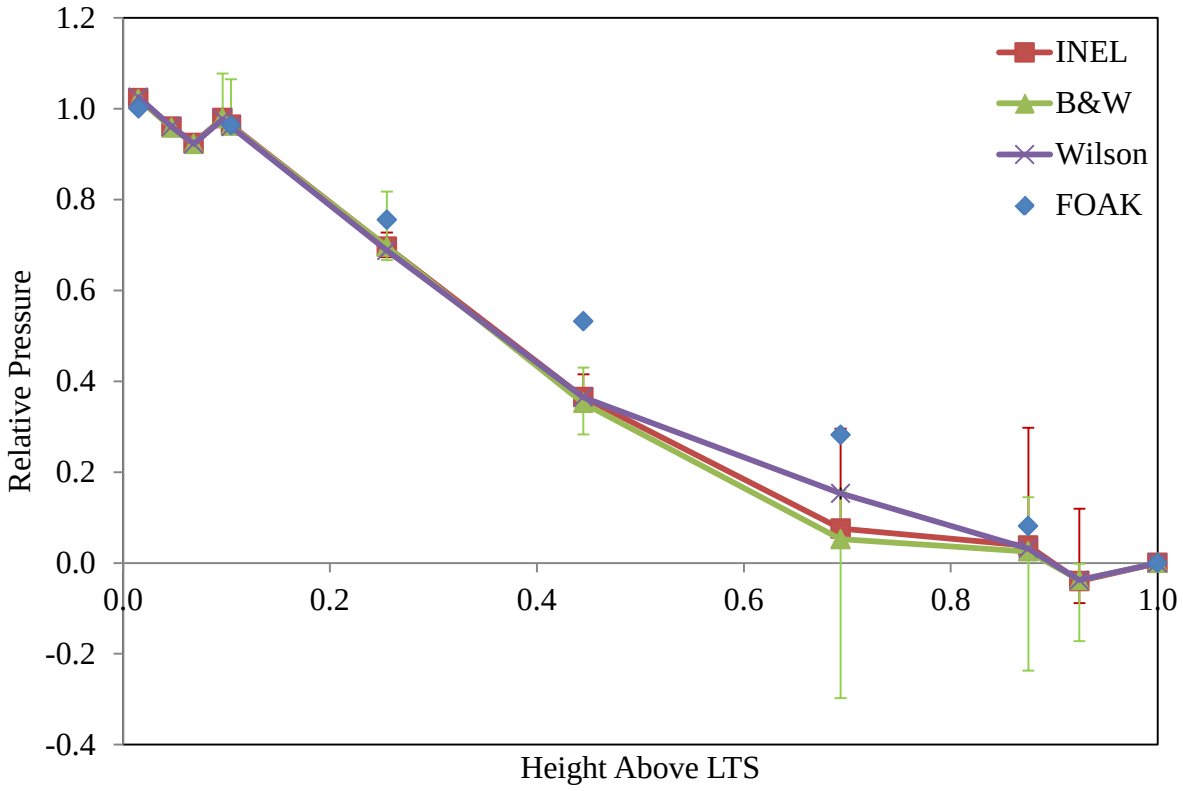

Figure 19: Relative Pressure Profile at 95% Power for the Default Slug Drag Models

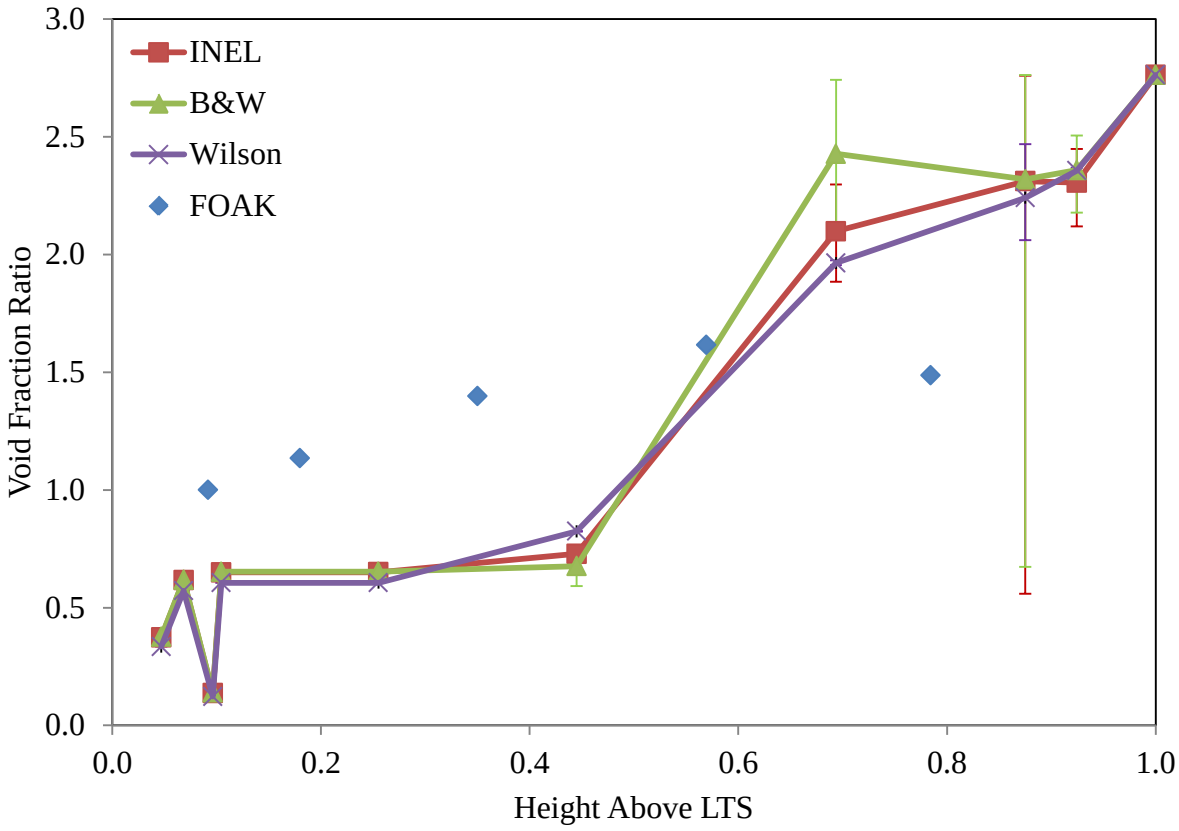

Figure 20: Void Fraction Ratio Profiles at 95% Power for the Default Slug Drag Models

4.1.2: 85% Power

Figure 21 and Figure 22 show the relative pressure and void fraction ratio profiles for each slug drag model at 85% power, respectively. At 85% Power, the discrepancy between the relative pressure profiles of the Wilson model versus both the INEL model and the B&W model is more noticeable than at 95% power. As the void fraction ratio profiles indicate, the Wilson is dragging down more vapor than the INEL and B&W models, which creates a more even density profile, and in turn a more consistent relative pressure profile over the downcomer. The flow regime data from RELAP indicates that the INEL and B&W models switch from slug to bubbly flow at 0.2550 above the LTS, while the Wilson model stays in the slug flow regime until the volume immediately above the orifice plate. The INEL and B&W models suggest a liquid level

at 0.2550 above the LTS, with very little vapor below that point. In the Wilson model, there appears to be a slug flow liquid level at 0.2550 above the LTS that disagrees with the FOAK data.

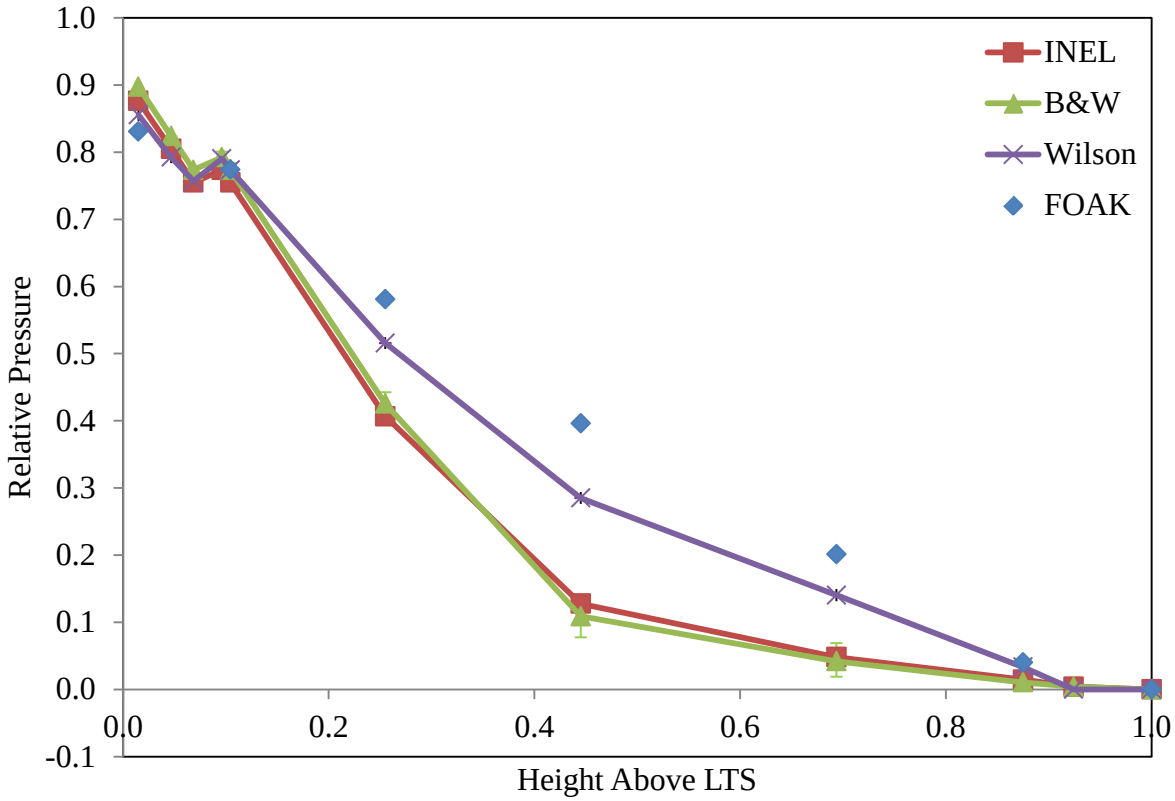

Figure 21: Relative Pressure Profiles at 85% Power for the Default Slug Drag Models

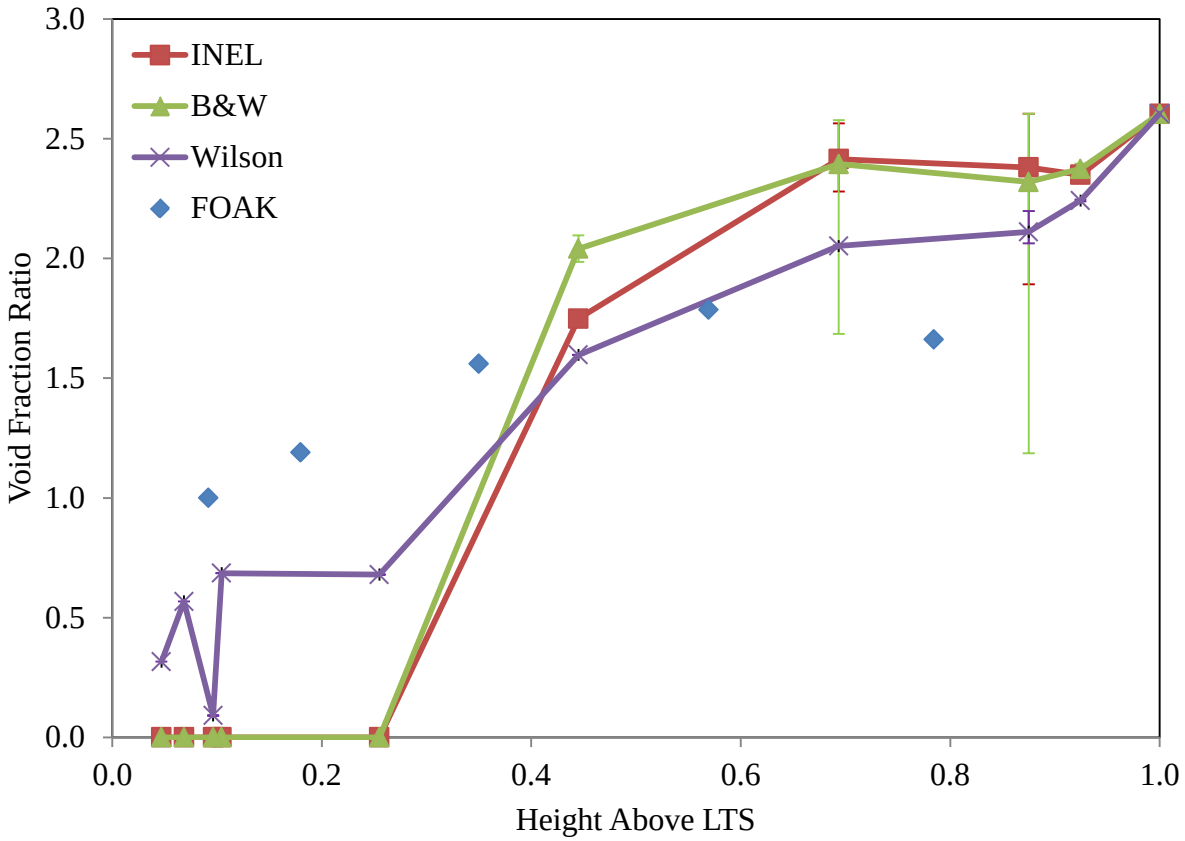

Figure 22: Void Fraction Ratio Profiles at 85% Power for the Default Slug Drag Models

4.1.3: 75% Power

Figure 23 and Figure 24 show the relative pressure and void fraction ratio profiles at 75% power, respectively. All three models over-predicted the amount of steam in the upper region of the downcomer, and under-predicted the amount of steam in the lower portion of the downcomer. Similar to the case with 85% power, all three models show the development of a liquid level at 0.2550 above the LTS, with the Wilson model indicating slug flow at 0.2550 above the LTS and bubbly flow at 0.1044 above the LTS. The disproportionate distribution of liquid and vapor indicates that the default models are under-predicting the interphase friction, as the liquid phase in the model is failing to drag the vapor phase down. Since there is more vapor in the upper region of the downcomer, the overall density will be less in the upper region and the pressure gradient will also be under-predicted in the upper region. However, with a deficit of

vapor in the bottom of the downcomer, the density is much higher than the FOAK data would have indicated, resulting in an over-predicted pressure gradient. If the interphase friction were to be increased, then the vapor should achieve a distribution more similar to that of the FOAK profile, and thus the pressure profile predicted by RELAP should also match the FOAK pressure profile.

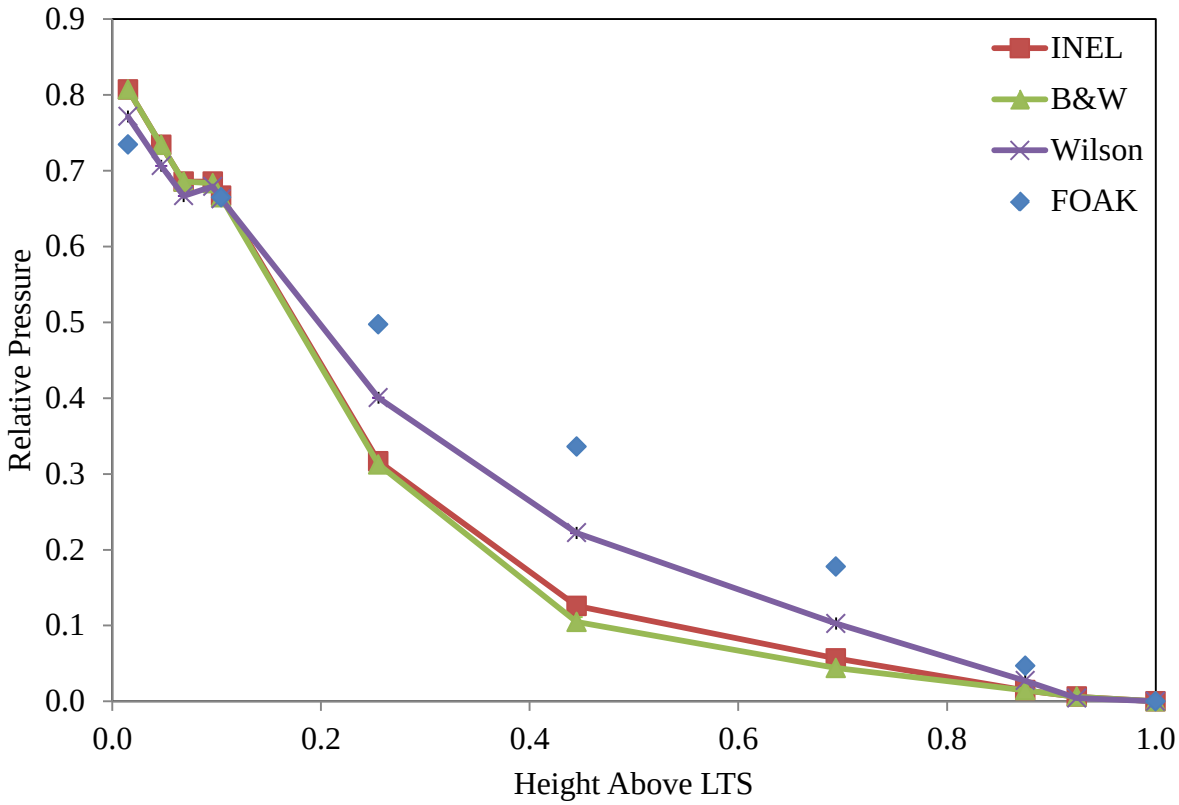

Figure 23: Relative Pressure Profiles at 75% Power for the Default Slug Drag Models

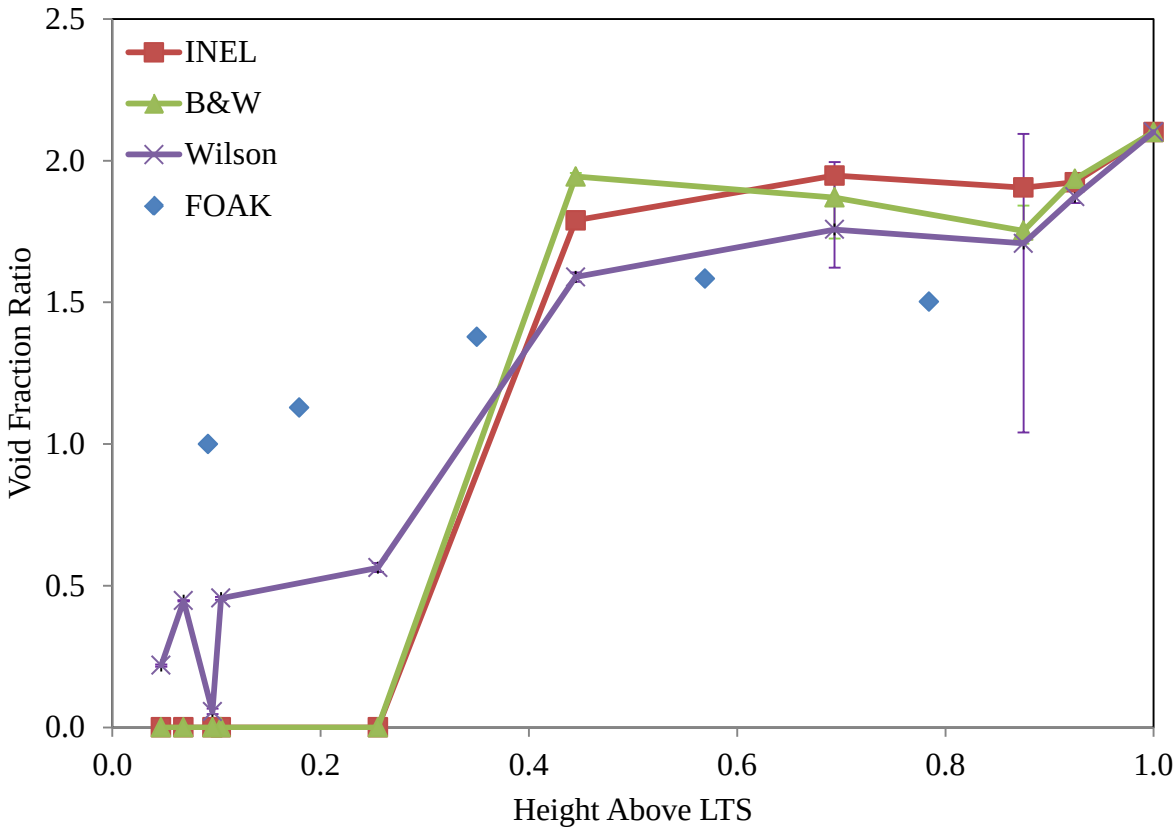

Figure 24: Void Fraction Ratio Profiles at 75% Power for the Default Slug Drag Models

4.1.4: 65% Power

At 65% power, the pressure profile seen in Figure 25 looks very similar to those seen at 95%, 85% and 75% power, with the pressure change in the lower part of the downcomer is much greater than the FOAK data indicates. However, the void fraction ratio profile shown in Figure 26, is much different, as the INEL and B&W models suggest a liquid level, with considerable vapor volume, at 0.2550 above the LTS. At that height, there is slug flow in the INEL model and bubbly flow in the B&W model, that contradict the FOAK data. The Wilson model indicates slug flow until it reaches its liquid level, with an insignificant amount of vapor carry-under at 0.1044 above the LTS. As is true at higher power levels, at 65% power there is insufficient interphase friction in the slug flow regime to drag the vapor to the lower portions of the downcomer, resulting in excess vapor at the top and excess liquid at the bottom. In turn, the

density is under-predicted at the top of the downcomer and over-predicted at the bottom. This results in the pressure gradient at the top is under-predicted while it is over-predicted at the bottom, which is balanced by RELAP to achieve the desired pressure change over the downcomer.

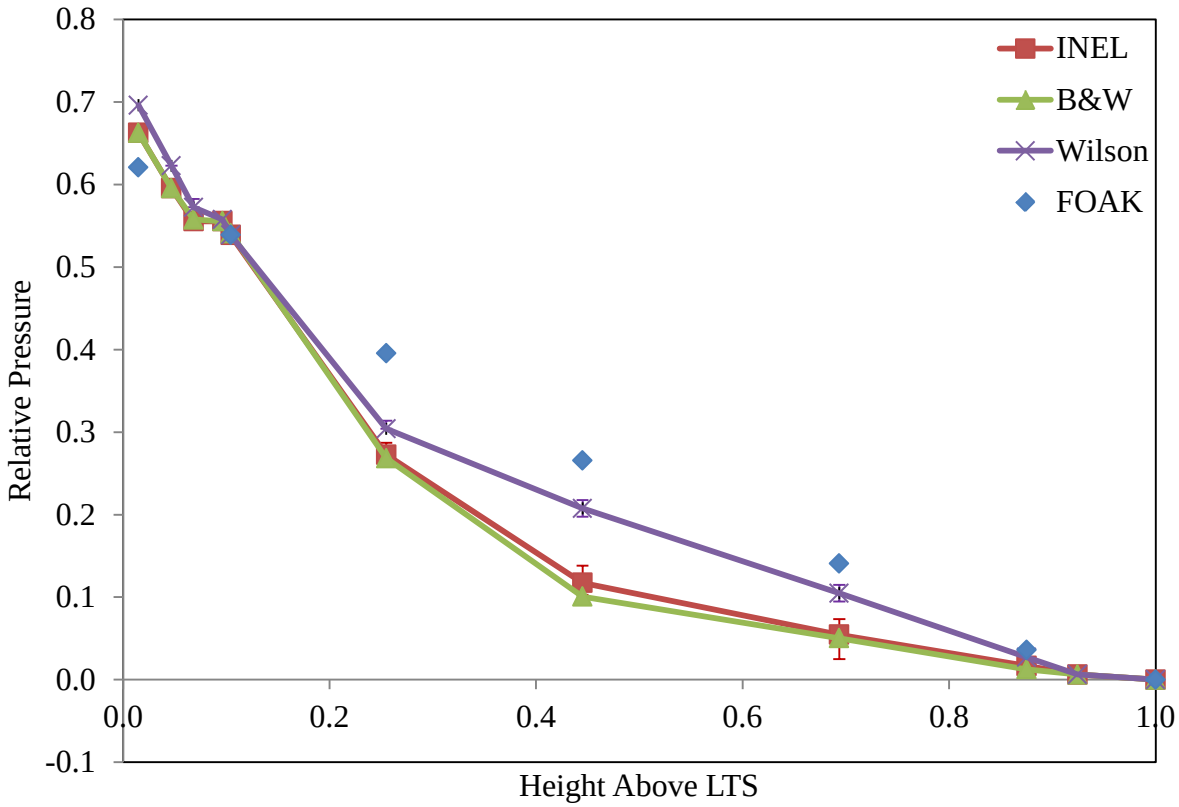

Figure 25: Relative Pressure Profiles at 65% Power for the Default Slug Drag Models

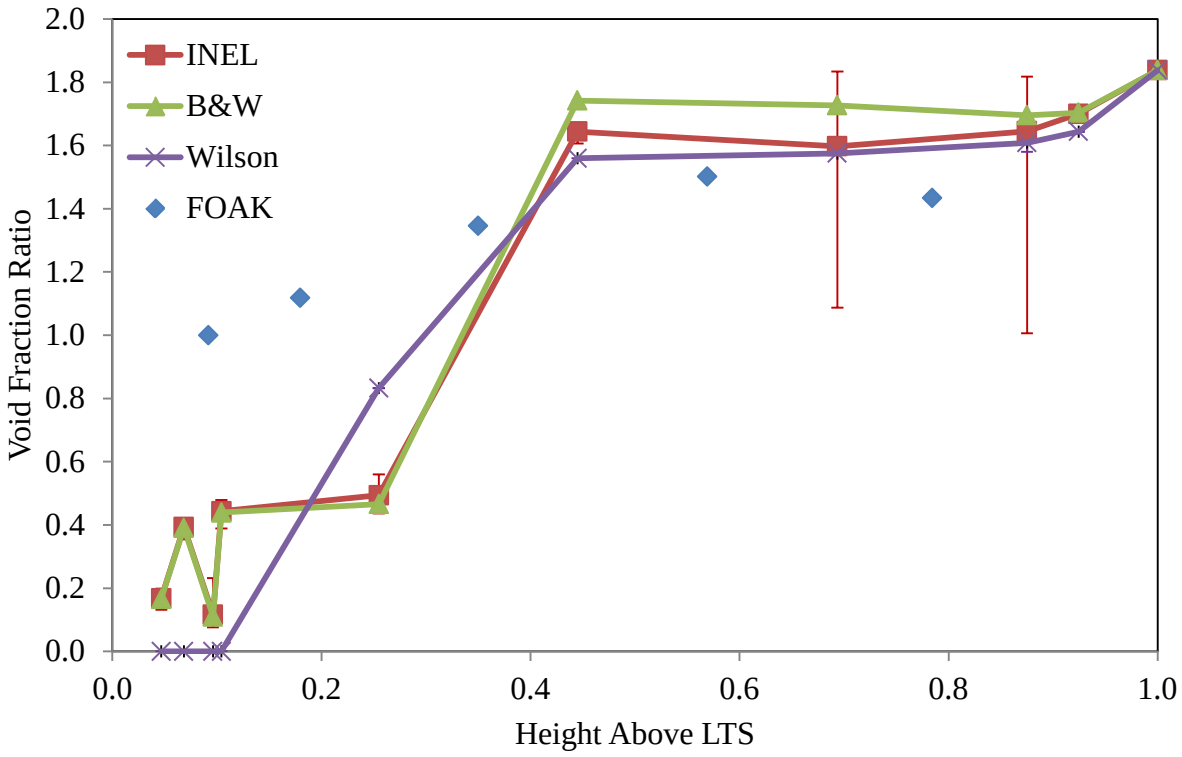

Figure 26: Void Fraction Ratio Profiles at 65% Power for the Default Slug Drag Models

4.1.5: 55% Power

At 55% power, the trend of under-predicted pressure gradient at the top of the downcomer, with over-predicted pressure gradient at the bottom of the downcomer is consistent with that seen at higher power levels, as shown in Figure 27. Similarly, the void fraction ratio profile at 55% shown in Figure 28 indicates that there is a lack of slug flow interphase friction in the system, with excessive vapor in the slug flow in the upper portions of the downcomer. One difference from higher power levels is the common liquid level seen at 0.1044 above the LTS amongst all three models, with little vapor carry-under.

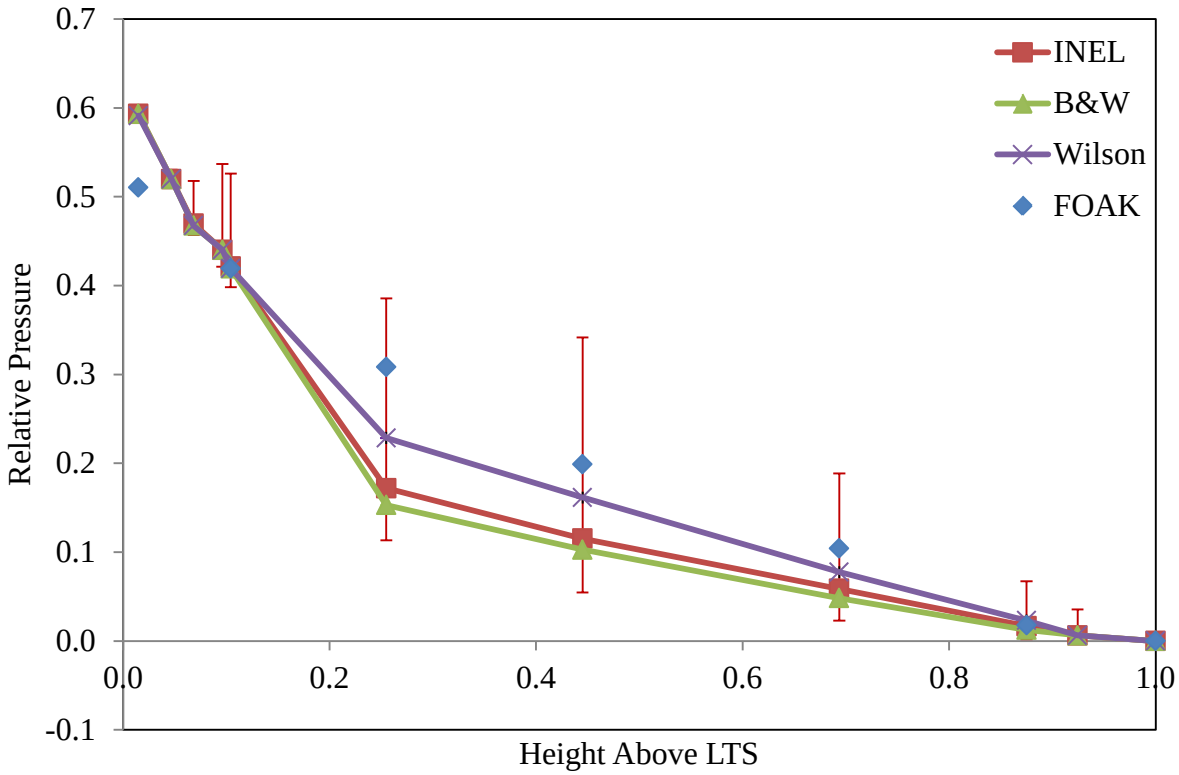

Figure 27: Relative Pressure Profiles at 55% Power for the Default Slug Drag Models

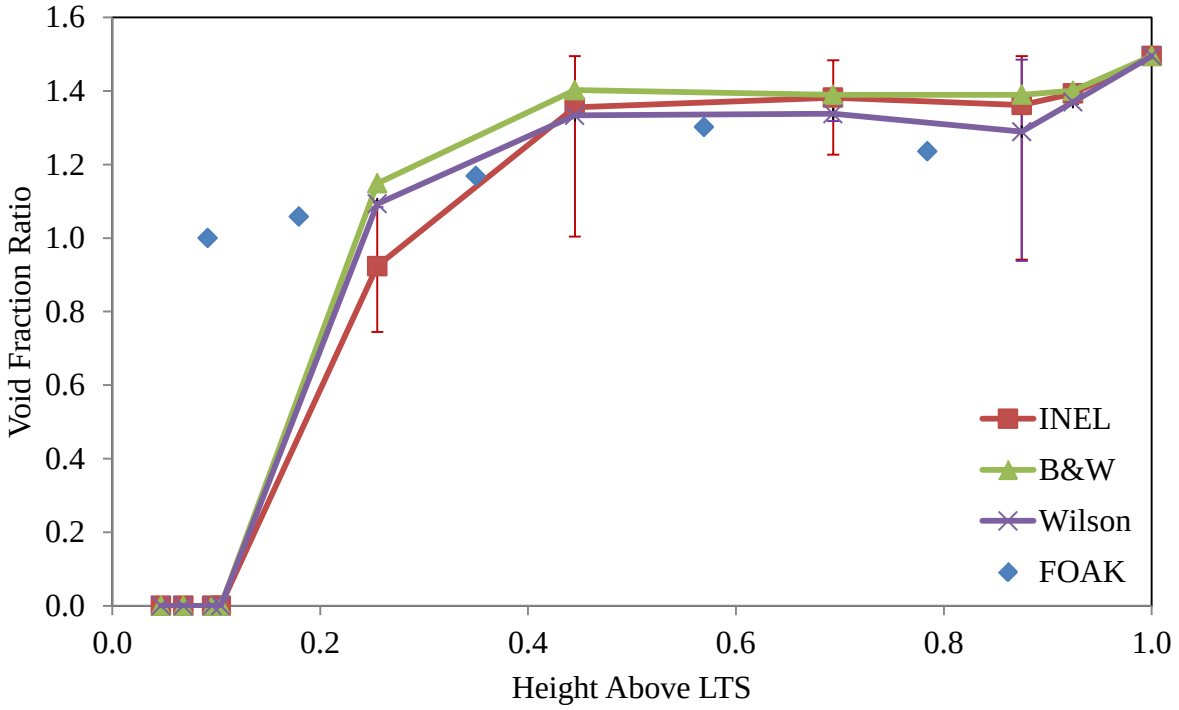

Figure 28: Void Fraction Ratio Profiles at 55% Power for the Default Slug Drag Models

4.1.6: 45% Power

At 45% power, the models show a much closer approximation to the pressure profile that has been observed at higher power levels. Figure 29 suggests a close approximation of the pressure gradient in the INEL and B&W models between the aspirator ports at 1.0000 above the LTS and the pressure tap at 0.4450 above the LTS, while the Wilson model closely mirrors the relative pressure profile from the aspirator port to the orifice plate at 0.0919 above the LTS, with the largest difference in relative pressure occurring at 0.2550 above the LTS at 0.0147. In the void fraction ratio profiles shown in Figure 30, all three models indicate a liquid level with very little vapor carry-under at 0.1044 above the LTS, with excessive vapor above the liquid level. As is the case with higher power levels, this indicates that the interphase friction is insufficiently dragging the vapor down where slug flow is the predominant flow regime.

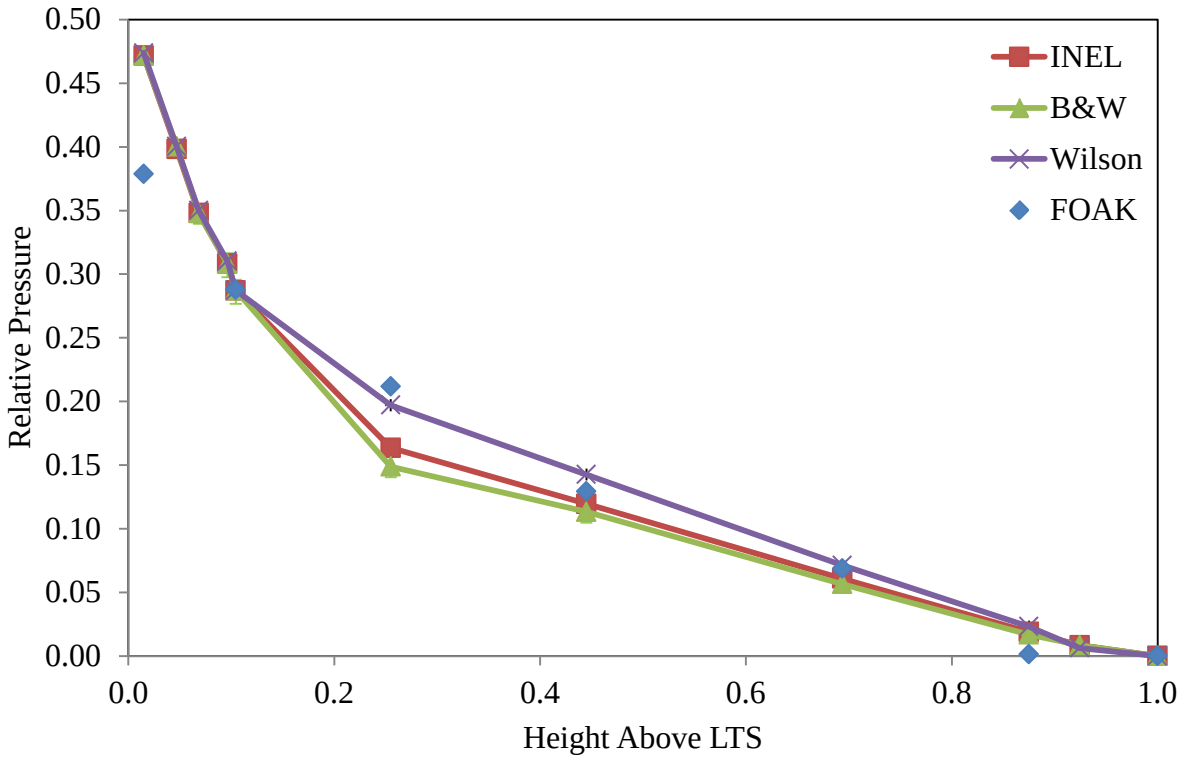

Figure 29: Relative Pressure Profiles at 45% Power for the Default Slug Drag Models

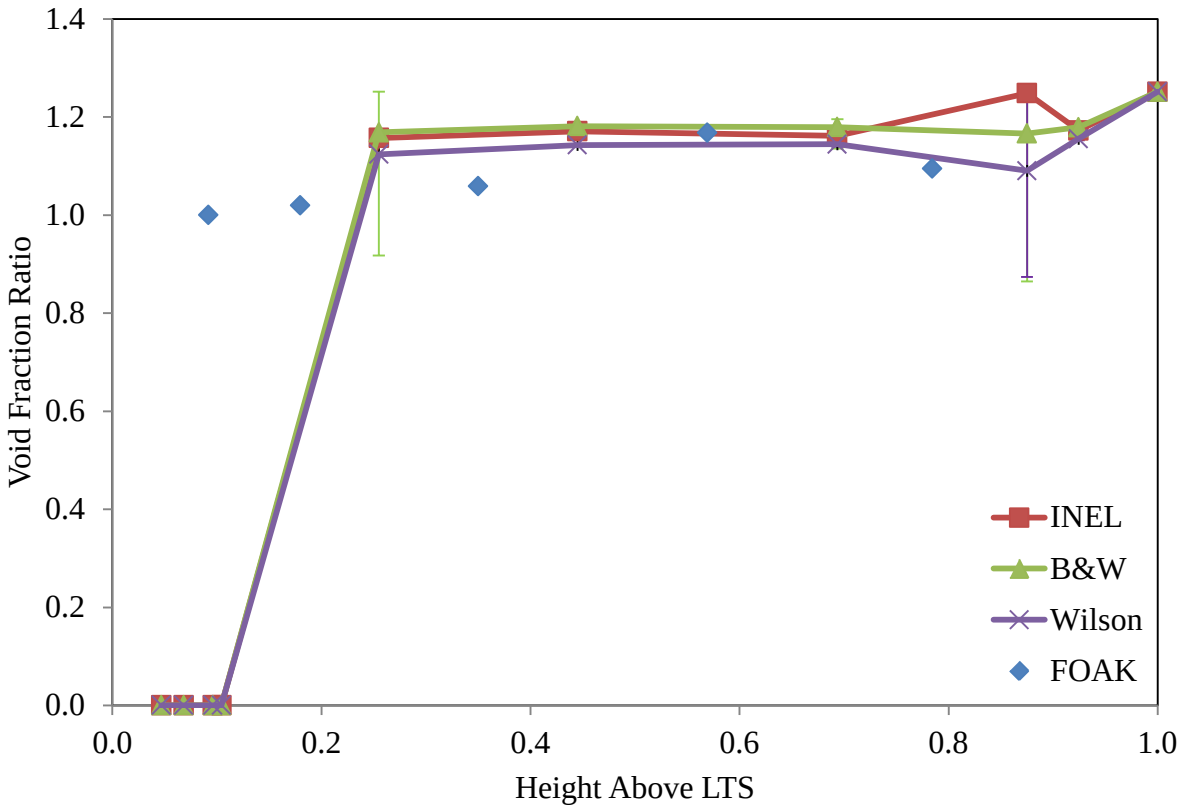

Figure 30: Void Fraction Ratio Profiles at 45% Power for the Default Slug Drag Models

4.2: Optimizing the Pressure Profile

As discussed earlier, the leading cause for the pressure profiles to be modeled incorrectly related to an under-prediction of the interphase friction between the liquid and vapor phases in the OTSG downcomer. Previously, a drift flux velocity was proposed to adjust the interphase friction, however, that was done to decrease the interphase friction in scenarios where it had been over predicted. [1,3,4,9,10,17,18,25] The version of RELAP5/MOD2 provided by Areva, Inc. contained two different options for adjusting the interphase friction by adding coefficients to the calculation of the friction factor, rather than adjusting the velocity. Those options were the B&W modified slug drag model and the Wilson slug drag model.

While the default Wilson model provided relative pressure and void fraction ratio profiles for the downcomer that more closely resembled those of the FOAK data, the B&W modified slug drag model was chosen to be studied more extensively, as it could be better correlated to the original INEL slug drag model. As stated earlier, parametric studies focused on the interphase friction model coefficient, M_{st}, as increases in M_{st} would also increase the interphase friction and the value of M_{st} could be easily adjusted between model runs in the RELAP input file. There was not enough data to suggest that changing any other parameters within the B&W modified slug drag model would affect the interphase friction between the vapor and liquid phases. Nonetheless, parametric studies were conducted to see if there was any impact on the downcomer model, only to find that no consistent pattern could be determined that would improve the interphase friction prediction. Thus, all other parameters for the B&W modified slug drag model were held constant at their default values.

4.2.1: Varying M_{st}

4.2.1.1: 95% Power

To determine the best M_{st} value to be used for the B&W modified slug drag model, a series of model runs were conducted, where the least squares pressure error for the downcomer was calculated for the pressure taps above the orifice plate. Figure 31 shows the least squares pressure error for a series of M_{st} values ranging from 0.2718 (the default value) to 22.4532, when the downcomer is operating at 95% power. The chart indicates whether the model runs did or did not converge to steady state. As the figure shows, the least squares error in the pressure profile decreases rather dramatically with increasing M_{st} from an error of 0.2947 at M_{st} = 0.2708, to a minimum error of 0.0306 is achieved at M_{st} = 5.1517. Then the error only slightly increases with increasing M_{st} values, indicating that when trying to model the downcomer, overestimating

the M_{st} value would be less serious than underestimating the M_{st} value. Also noteworthy is that the model has a tendency to fail to converge to steady state when the interphase friction is low, but this does not appear to be a problem at 95% power once the interphase friction is above a certain value.

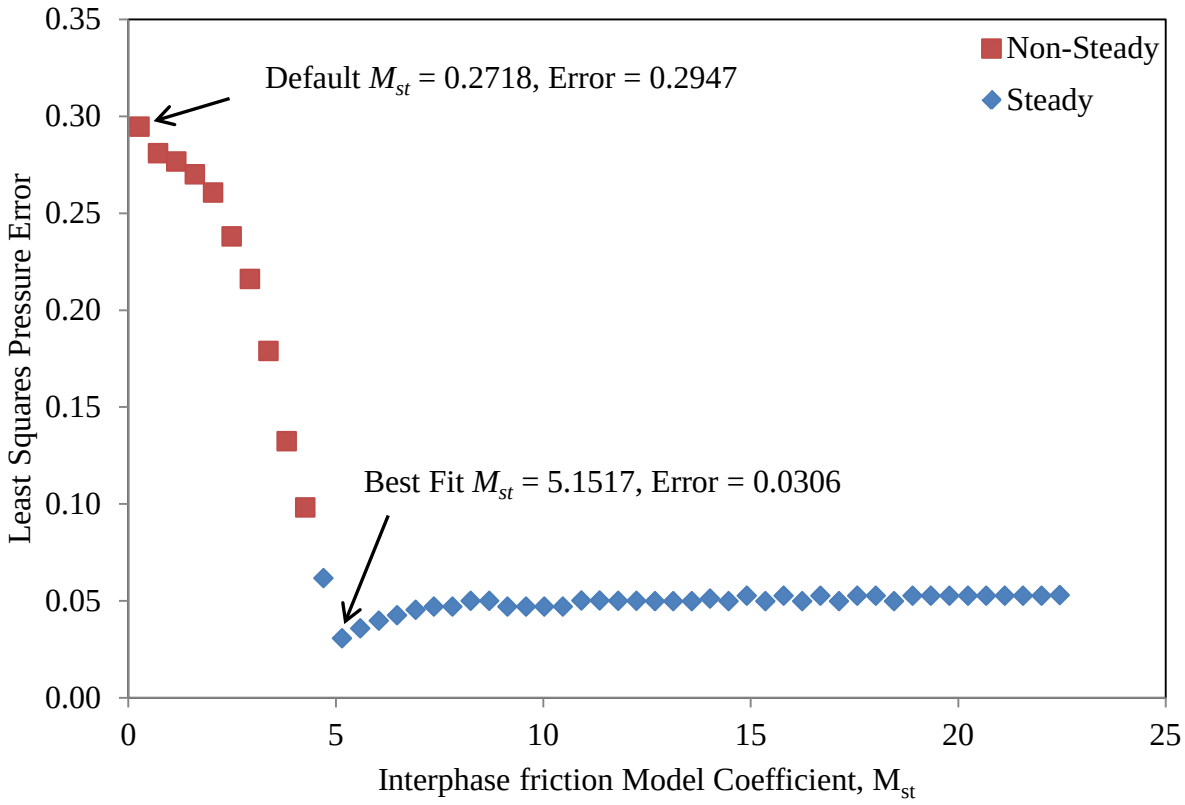

Figure 31: Least Squares Pressure Error Above the Orifice Plate at 95% Power for Varying Interphase Friction Model Coefficient Values

A closer look at the relative pressure and void fraction ratio profiles for individual M_{st} values is offered in Figure 32 and Figure 33, respectively. As the relative pressure profiles indicate, setting M_{st} to 5.1517 provides a very close approximation to the FOAK relative pressure profile above the orifice plate, as does the case with M_{st} = 22.4532. Below the orifice plate, it appears that the pressure is slightly under-predicted for M_{st} = 5.1517, and significantly under-predicted for M_{st} = 22.4532. There are two key factors that affect the pressure rise between the tap above the orifice plate and the tap 0.0150 above the LTS; the density of the two-phase

mixture below the orifice plate and the pressure loss caused by the orifice plate. As the void fraction ratio profiles indicate, for the higher M_{st} values, more vapor is being dragged through the orifice plate, lowering the density of the mixture entering the tube nest. RELAP data shows that the pressure rise from the center of the branch connection, with a height of 0.0684 above the LTS, to the pressure tap 0.0150 above the LTS, is 0.0985 when M_{st} = 0.2718 and 0.0671 for M_{st} = 22.4532, a difference of 0.0314. However, the pressure drop caused by the orifice plate was calculated to be 0.0545 for M_{st} = 0.2718 and 0.1195 for M_{st} = 22.4532, a difference of 0.0650. This would indicate that the major factors regarding the orifice plate pressure rise would be the density at the orifice plate, which is addressed by adjusting M_{st}, and the orifice plate energy loss factor, K_L, which is discussed in Section 4.2.3.

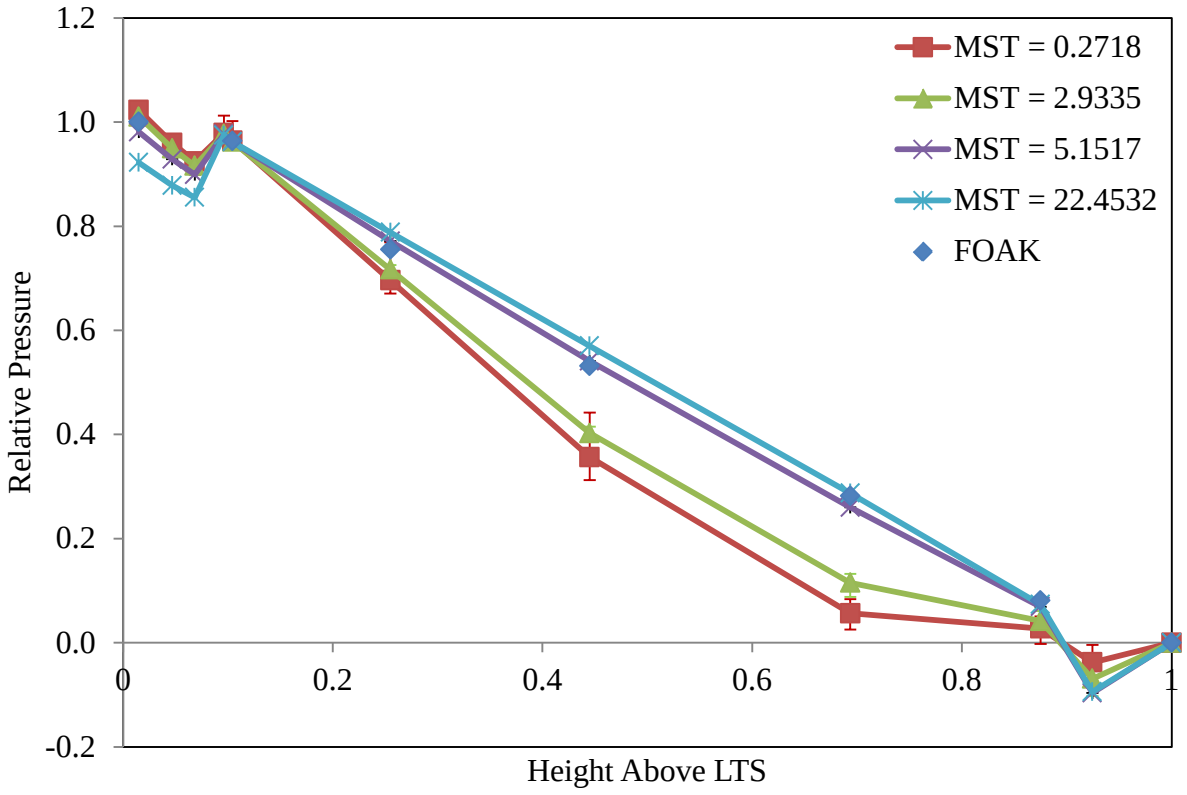

Figure 32: Relative Pressure Profiles for Varying Interphase Friction Model Coefficient Values at 95% Power

Overall, the void fraction ratio profile for M_{st} = 5.1517 does not seem to match the FOAK void fraction ratio profile as the relative pressure profile match would suggest. The FOAK profile indicates a curve in the void fraction ratio profile, with a maximum void fraction ratio at 0.6936 above the LTS, while the RELAP void fraction ratio profile is much flatter. Also, the RELAP model runs indicate a dip in the void fraction ratio profile at the orifice plate. The most likely reason for these discrepancies would be that in the FOAK report, void fraction is derived from the pressure data, under the assumption of several simplifications. The key assumptions being that the pressure is purely hydrostatic and that the void fraction can be linearly extrapolated to the orifice plate from the two closest values. RELAP has the ability to take into account other factors such as frictional losses and damming by the orifice plate, which can cause the RELAP void fraction ratio profile to appear different from the FOAK profile, even when the profiles for relative pressure nearly match.

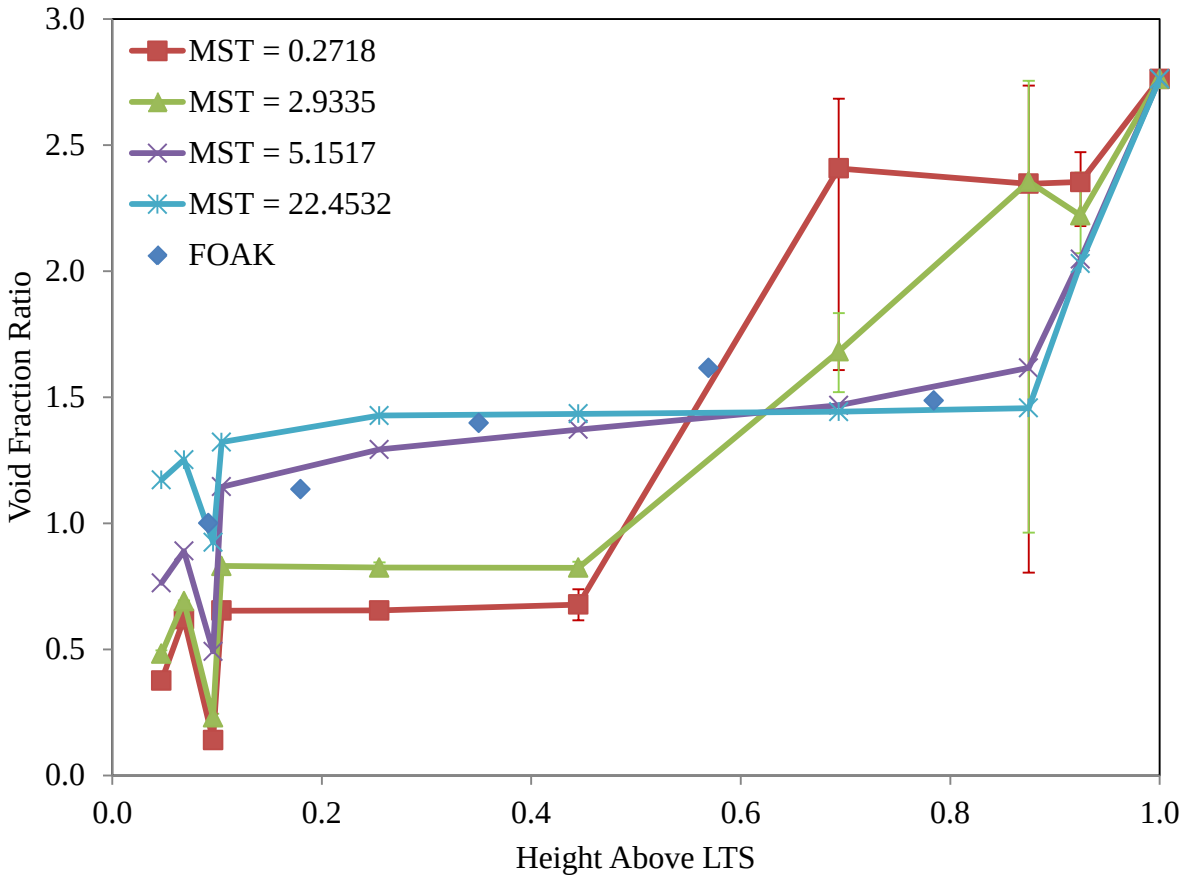

Figure 33: Void Fraction Ratio Profiles for Varying Interphase Friction Model Coefficient Values at 95% Power

4.2.1.2: 85% Power

Figure 34 shows the total pressure error for each model run conducted at 85% power, using the same M_{st} values as were examined at 95% power. Similar to the case at 95% power, the error drops off at a much greater rate for increasing M_{st} values until reaching a minimum, before increasing more modestly for higher M_{st} values. However, at 85% power, the error minimum was 0.0381 and occurred at an M_{st} value of 6.9262, which was a run that failed to converge to steady state. Since the run did not converge to steady state, the pressure error is calculated using the average pressure at each node over the final 100 seconds of the 900-second model run.

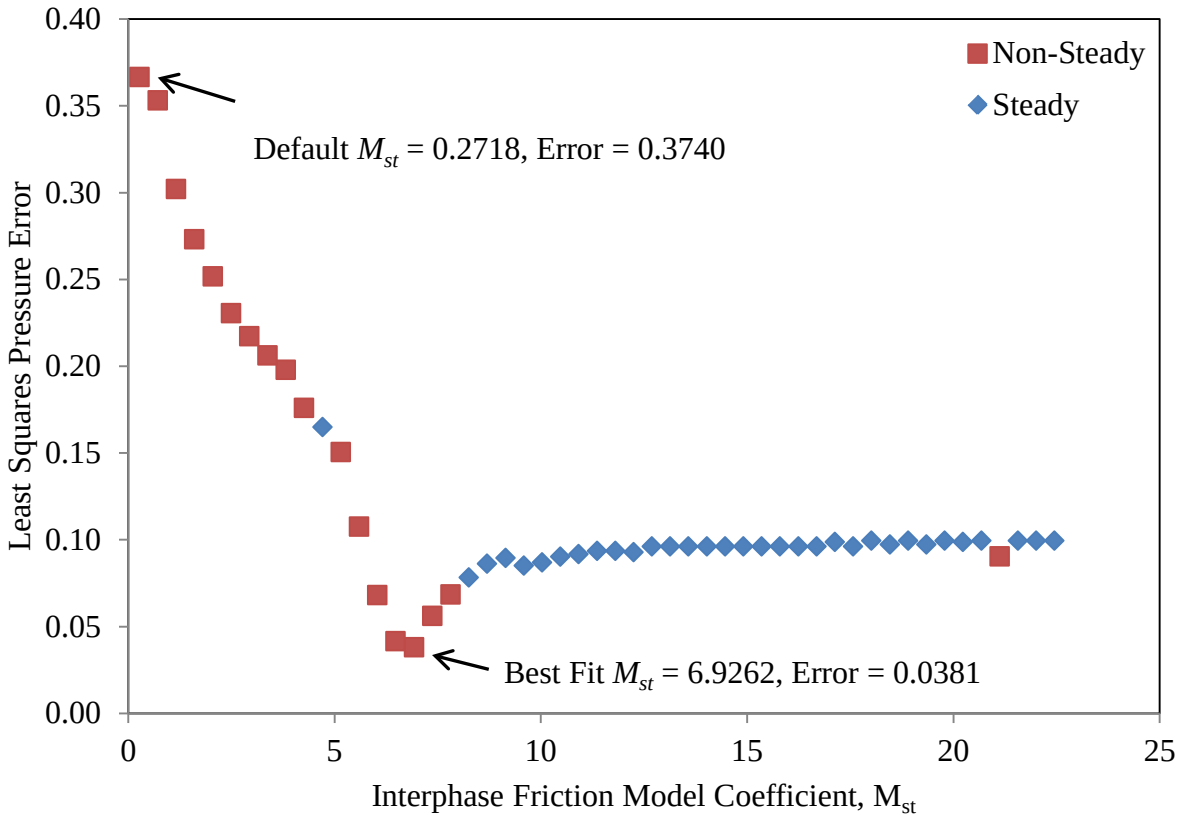

Figure 34: Least Squares Pressure Error Above the Orifice Plate at 85% Power for Varying Interphase Friction Model Coefficient Values

In Figure 35 and Figure 36, the relative pressure and void fraction ratio profiles, respectively, at 85% power are compared, and it is shown that at 85% power for M_{st} = 5.1517, the interphase friction is inadequate to drag the vapor to the bottom of the downcomer and through the orifice plate. However, at M_{st} = 6.9262, the amount of vapor at the orifice plate is only slightly overestimated, similarly to the case with M_{st} = 5.1517 for 95% power.

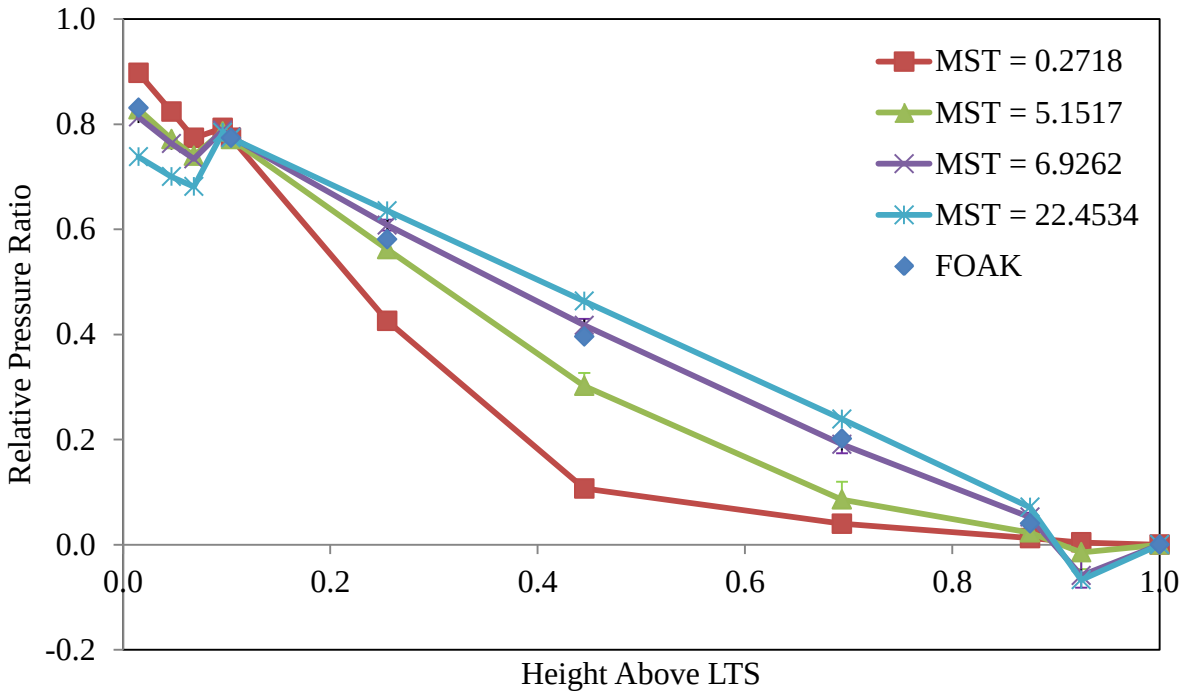

Figure 35: Relative Pressure Profiles at 85% Power for Varying Interphase Friction Model Coefficient Values

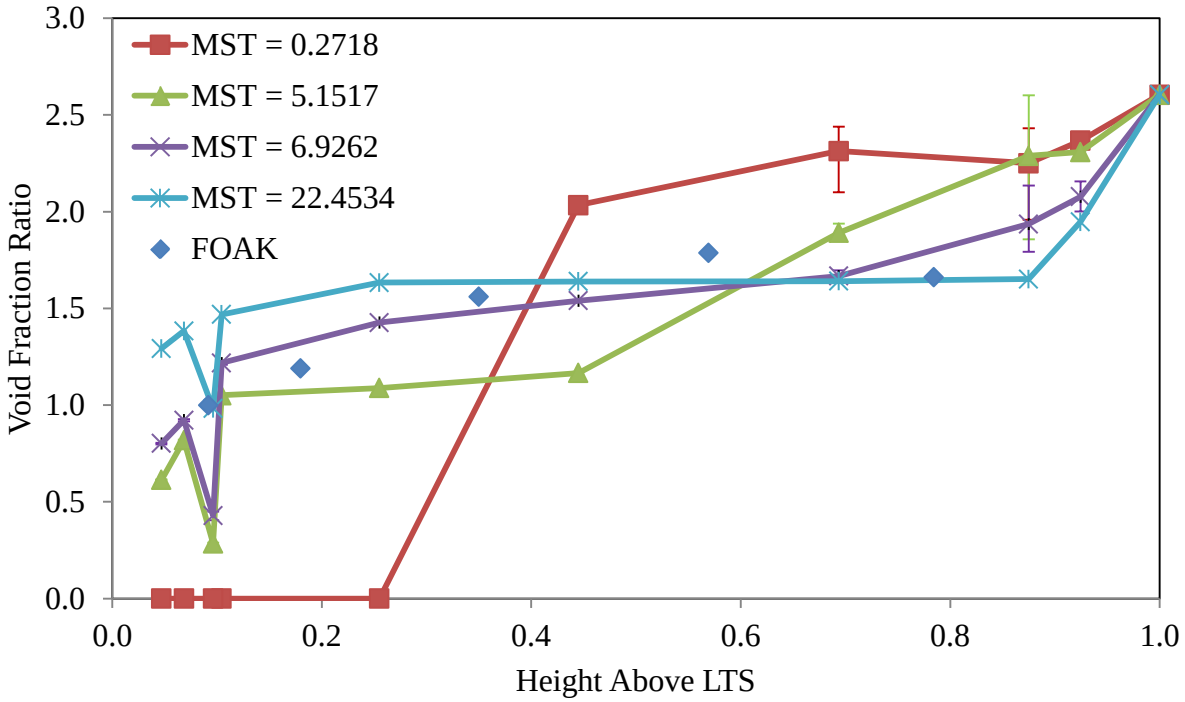

Figure 36: Void Fraction Ratio Profiles at 85% Power for Varying Interphase Friction Model Coefficient Values

4.2.1.3: 75% Power

At 75% power, the trend of increasing the M_{st} value to achieve minimal error continues, with a total downcomer pressure error of 0.0342 at an M_{st} value of 9.5880, as can be seen in Figure 37. The relative pressure and void fraction ratio profiles for 75% power shown in Figure 38 and Figure 39, respectively, show similar patterns to what has been seen at 95% and 85% power, although the void fraction ratio for the volumes leading up to the orifice plate appear to have slightly less vapor than seen in the 95% and 85% power runs.

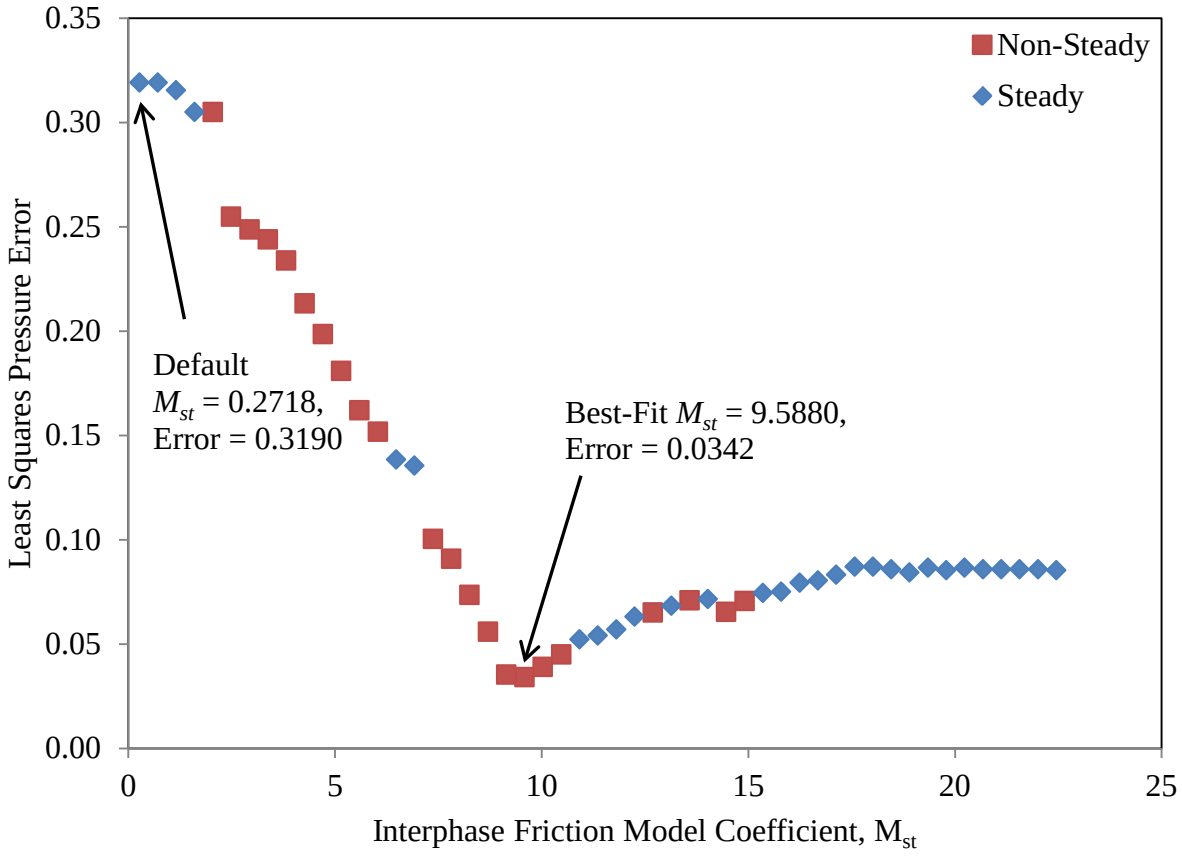

Figure 37: Least Squares Pressure Error Above the Orifice Plate at 75% Power for Varying Interphase Friction Model Coefficient Values

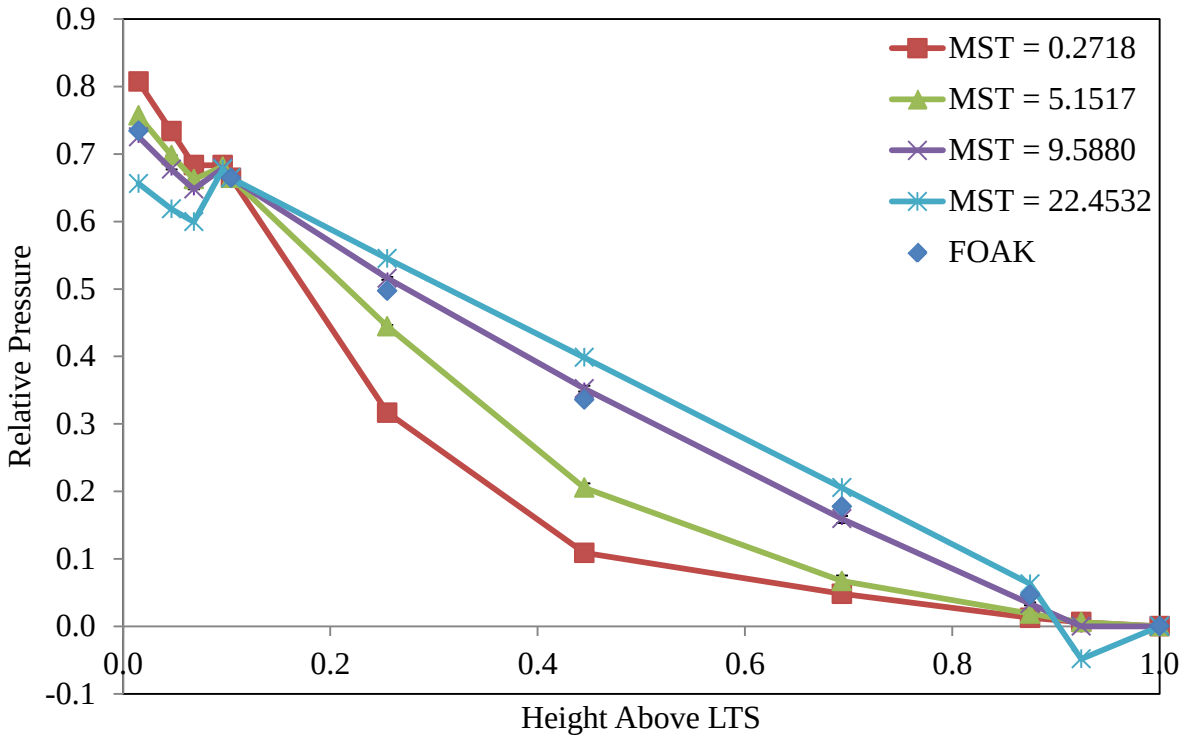

Figure 38: Relative Pressure Profiles at 75% Power for Varying Interphase Friction Model Coefficient Values

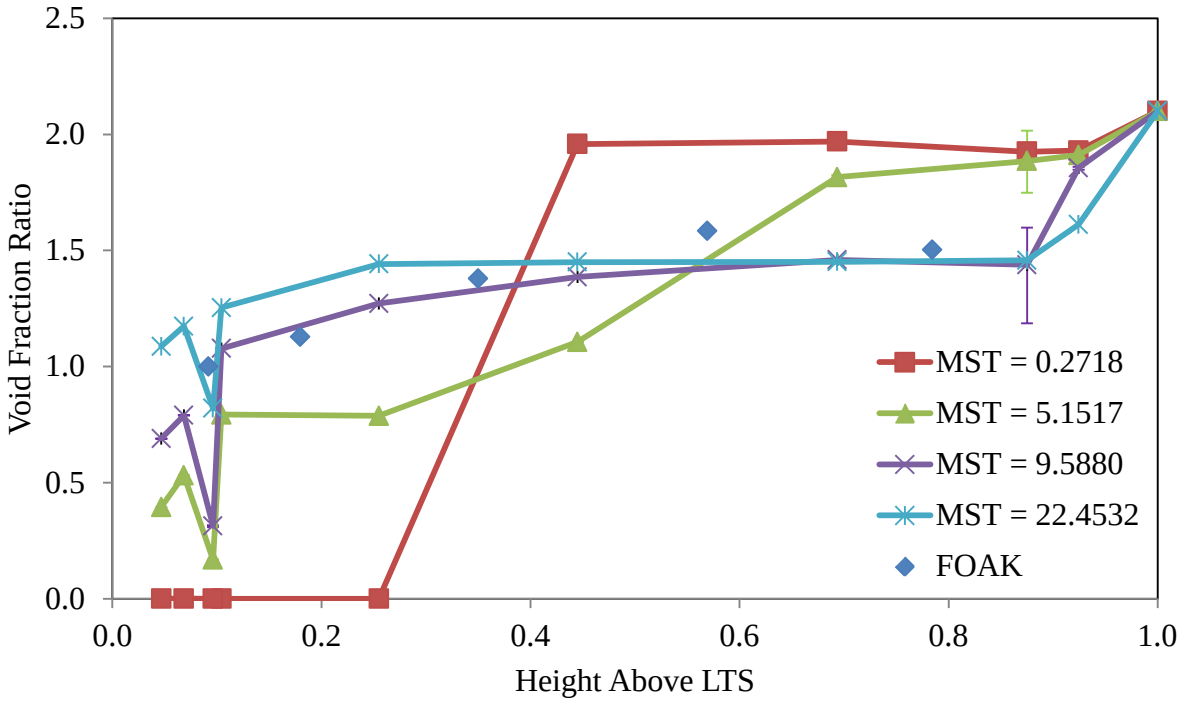

Figure 39: Void Fraction Ratio Profiles at 75% Power for Varying Interphase Friction Model Coefficient Values

4.2.1.4: 65% Power

Figure 40 shows that the trend seen for pressure error at higher power levels continues for 65% power, with the sharp decrease in pressure error for increasing M_{st} as M_{st} approaches the value of minimum error, and then a smaller increase in error for M_{st} values that are greater. The minimum error at 65% power was 0.0154 at M_{st} = 11.3625. While the pressure profiles shown in Figure 41 are similar to those seen at higher power levels, there is a noticeable difference for the best-fit M_{st} void fraction ratio profile shown in Figure 42, in that the void fraction ratio predicted in the volumes above the orifice plate is less than the void fraction ratio calculated in the FOAK report.

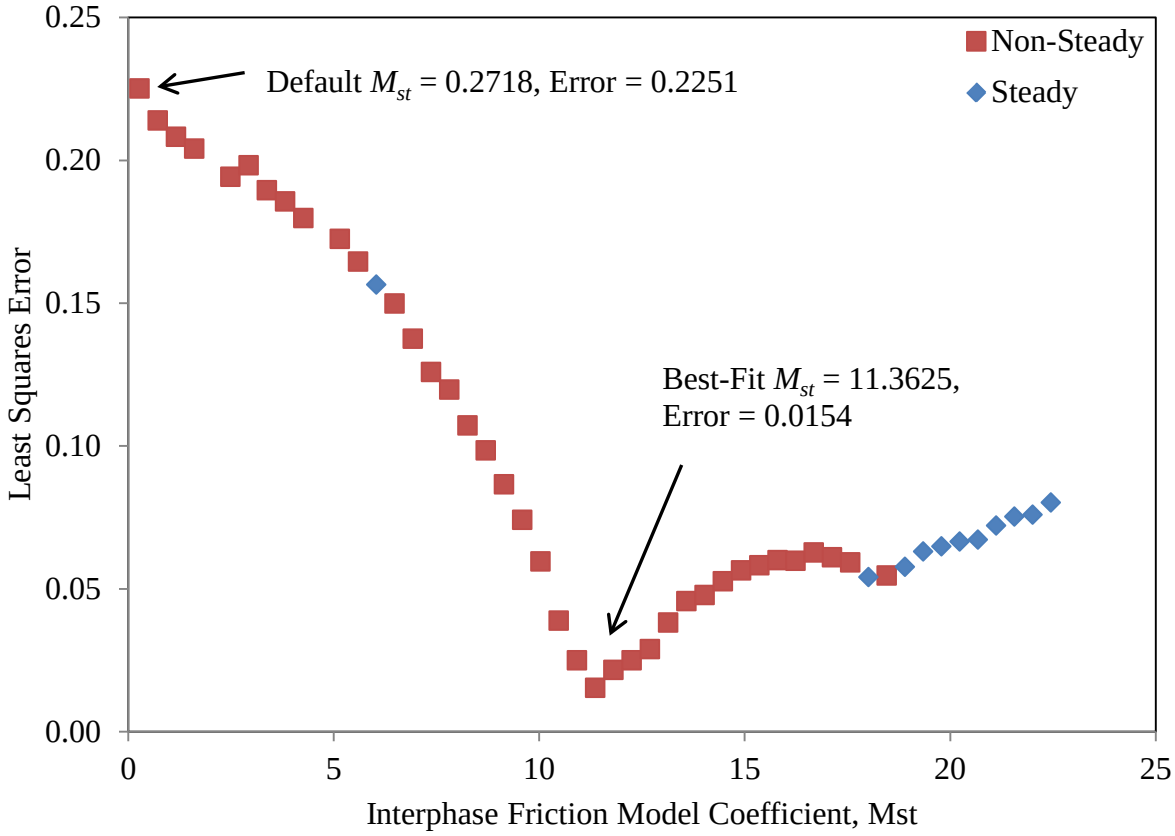

Figure 40: Least Squares Pressure Error Above the Orifice Plate at 65% Power for Varying Interphase Friction Model Coefficient Values

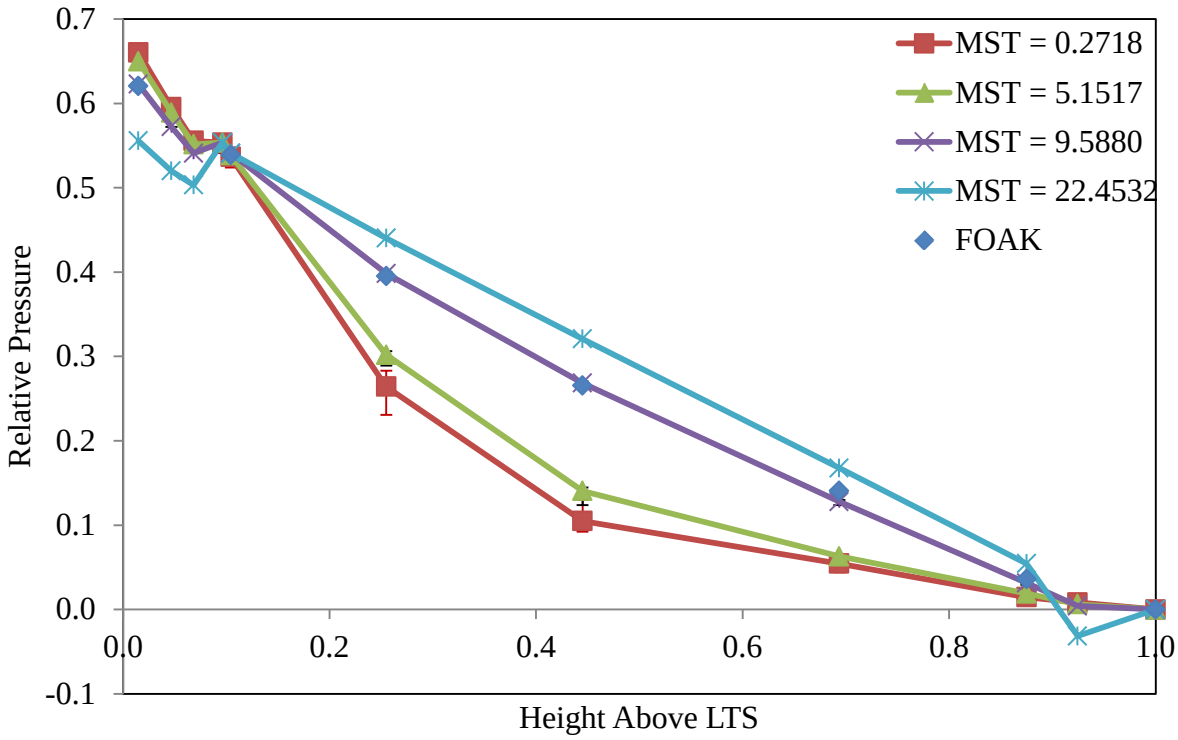

Figure 41: Relative Pressure Profiles at 65% Power for Varying Interphase Friction Model Coefficient M_{st} Values

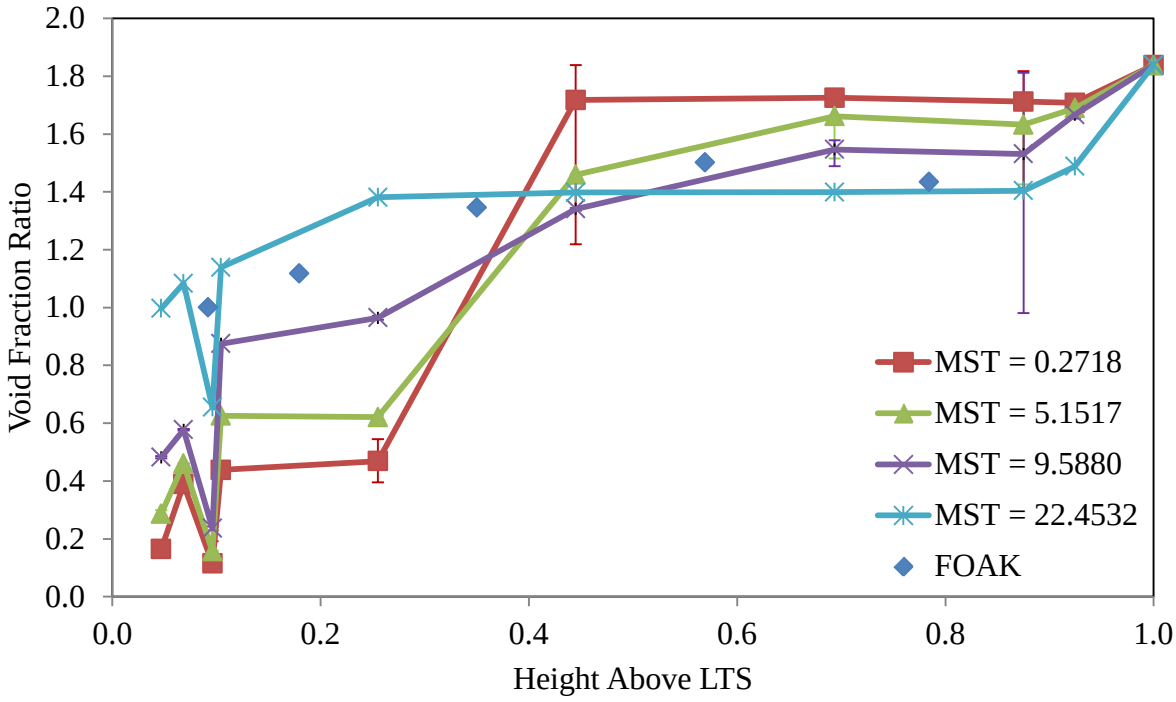

Figure 42: Void Fraction Ratio Profiles at 65% Power for Varying Interphase Friction Model Coefficient Values

4.2.1.5: 55% Power

At 55% power, the trend of increasing M_{st} with decreasing power level, to achieve the best-fit solution continues, as is evidenced in Figure 43. The minimum pressure error was 0.0160 with M_{st} = 14.0243. In Figure 44, the relative pressure profiles look as would be expected compared to those seen at higher power levels, but the void fraction ratio profiles shown in Figure 45 reveal that the void fraction ratio being predicted by RELAP at the best-fit M_{st} is less than the FOAK data would indicate in the volumes above the orifice plate.

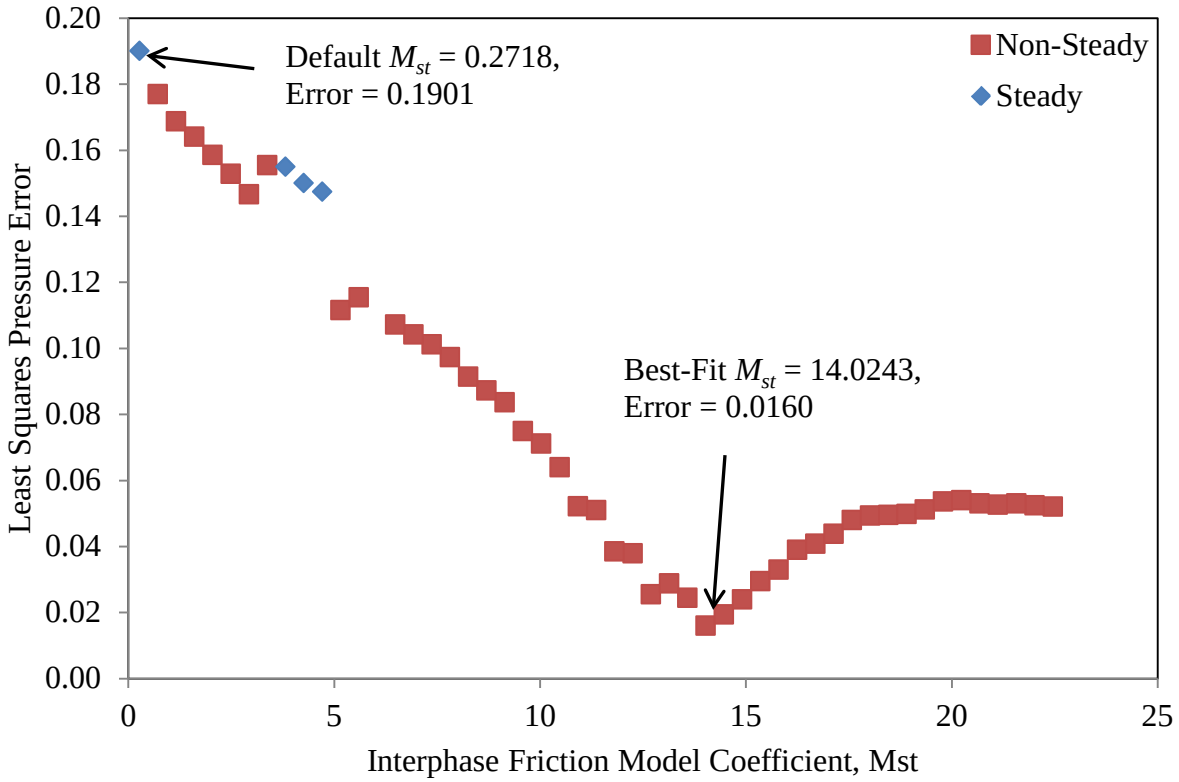

Figure 43: Least Squares Pressure Error Above the Orifice Plate at 55% Power for Varying Interphase Friction Model Coefficient Values

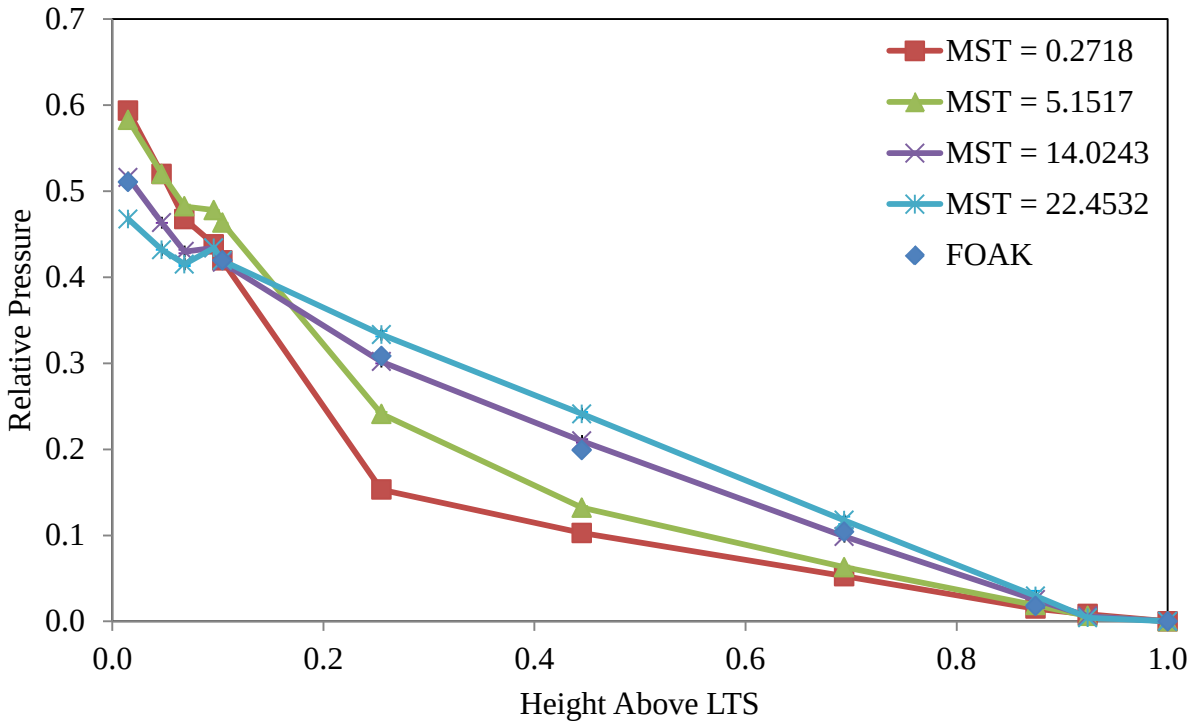

Figure 44: Relative Pressure Profiles at 55% Power for Varying Interphase Friction Model Coefficient Values

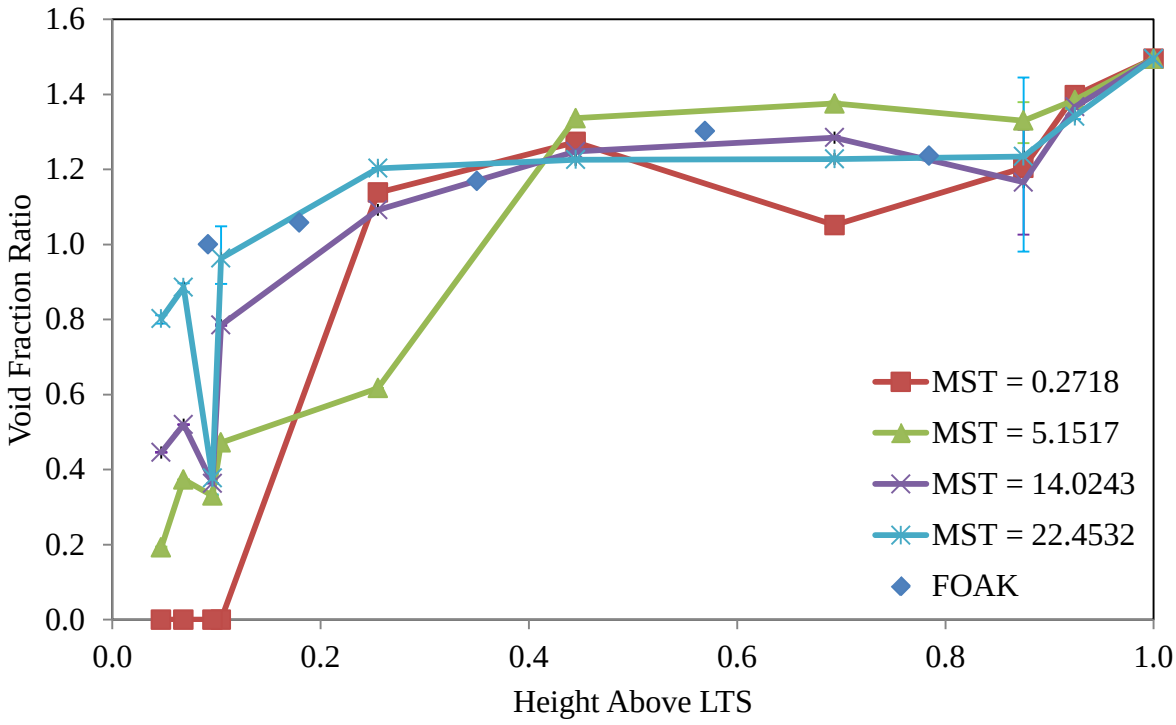

Figure 45: Void Fraction Ratio Profiles at 55% Power for Varying Interphase Friction Model Coefficient Values

4.2.1.6: 45% Power

Many of the trends noticed at higher power levels do not appear to continue when the power level is dropped to 45% power. First, as evidenced in Figure 46, the pressure error does not drop sharply with increasing M_{st} and only increase slightly after achieving a minimum error, but instead the pattern appears to be more parabolic at 45% power. The minimum pressure error is 0.0287 and occurs with M_{st} = 11.8061, which goes against a trend of increasing M_{st} to achieve a minimum error with decreasing the power level. The relative pressure profiles at 45% power shown in Figure 47 are consistent with those seen at higher power levels, given the knowledge of the inconsistency with the pressure error. In Figure 48, the void fraction ratio profiles at 45% power show that the void fraction ratio drops off in the volumes closest to the orifice plate in the RELAP runs, while the FOAK data indicates much higher void fraction ratios.

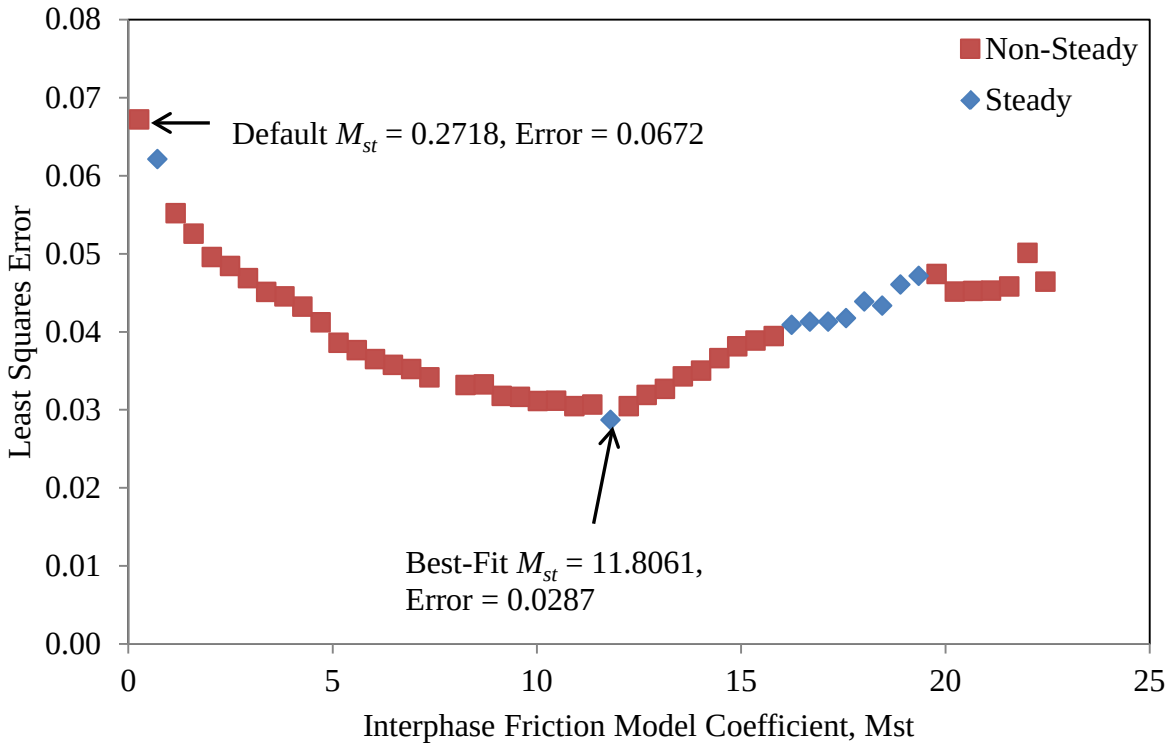

Figure 46: Least Squares Pressure Error Above the Orifice Plate at 45% Power for Varying Interphase Friction Model Coefficient Values

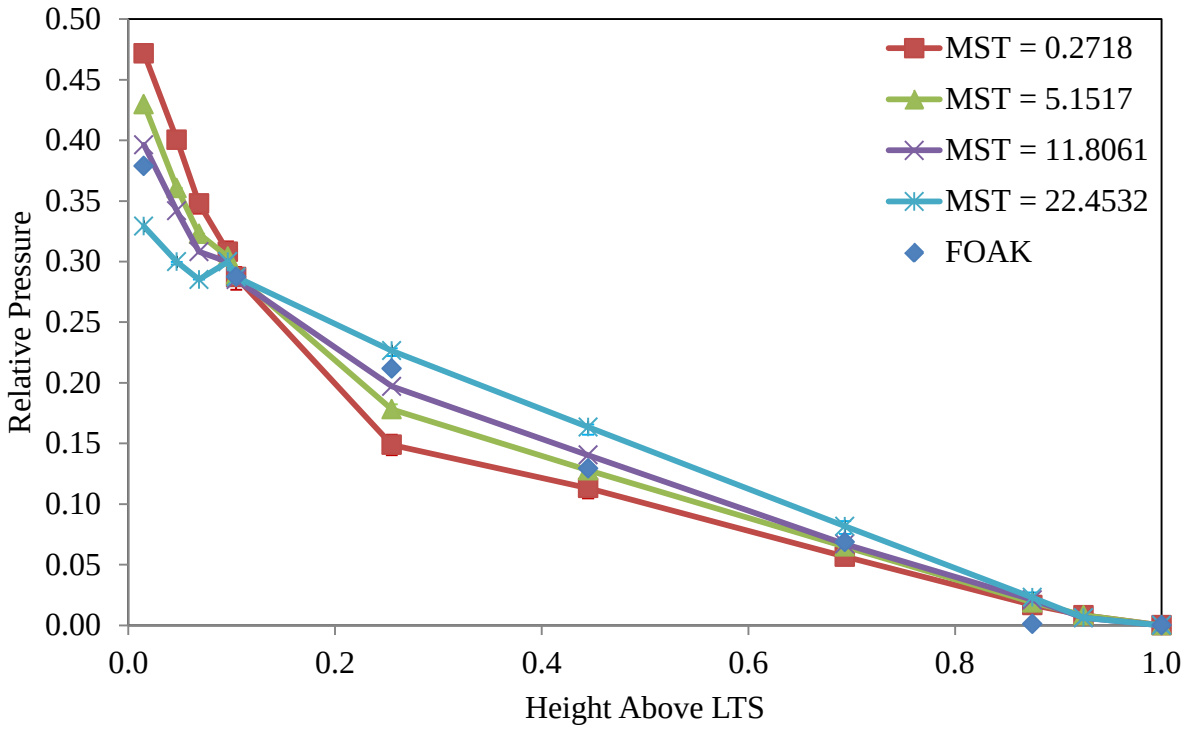

Figure 47: Relative Pressure Profiles at 45% Power for Varying Interphase Friction Model Coefficient Levels

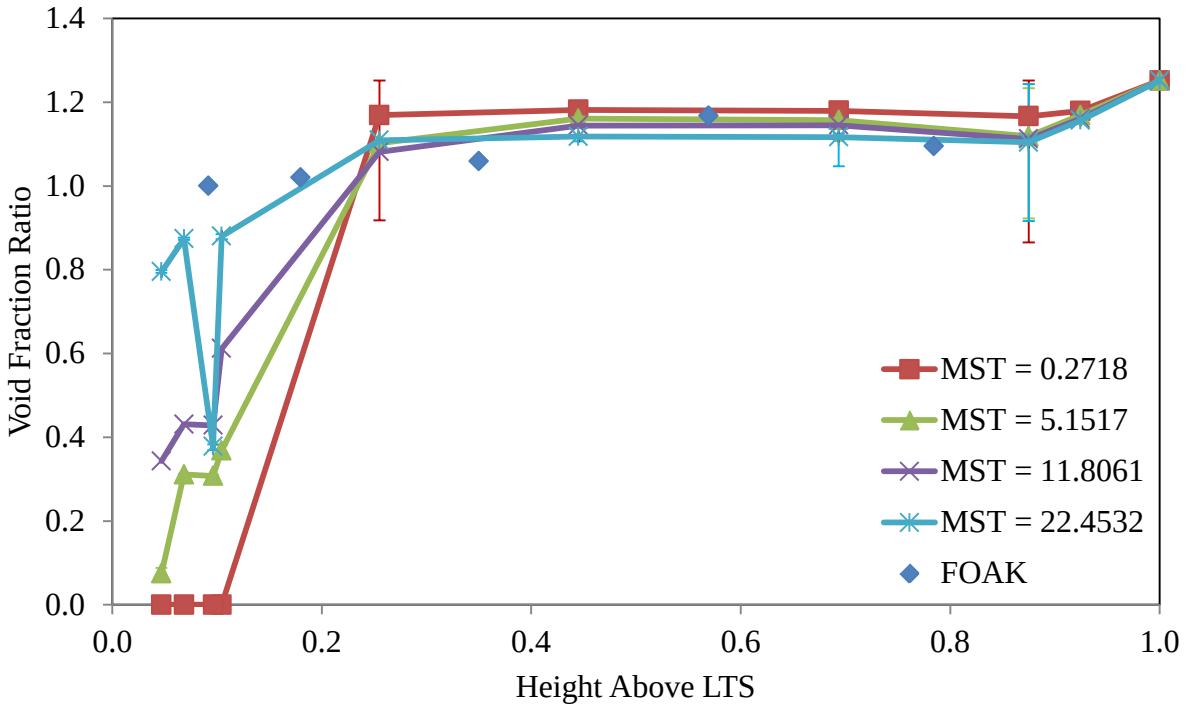

Figure 48: Void Fraction Ratio Profiles at 45% Power for Varying Interphase Friction Model Coefficient Levels

4.2.2: Varying Orifice Plate Energy Loss Factor

As noted earlier, while adjusting the M_{st} values for each power level helped improve the pressure profile for the main body of the downcomer, there remain some issues with the pressure profile at and below the orifice plate. Two adjustments could be made to the system, either by adjusting the orifice plate energy loss factor (also known as the k-factor), so as to produce an ideal pressure loss through the orifice plate, or by adjusting the M_{st} value so as to achieve a void fraction at the orifice plate that is more closely resembling that determined in the FOAK data. Since the M_{st} value has been fitted to the pressure profile and is already used to set the void fraction at the orifice plate, adjusting M_{st} was ruled out in favor of finding a better fitting energy loss factor for the orifice plate.

A positive value indicates that the model is under-predicting the pressure loss through the orifice plate, resulting in an over-predicted pressure rise over the total interval. A negative value indicates the model is over-predicting the pressure loss, and thus an under-predicted pressure rise over the total interval. Flow regime data has been included to help explain why discontinuities and anomalies in the profiles occur.

4.2.2.1: 95% Power

At 95% power, with M_{st} set to 5.1517, Figure 49 shows that ideal orifice plate energy loss factor should be 0.79, rather than at 0.90, the default value. In modeling the downcomer with different energy loss factors for the orifice plate, the orifice plate pressure error leveled off around K_L = 0.3, which coincided with the flow regime in the volume directly above the orifice plate changing from slug flow to bubbly flow.

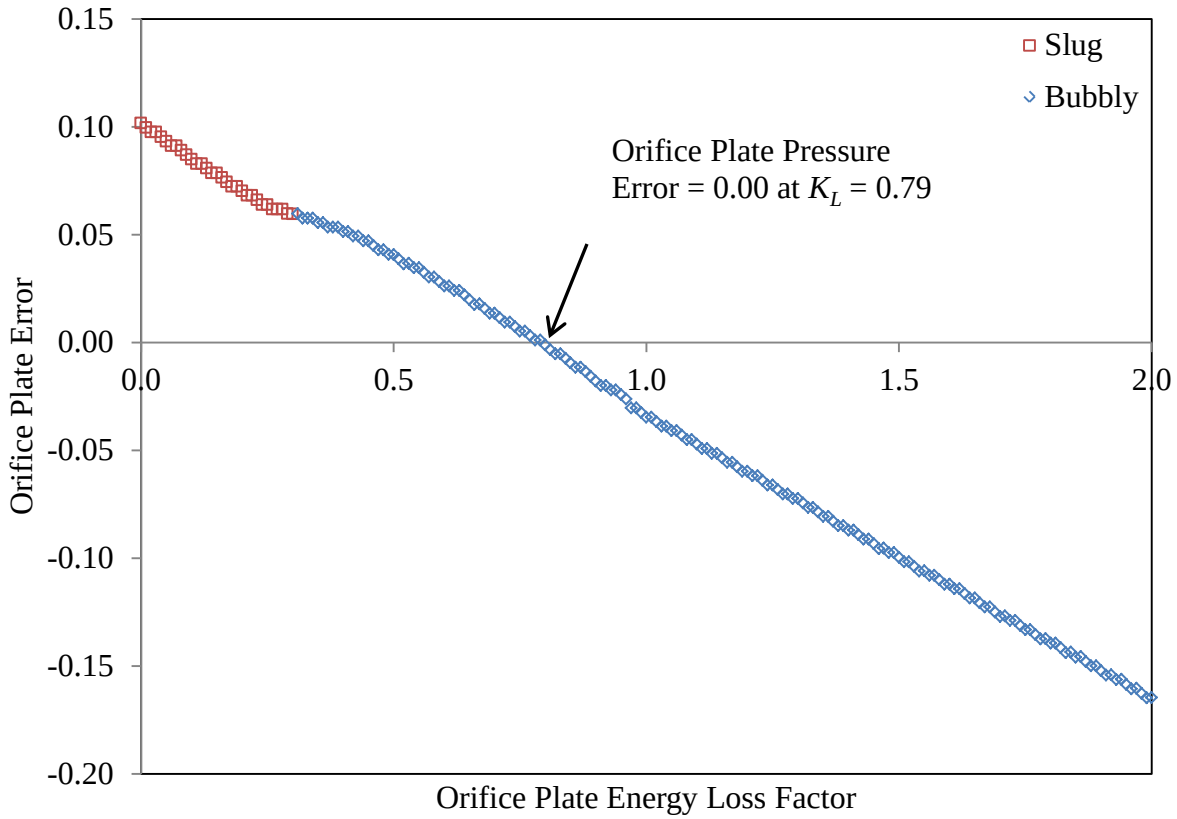

Figure 49: Orifice Plate Pressure Errors for Varying Orifice Plate Energy Loss Factor at 95% Power

4.2.2.2: 85% Power

With 85% power and M_{st} = 6.9262, the ideal orifice plate energy loss factor is 0.75, as is indicated in Figure 50. Similar to 95% power, a leveling in the pressure error at K_L = 0.37 coincides with a flow regime change from slug to bubbly flow in the volume directly above the orifice plate.

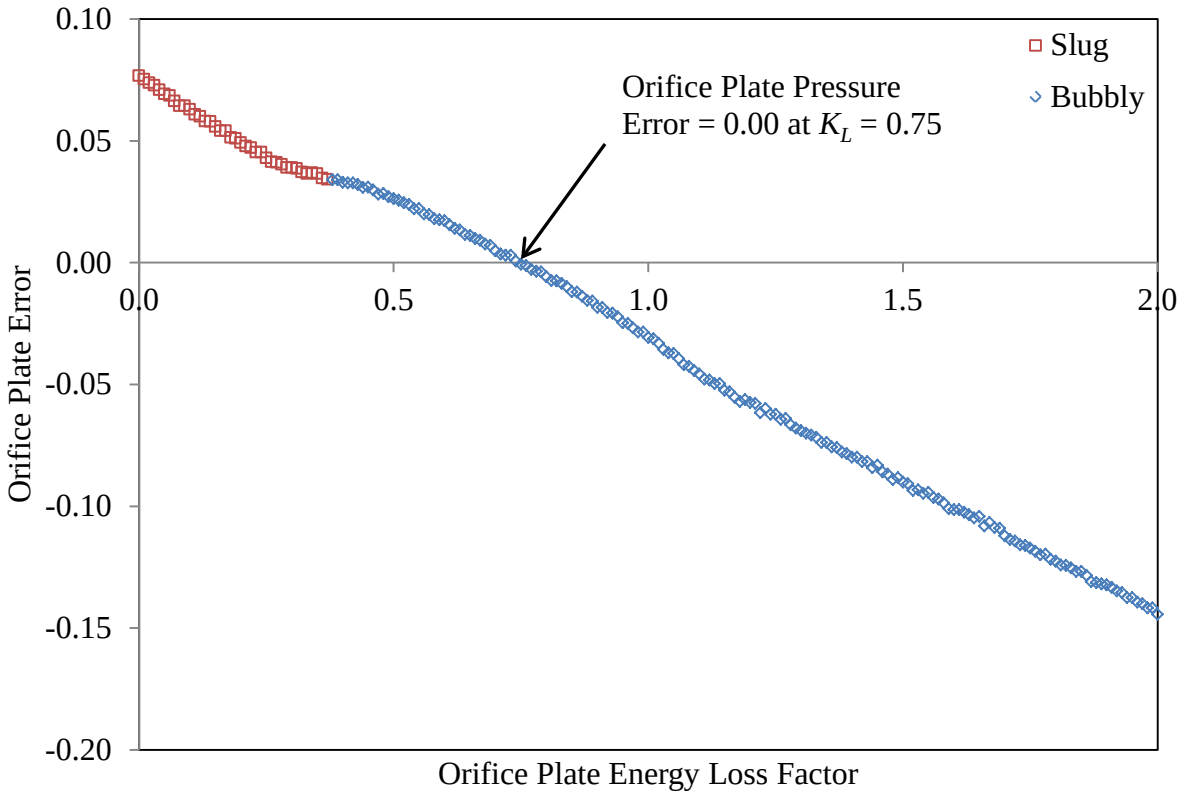

Figure 50: Orifice Plate Pressure Errors for Varying Orifice Plate Energy Loss Factor at 85% Power

4.2.2.3: 75% Power

At 75% power, with M_{st} = 9.5880, the ideal orifice plate energy loss factor is 0.79, as Figure 51 shows. As the orifice plate energy loss factor approaches 0.48, the orifice plate pressure error levels, just as the flow regime in the volume above the orifice plate switches from slug to bubbly flow, similar to the profiles of 95% and 85% power.

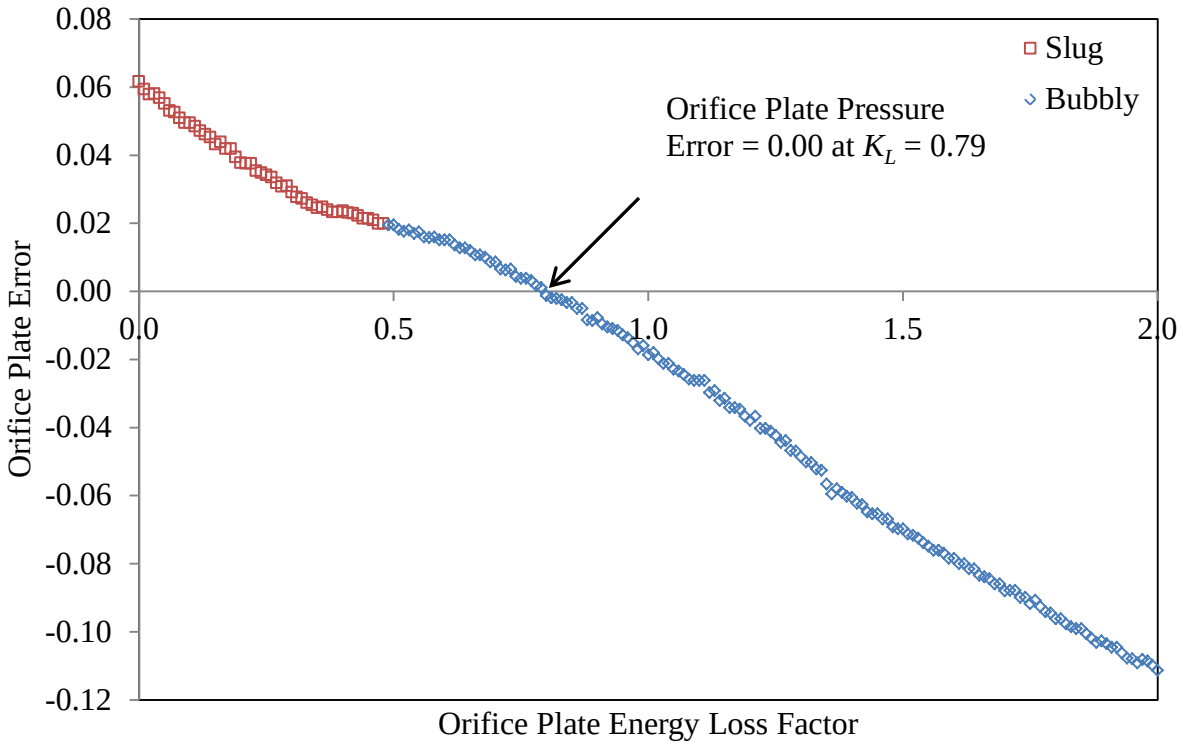

Figure 51: Orifice Plate Pressure Errors for Varying Orifice Plate Energy Loss Factor at 75% Power

4.2.2.4: 65% Power

In the case of 65% power, with M_{st} = 11.3625, the profile shown in Figure 52 reveals that the ideal energy loss factor is 0.94. Unlike at higher power levels, the orifice plate pressure error does not level, but instead the pressure error takes on the profile of a cubic curve, with the transition from slug to bubbly flow occurring at the point of inflection. In Figure 53, the void fraction ratios in the volumes immediately above and below the orifice plate are shown for each orifice plate energy loss factor. The jump discontinuity in the void fraction ratio below that occurs at K_L = 0.63 coincides with the point of inflection of the orifice plate pressure error curve.

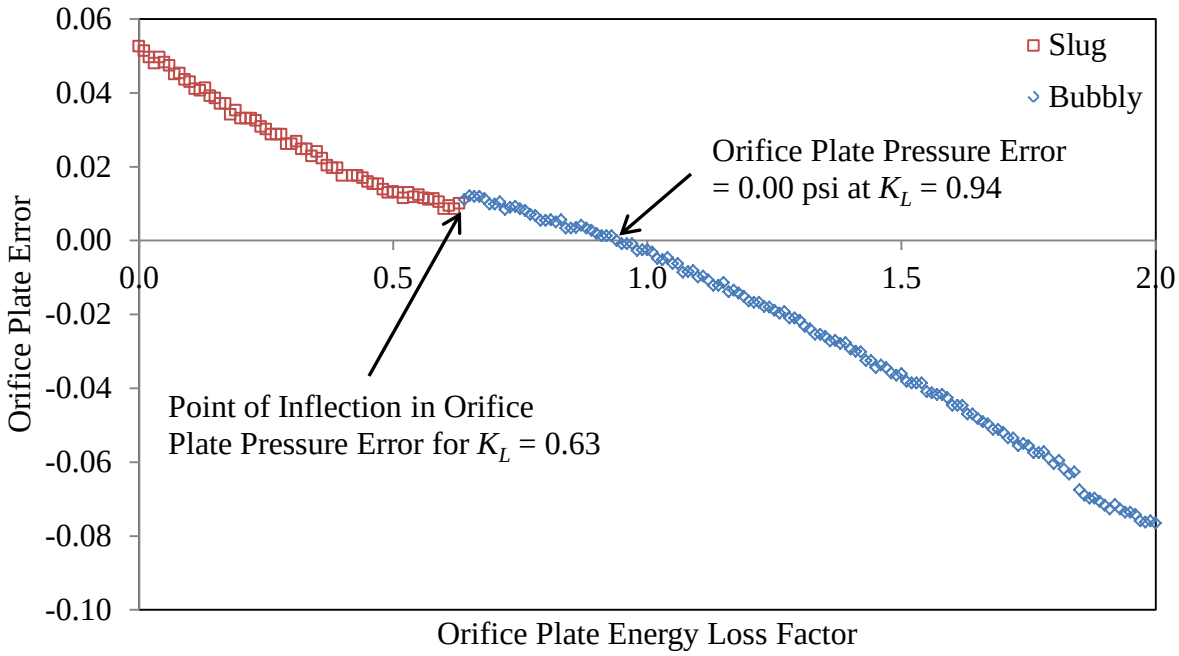

Figure 52: Orifice Plate Pressure Errors for Varying Orifice Plate Energy Loss Factor at 65% Power

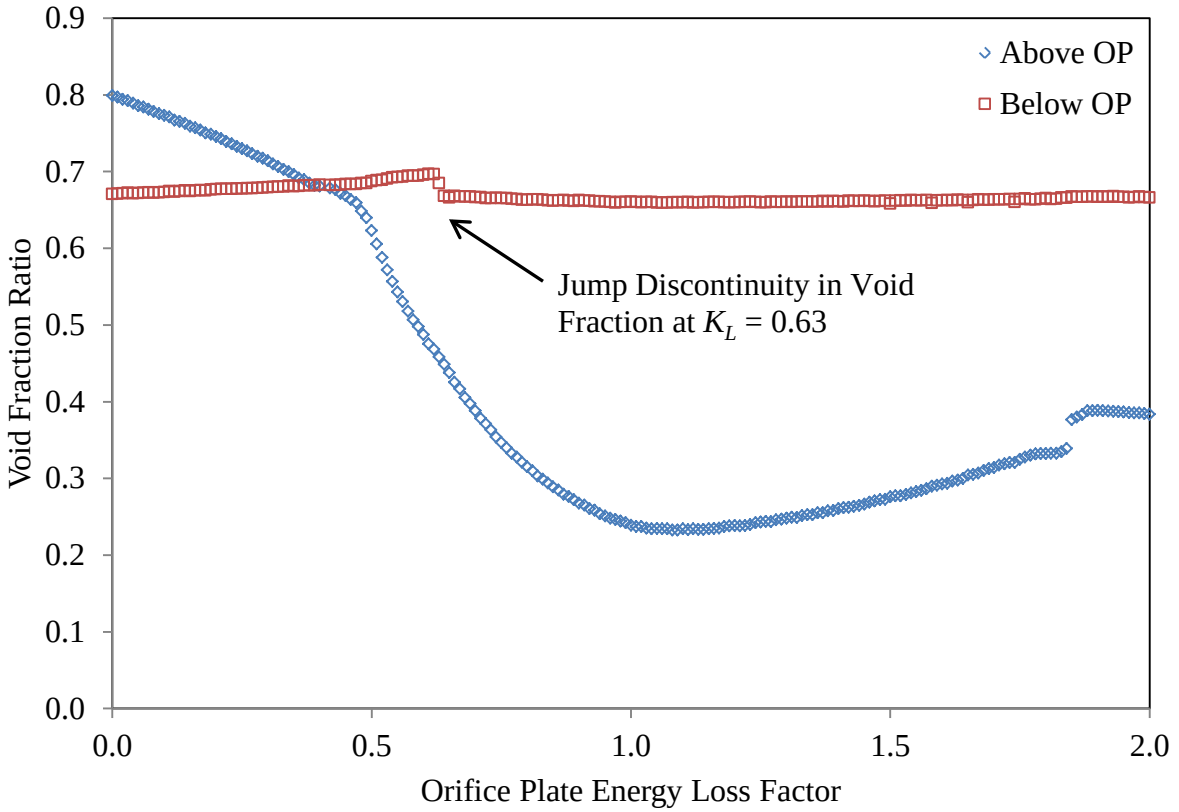

Figure 53: Void Fraction Ratio Above and Below the Orifice Plate for Varying Orifice Plate Energy Loss Factor at 65% Power

4.2.2.5: 55% Power

At 55% power, with M_{st} = 14.0243, the orifice plate energy loss factor that produces zero pressure error is 1.27. The cubic curve seen in Figure 54, is very similar to the cubic curve seen at 65% power. The transition from slug to bubbly flow in the volume above the orifice plate occurs at the point of inflection in the curve, where K_L = 0.87. As is the case with 65% power, the void fraction ratio below the orifice plate experiences a jump discontinuity at the same value for the energy loss factor as the point of inflection, which is shown in Figure 55.

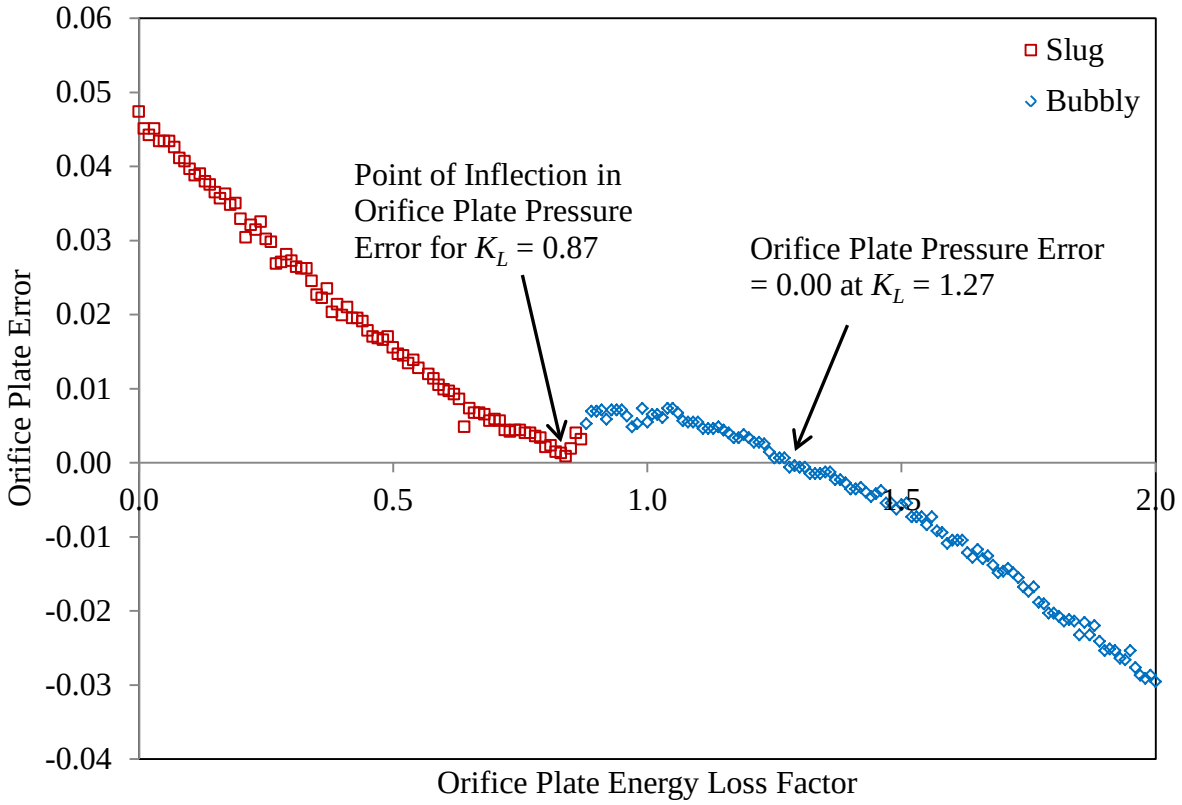

Figure 54: Orifice Plate Pressure Errors for Varying Orifice Plate Energy Loss Factor at 55% Power

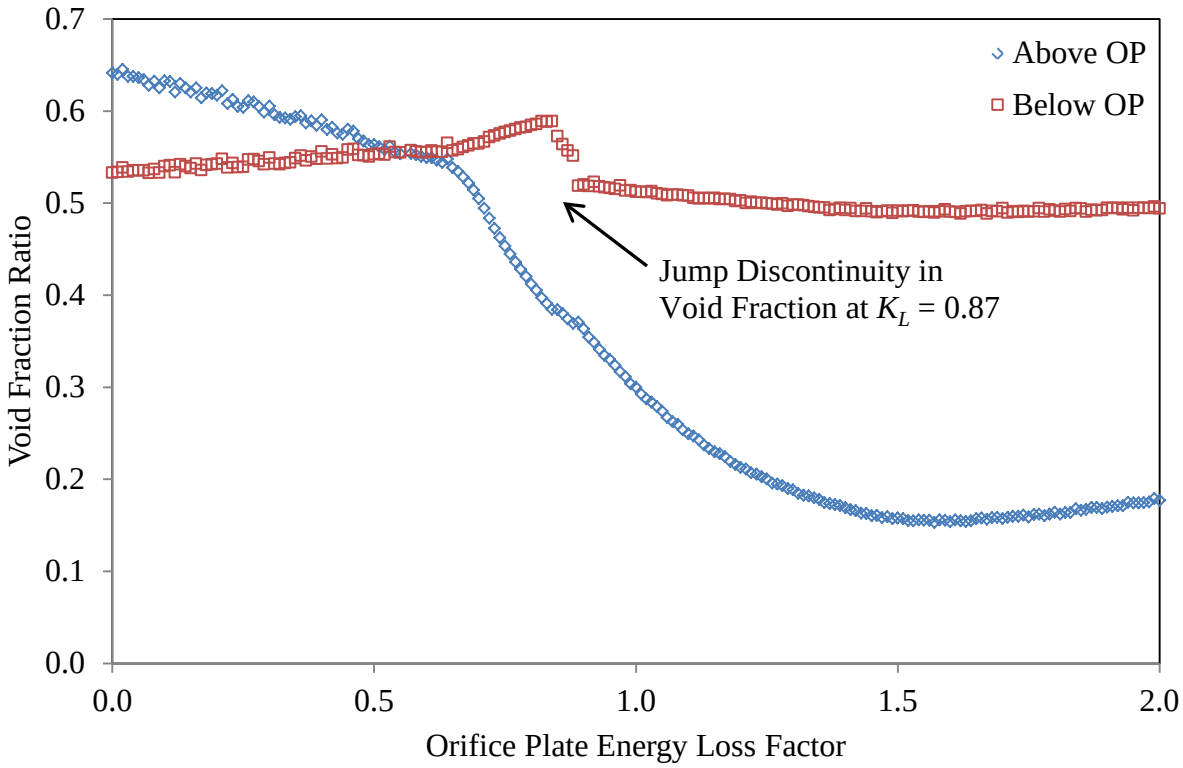

Figure 55: Void Fraction Ratio Above and Below the Orifice Plate for Varying Orifice Plate Energy Loss Factor at 55% Power

4.2.2.6: 45% Power

At 45% power, the orifice plate pressure error takes on a much different form when compared to the orifice plate energy loss factors, as can be seen in Figure 56. For the possible orifice plate energy loss factors that were examined, there was no value for which the orifice plate pressure error was zero. Instead, there is a minimum orifice plate error of 0.0044 for K_L = 1.21. One explanation for this difference would be due to the instabilities that were observed at lower power levels discussed with the FOAK data in Section 2.2.

Since the pattern of the chart for 45% power is unique compared to the trends of the higher power levels, an in depth analysis of the flow regimes in the downcomer were looked at to try to determine any correlations between flow regimes and discontinuities in the chart. The flow regimes for the volume immediately above the orifice plate, the volume immediately below

the orifice plate and the volume that connects the bottom of the downcomer to the tube nest were examined, as they were the only volumes to experience a flow regime change between all of the model runs for varying energy loss factors. In Figure 56, the flow regime sequence is identified by a three-letter code, with the first letter representing the flow regime above the orifice plate, the second letter signifying the flow regime below the orifice plate, and the flow regime for the connection from the downcomer to the tube nest being represented by the third letter. The letter "B" stands for bubbly flow while the letter "S" represents slug flow. Table 8 provides an alternative description of the flow regime sequences and codes. While there are several changes in flow regime patterns, which usually are indicative of discontinuities and jumps in such a profile, there does not appear to be any clear correlation with the changes in flow regime and such discontinuities at 45% power.

Table 8: Flow Regime Sequence Codes for Figure 56

	Flow Regime		
Code	Above Orifice Plate	Below Orifice Plate	Downcomer-Tube Nest Connection
SSB	Slug	Slug	Bubbly
SSS	Slug	Slug	Slug
BSS	Bubbly	Slug	Slug
BSB	Bubbly	Slug	Bubbly
BBB	Bubbly	Bubbly	Bubbly

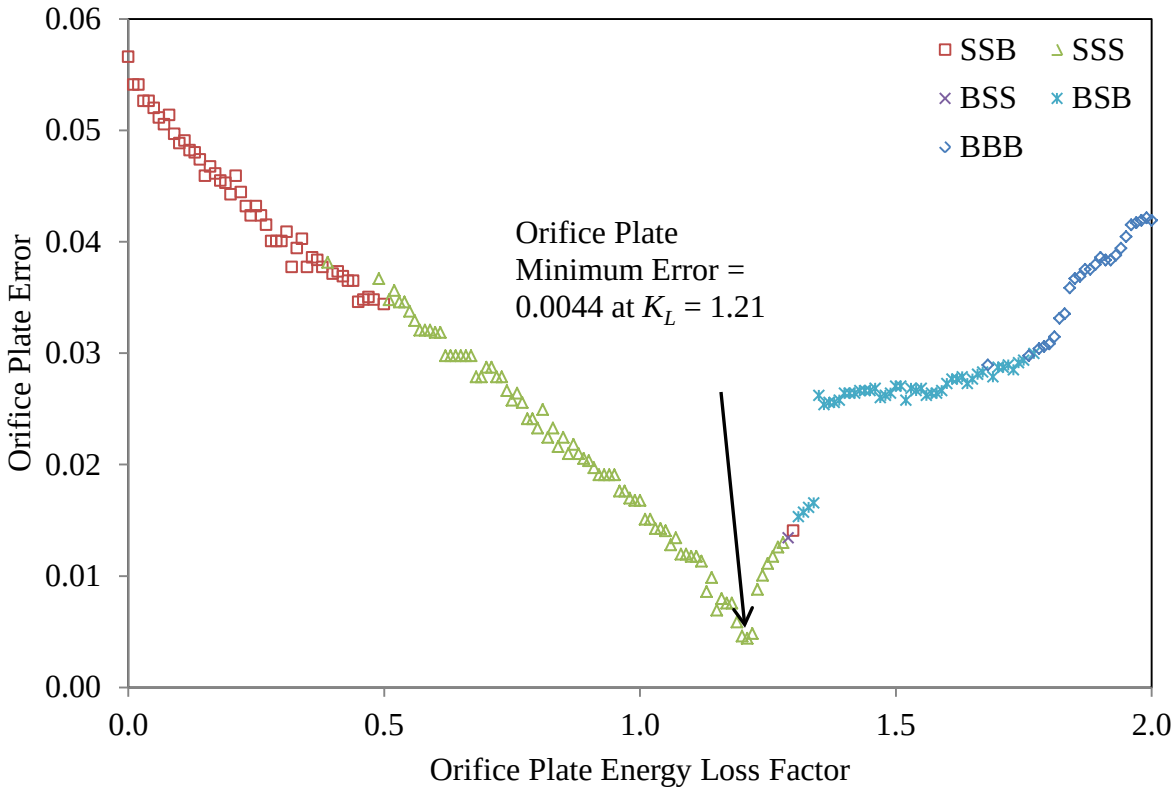

Figure 56: Orifice Plate Pressure Error for Varying Orifice Plate Energy Loss Factor at 45% Power

Figure 57 shows how the void fraction ratio above and below the orifice plate vary with respect to the orifice plate energy loss factor, with the void fraction ratio below the orifice plate displaying an inversely proportional relation to the orifice plate pressure error. This should be expected as the void fraction ratio is proportional to the density below the orifice plate, which governs the pressure rise between the orifice plate and the pressure tap at 0.0150 above the LTS.

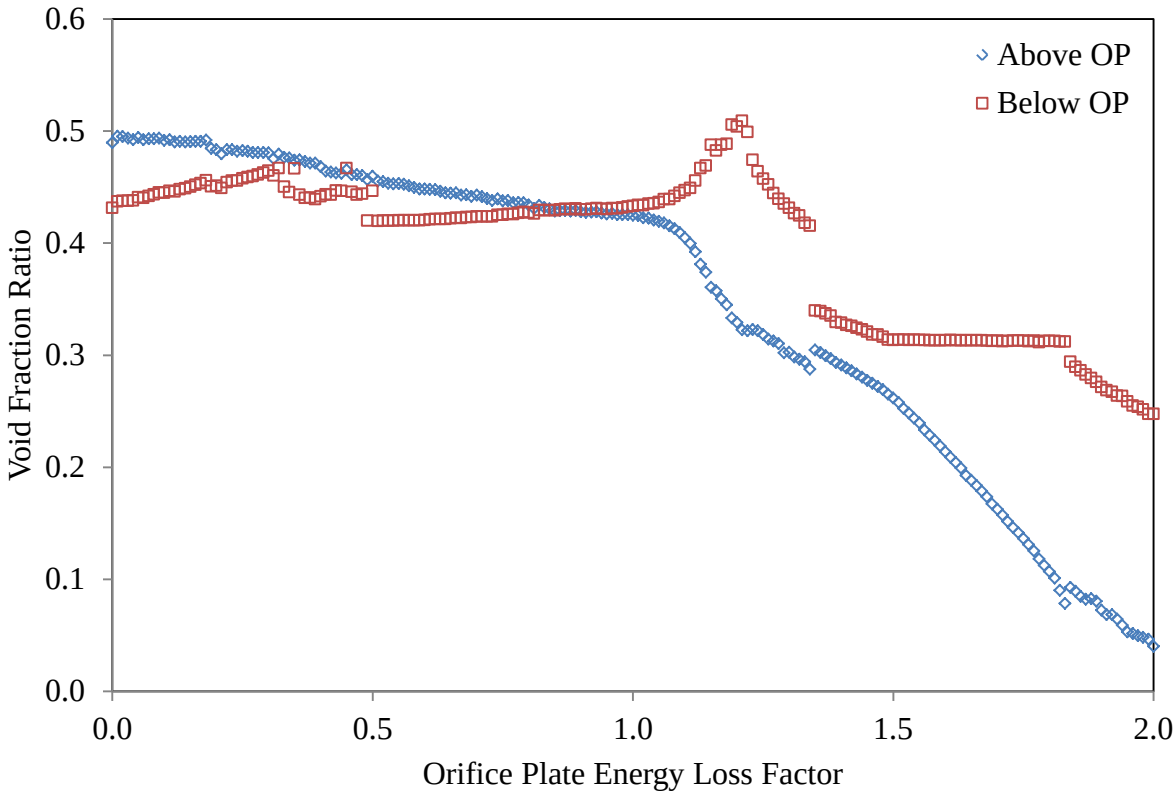

Figure 57: Void Fraction Ratio Above and Below the Orifice Plate for Varying Orifice Plate Energy Loss Factor at 45% Power

4.2.3: Integrating M_{st} and Orifice Plate Energy Loss Factor

A summary of the M_{st} values and orifice plate energy loss factors that best replicate the FOAK data for the downcomer model is provided in Table 9. In general, the best-fit M_{st} value increases with respect to decreasing power level, while there does not appear to be a clear correlation between the orifice plate energy loss factor and power level. It is known that the thermohydraulic properties of the actual downcomer are more unstable at lower power levels, and that perhaps RELAP is finding that same instability when it attempts to model the downcomer at the lower power levels.

Table 9: Summary of Best-Fit M_{st} Values with Best-Fit Orifice Plate Energy Loss Factors

Power Level	M_{st}	K_L
95%	5.1517	0.79
85%	6.9262	0.75
75%	9.5880	0.79
65%	11.3625	0.94
55%	14.0243	1.27
45%	11.8061	1.21

While the values in Table 9 represent an ideal value for each specific power level, it is a goal of this project to determine a best-case set of parameters for all power levels. An overall orifice plate pressure error can be determined using a least squares method from each of the power levels, operating at the power level's respective best-fit M_{st} value. In Figure 58, the least squares orifice plate pressure error for all power levels is plotted with respect to the orifice plate energy loss factor, with a minimum least squares error occurring at $K_L = 0.79$.

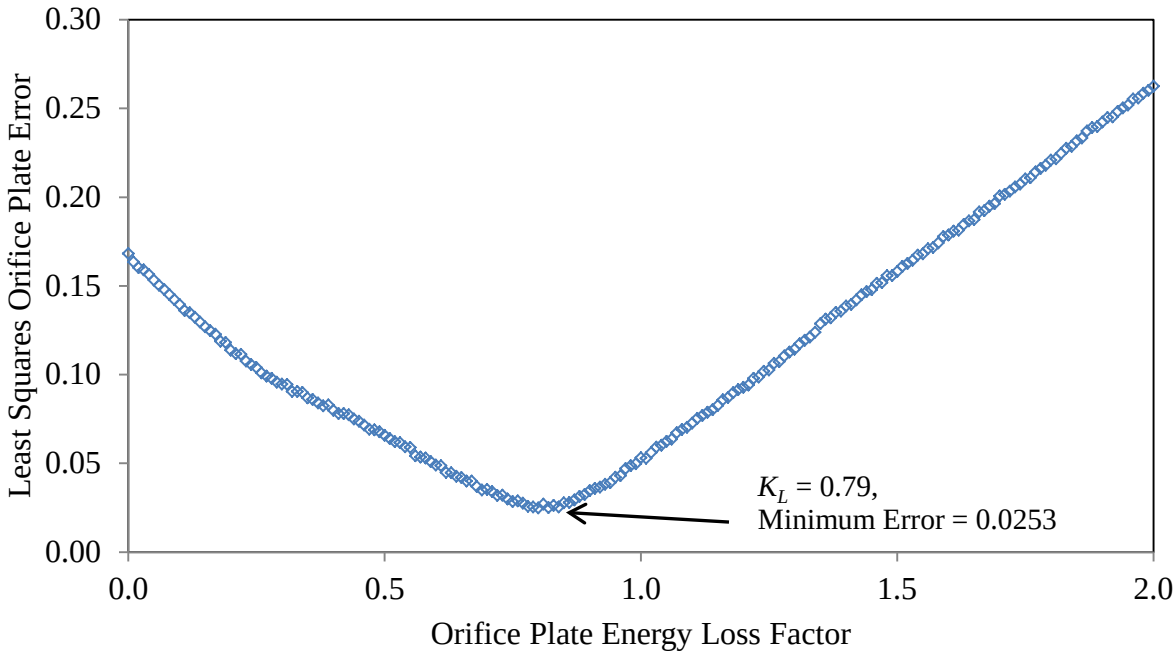

Figure 58: Least Squares Orifice Plate Pressure Error for all Power Levels at Varying Orifice Plate Energy Loss Factors

With the orifice plate energy loss factor set to $K_L = 0.79$, a final series of model runs were conducted for each power level to determine the final best-fit M_{st} values for each power level, as well as a best-fit M_{st} value for all power levels. This was done because the two parameters are not entirely independent, as the orifice plate energy loss factor would impact the pressure and void fraction ratio in the volumes immediately above the orifice plate. Table 10 lists the best-fit M_{st} values as well as the least squares best fit for all power levels, along with the pressure error for the given power level and M_{st} value. Figure 59 shows how the M_{st} values change with respect to power level, and how the best-fit M_{st} values appear to fit a linear correlation. An exception is made for the M_{st} value at 45% power due to the numerous fluctuations in data with both the FOAK study and RELAP5 modeling. Such a correlation could be useful for predicting the appropriate M_{st} values at power levels exceeding 95%, except that there would exist a power level at which M_{st} would equal zero. In the case of the overall best-fit M_{st} value, the least squares error averaged for all six power levels is provided, while Figure 60 shows the average least squares pressure error for each M_{st} value.

Table 10: Best-Fit M_{st} Values for $K_L = 0.79$

Power Level	M_{st}	Error
95%	5.1517	0.0307
85%	6.9262	0.0374
75%	9.5880	0.0356
65%	11.3625	0.0174
55%	14.9115	0.0173
45%	11.3625	0.0303
Overall	11.8061	0.0495

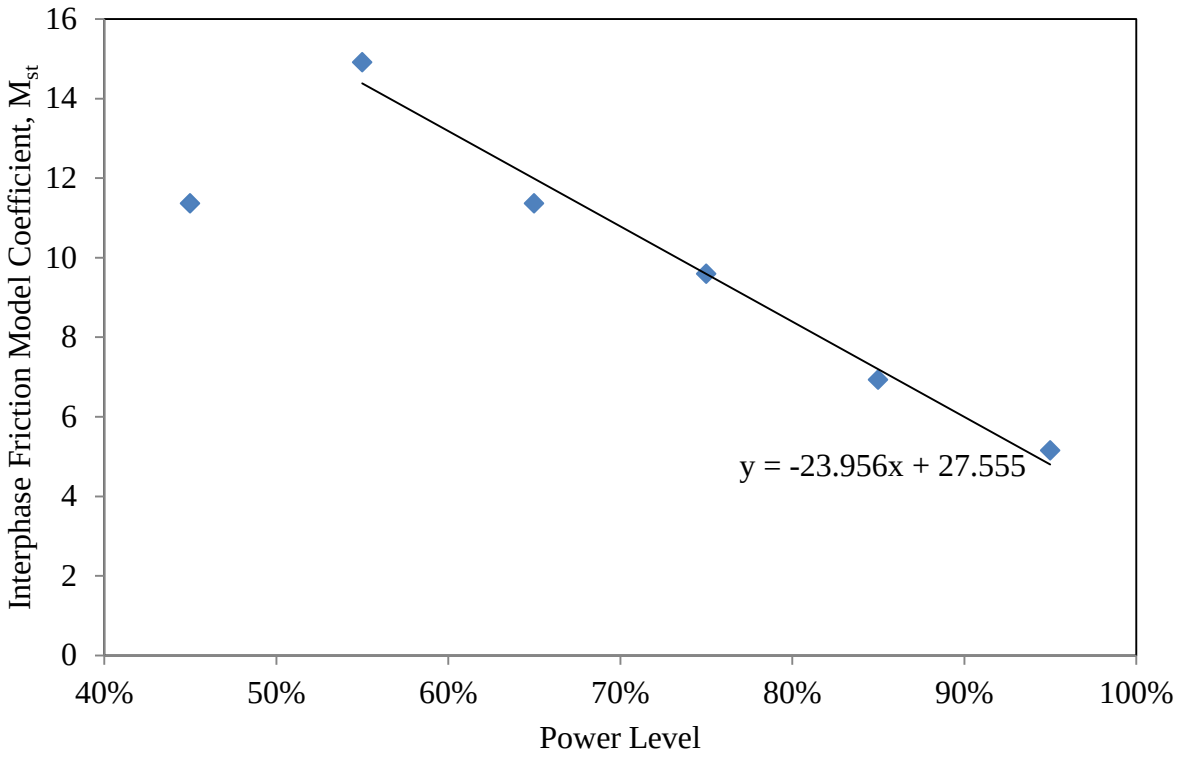

Figure 59: Interphase Friction Model Coefficients for Various Power Levels

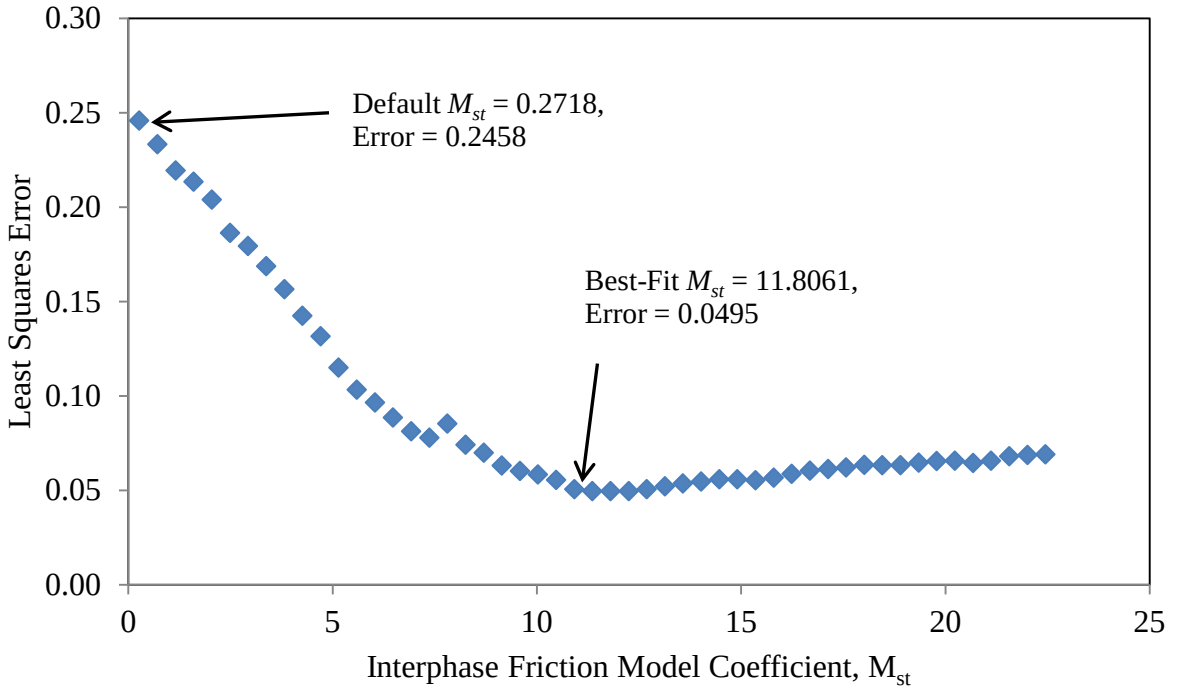

Figure 60: Average Least Squares Pressure Error for All Power Levels with an Orifice Plate Energy Loss Factor of 0.79

4.3: Spatial Resolution Study

As discussed earlier, the main body of the downcomer model featured a total of 10 volumes, with five pressure taps 0.0075 long, centered at the location of pressure taps, separated by a single volume apiece of varying length. There was some concern that having such large volumes within the downcomer may create discrepancies with how the downcomer is modeled and the validity of the data that was received from RELAP. To ensure that the spatial resolution of the downcomer was not a factor in the results that were obtained, a few sample model runs were chosen to be run and analyzed at both the standard resolution, but also at a higher spatial resolution, where each of the larger volumes in the main body of the downcomer are broken up into eight segments. Rather than analyzing the data output in text files by the shell program, output from the RELAP major edits was analyzed, so as to get the full effect of the resolution difference between model runs. As only one point in time would be analyzed, only steady state model runs were studied, for the sake of simplicity.

4.3.1: 95% Power, M_{st} = 5.1517

In Figure 61, the relative pressure profiles for 95% power and M_{st} = 5.1517 are shown for both the high resolution and low resolution RELAP model runs, along with the FOAK data to provide a standard for comparison. While the relative pressure profiles appear to be nearly identical to each other, there are some slight differences in the data. Both model runs converged to steady state, however the low resolution model run had a least squares error of 0.0307 while the high resolution model run had a least squares error of 0.0304 for the FOAK data points above the orifice plate. A look at individual points within each model run reveals that the pressure at

any of the given FOAK data points only differs by 0.0021, which given the pressures at which the OTSG downcomer is operating, may be considered to be insignificant.

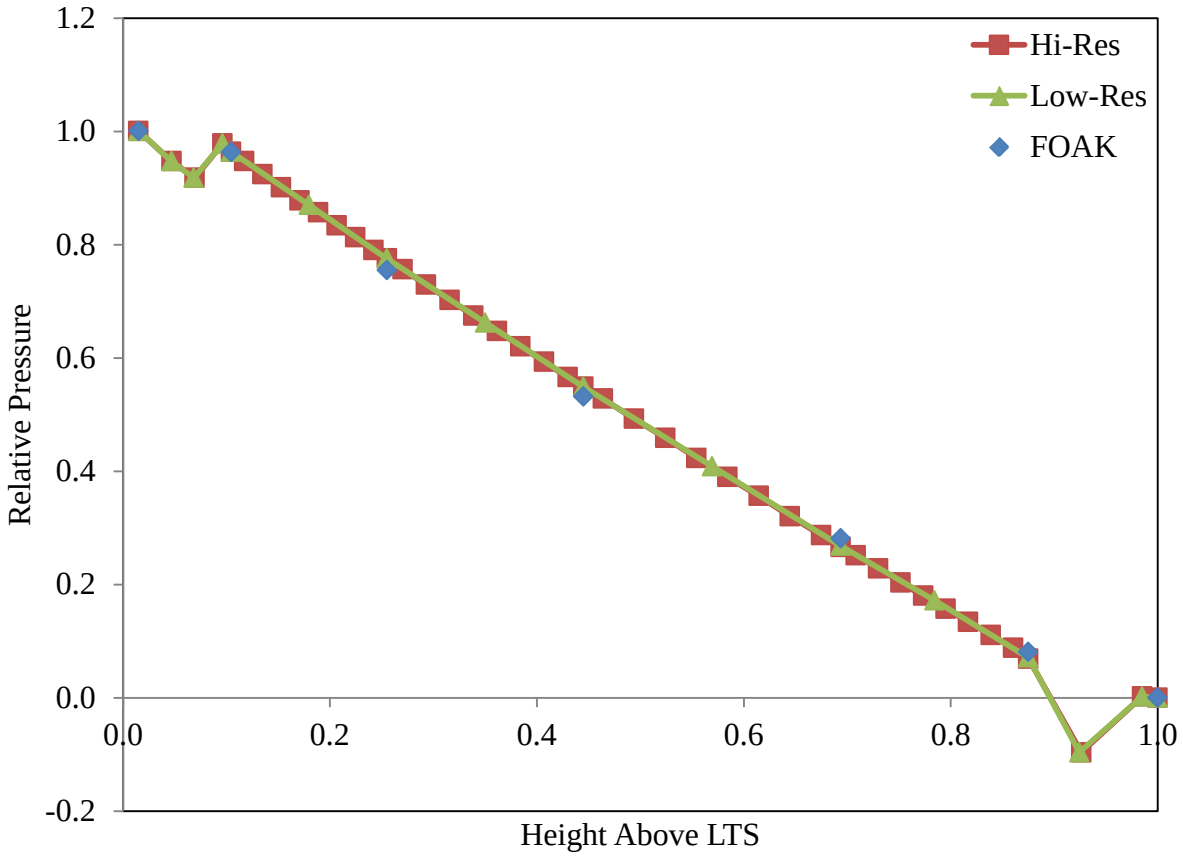

Figure 61: Relative Pressure Profile Comparison for 95% Power, M_{st} = 5.1517

Meanwhile, the void fraction ratio profiles provided in Figure 62 show that when the profile of a parameter is more curvaceous, the high-resolution model data serves as a smoother profile than the low-resolution model. In some instances, the smoothing of the profile may have a significant impact on the value of a given point. For example, the void fraction ratio predicted at the exit of the mixing section of the downcomer, the low-resolution model run predicted a void fraction ratio of 1.584 and the high-resolution model run predicted a void fraction ratio of 1.759. However, this difference does not appear to have a significant impact on void fraction ratio downstream of the mixing section, and most importantly at and below the orifice plate.

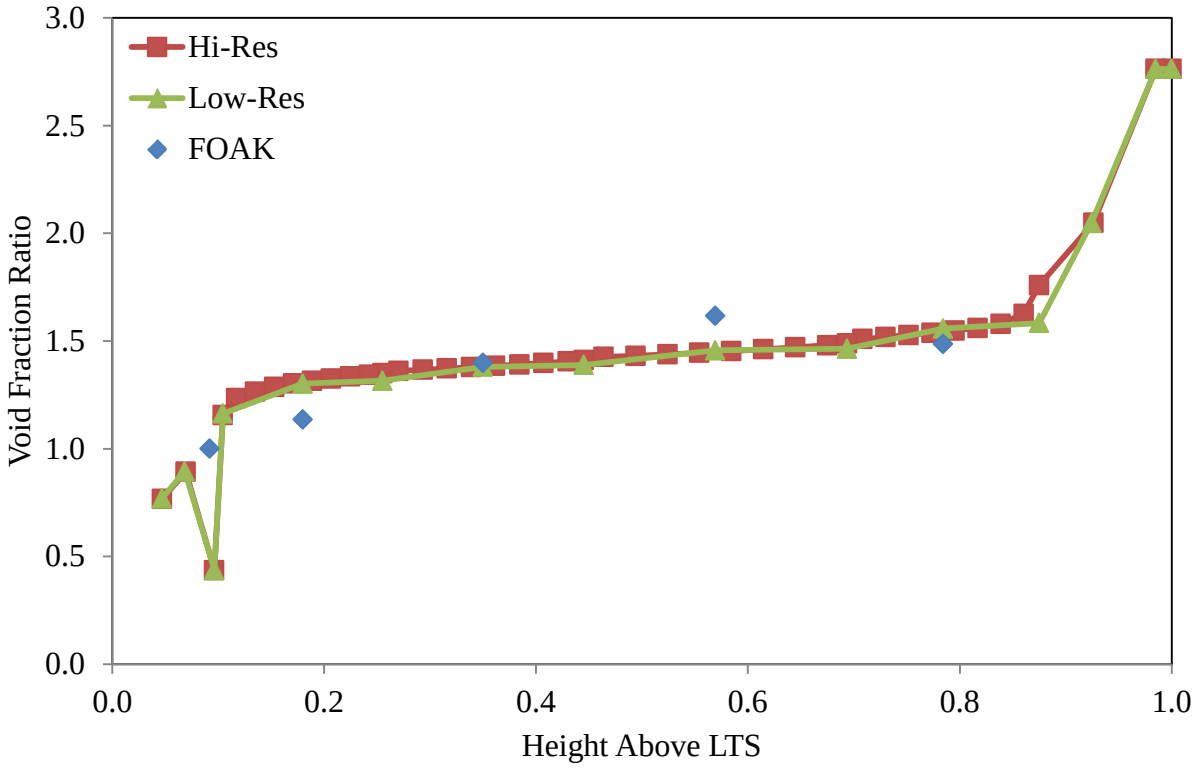

Figure 62: Void Fraction Ratio Profile Comparison for 95% Power, M_{st} = 5.1517

4.3.2: 95% Power, M_{st} = 11.8061

When the M_{st} value is raised to 11.8061, the relative pressure profiles between the high and low-resolution model runs continue to be nearly identical to each other, as shown in Figure 63. However, this similarity also carries over to the void fraction ratio profiles shown in Figure 64. With the increased interphase friction, the void fraction ratio profile becomes much more uniform throughout the downcomer, making the lower resolution model appear much closer to the higher resolution model than was the case in Figure 62. The only place in the downcomer where the higher resolution appears to overestimate the void fraction ratio near the orifice plate, which appears to be more the result of profile smoothing rather than an error in the data from the resolution.

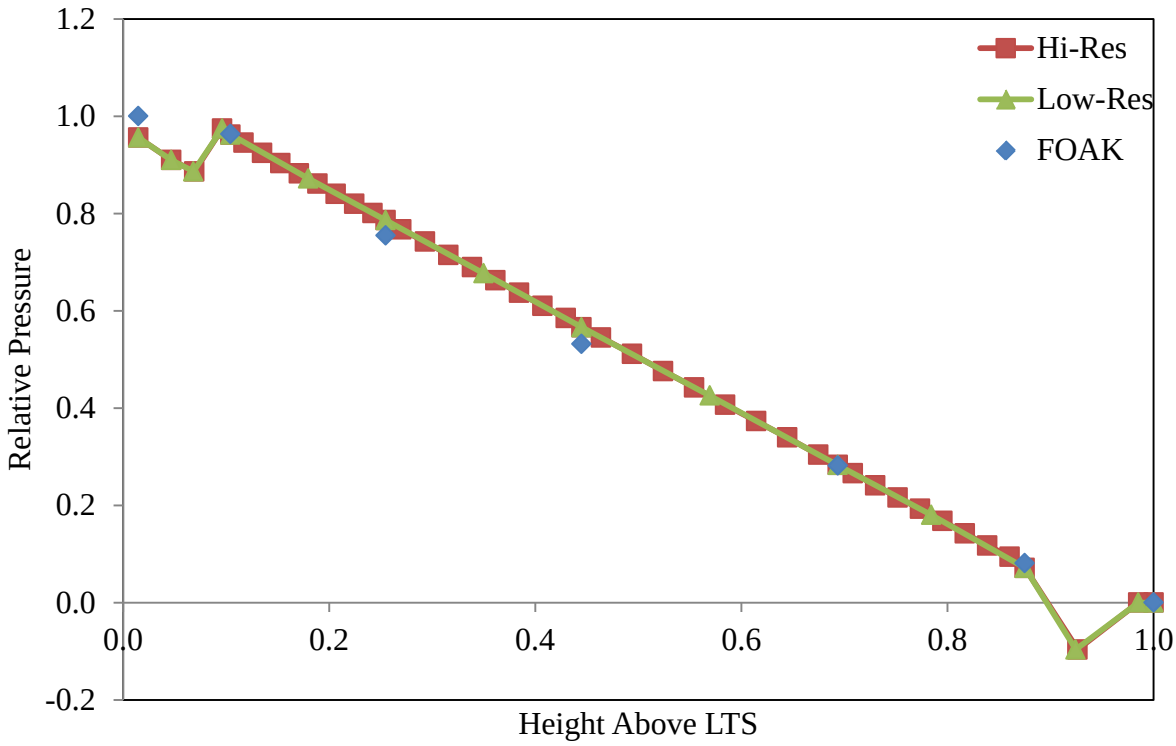

Figure 63: Relative Pressure Profile Comparison for 95% Power, M_{st} = 11.8061

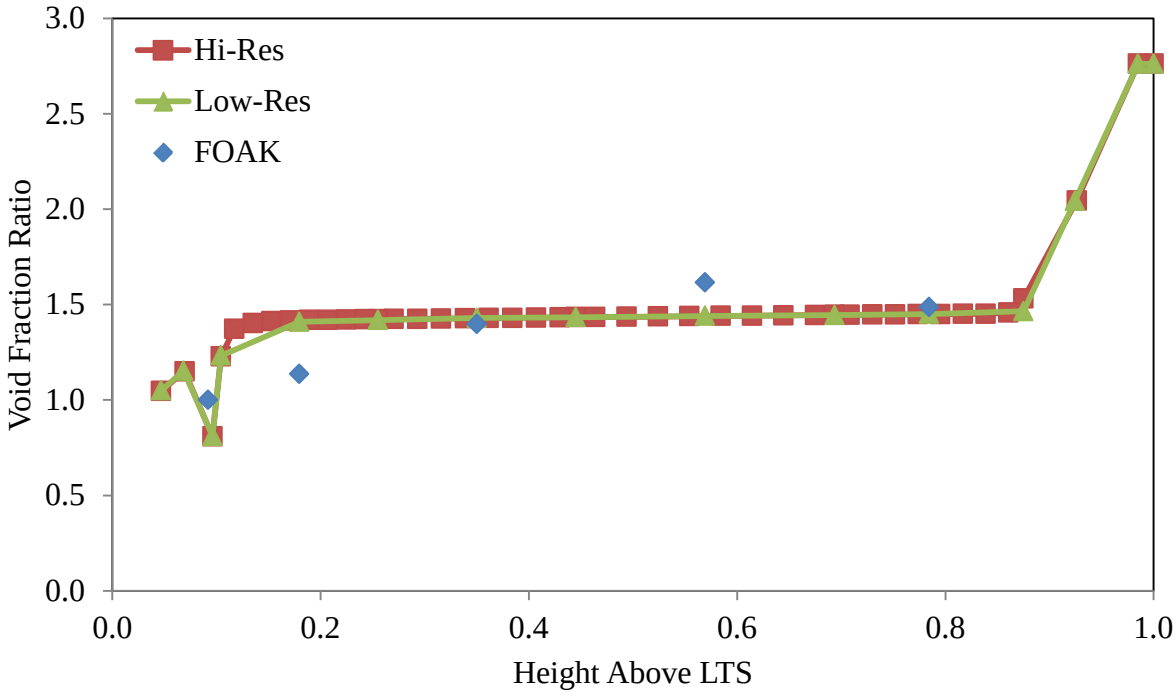

Figure 64: Void Fraction Ratio Profile Comparison for 95% Power, M_{st} = 11.8061

4.3.3: 75% Power, M_{st} = 11.8061

At 75% power with M_{st} = 11.8061, the relative pressure profile also appears to be largely unaffected by the change in resolution, as evidenced by Figure 65. However, the void fraction ratio profiles shown in Figure 66 reveal a difference in the void fraction ratio at the exit of the mixing section that cannot be explained as a simple smoothing error. While both model runs converged to steady state, and the least squares pressure errors were 0.0600 and 0.0621 for the low resolution and high resolution model runs, respectively, the void fraction ratio at the exit of the mixing section is 1.8330 for the high resolution model run and 1.3592 for the low resolution model run, a difference of over 22%. However, as Figure 66 shows, this difference in the void fraction ratio exiting the mixing section does not affect the void fraction ratio at lower points in the downcomer, where the high-resolution model appears to be a smoothed version of the low-resolution model.

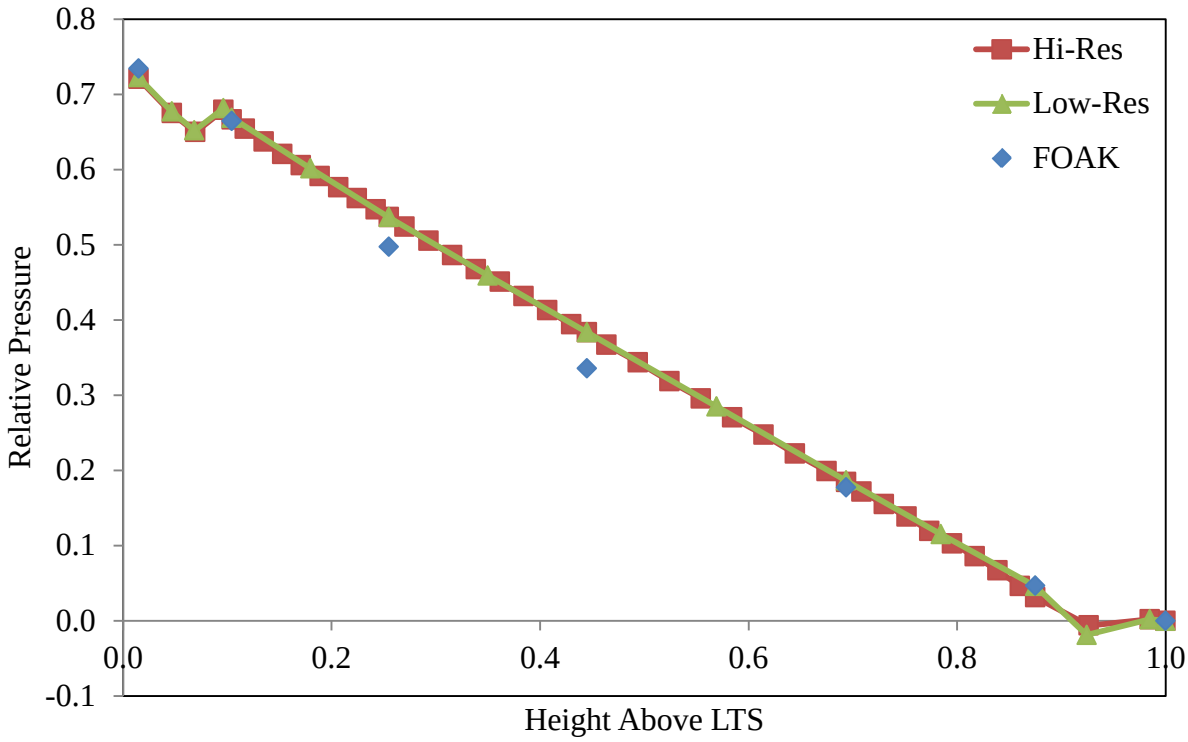

Figure 65: Relative Pressure Profile Comparison for 75% Power, M_{st} = 11.8061

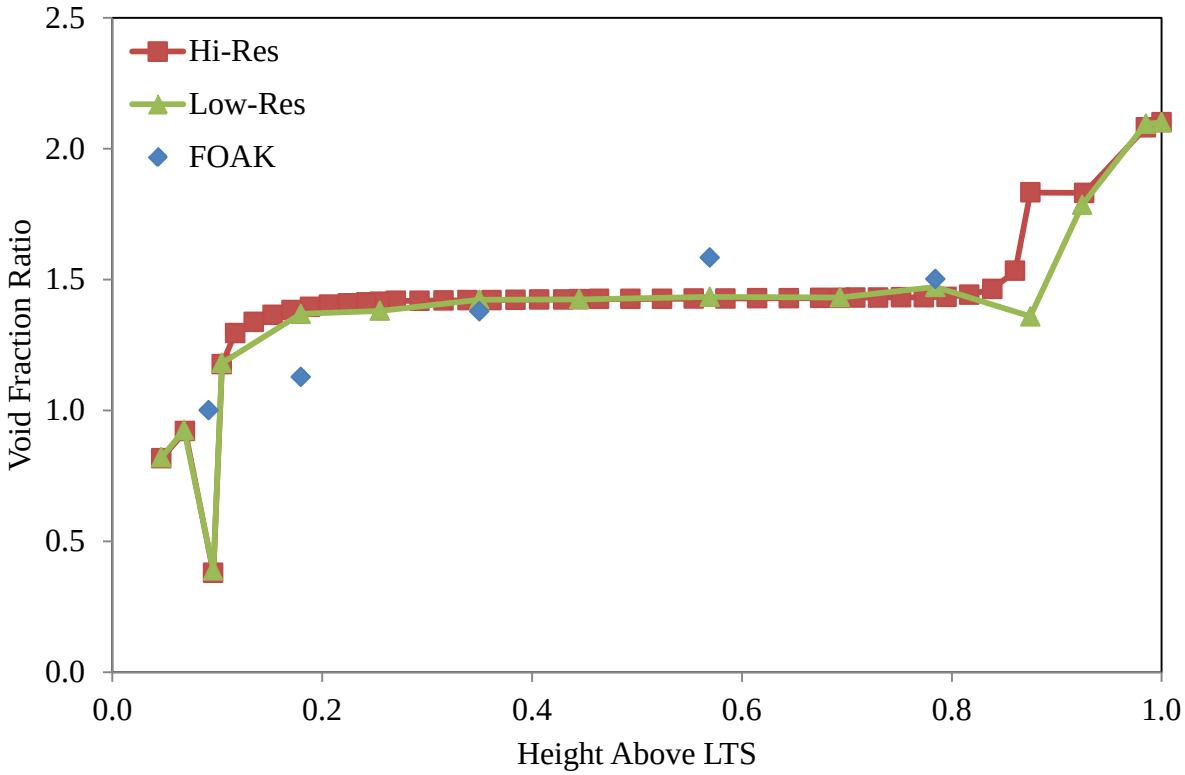

Figure 66: Void Fraction Ratio Profile Comparison for 75% Power, M_{st} = 11.8061

For the examples shown, the resolution does not appear to significantly impact the relative pressure profile, nor does it have an effect on the void fraction ratio immediately above, at or below the orifice plate, and only has an effect at the exit of the mixing chamber. Since this study is intended to focus primarily on the void fraction ratio in the vicinity of the orifice plate, then the effect that resolution has on void fraction ratio outside the mixing section is considered irrelevant to this particular study, but merit further investigation that is beyond the scope of this project. All further model data shown will focus on the void fraction ratio at and near the orifice plate, thus the usage of the low-resolution model remains valid.

4.4: Downcomer-Tube Nest Interaction

The OTSG downcomer model that has been developed only represents a small portion of the OTSG, although the downcomer model could be implemented into a full OTSG model. In order for that to occur, it is important to understand how the downcomer interacts with its boundaries, particularly those within the OTSG. For the OTSG downcomer model, there are three boundary conditions that determine the thermohydraulic properties within the downcomer: the mass flow rate of the feedwater, the static quality of the steam/water entering at the aspirator port, and the pressure rise that occurs within the downcomer. The mass flow rate of the feedwater is controlled externally of the OTSG, and has already been studied in Sections 4.1 and 4.2, as it is a function of the power level. Meanwhile, the aspirator port static quality and downcomer pressure rise are boundary conditions within the OTSG, as they describe interactions with the tube nest.

In all prior cases, the steam/water static quality at the aspirator port was assumed to be 1.0, i.e. the steam at the aspirator port was at saturation for the pressure specified within the FOAK report [5]. In a parametric study where the aspirator port static quality varied from 0.75 to 1.00, water property errors caused RELAP to fail to produce any results when the quality was below 0.95. For quality values between 0.95 and 1.0, RELAP model runs produced results that had insignificant variations in the relative pressure and void fraction ratio profiles.

Previously, the downcomer pressure rise has been set to the value reported in the FOAK report [5] for the corresponding power level. However, for a given power level, changes in the downcomer pressure affect the amount of steam that is added to the mixture through the aspirator port by RELAP, which has very significant consequences with regards to steam condensation, flow regime, interphase friction and vapor carry-under. For each power level, a parametric study

has been performed on the downcomer pressure rise, varying from 0.0105 to 2.2767, the static head of liquid water at 925 psi for the total height of the downcomer. [13] In Section 4.5, the FOAK downcomer pressure rise has been extrapolated to power levels exceeding 95% power, and compared to parametric studies on the downcomer pressure rise at those power levels.

In the results shown, the void fraction ratio at the orifice plate and at the FOAK data point at 0.1797 above the LTS are compared to the downcomer pressure rise. The reason for examining the orifice plate void fraction ratio is to understand the amount of carry-under that would occur in each case and to understand how the amount of carry-under changes with changes in the pressure profile. As has been observed in the void fraction ratio profiles, the RELAP model void fraction ratio values at the orifice plate differ from the FOAK values, largely because RELAP predicts a liquid buildup at the orifice plate, that is not taken into account with the linear extrapolation of the void fraction ratio in the FOAK data. A plot with error bars indicates that the RELAP model run for the given downcomer pressure rise did not converge to steady state, with the plot reflecting the average void fraction ratio for the final 100 seconds of a 900 second run, while the error bars reflect the high and low void fraction ratio during that time frame. Meanwhile, the FOAK data point at 0.1797 above the LTS provides insight into understanding the steam/water flow in the downcomer, with a minimized momentum effect from the feedwater nozzles.

The data has been broken up by flow regimes representative of significant volumes within the downcomer model to understand discontinuities in the void fraction ratio profile. The letter "D" indicates the annular-mist, or droplet flow regime, "S" indicates slug flow and "B" indicates bubbly flow. Each volume is identified as part of a three component sequence of flow regimes, the first letter being the mode-average flow regime for the volumes in the main body of

the downcomer (between 0.8750 and 0.1044 above the LTS), the second letter representing the flow regime in the volume immediately above the orifice plate, while the third letter represents the flow regime in the branch connection just below the orifice plate. Thus a sequence identified as "DSD" indicates that the predominant flow regime between 0.8750 above the LTS and 0.1044 above the LTS is annular-mist flow, the flow regime immediately above the orifice plate is slug flow and the flow regime below the orifice plate is annular-mist flow. Table 11 shows each regime sequence code that was observed in RELAP, along with the corresponding flow regime for each portion of the downcomer that is represented in the code.

Table 11: Flow Regime Sequences Used in Sections 4.4 and 4.5

	Flow Regime		
Code	Downcomer Mode	Above Orifice Plate	Below Orifice Plate
DDD	Annular-Mist	Annular-Mist	Annular-Mist
DSD	Annular-Mist	Slug	Annular-Mist
DSS	Annular-Mist	Slug	Slug
SSS	Slug	Slug	Slug
SBS	Slug	Bubbly	Slug
SBB	Slug	Bubbly	Bubbly
BBB	Bubbly	Bubbly	Bubbly

The appearance of annular-mist flow within the downcomer only occurs when the downcomer pressure rise is significantly less than what the FOAK data indicates. Since the amount of liquid being added to the system is constant for each power level, the appearance of droplet flow would indicate RELAP is adding an excess amount of steam in order to achieve the desired pressure rise within the downcomer. For the FOAK data, the density and void fraction ratio profiles calculated by RELAP indicate that slug flow should be the predominant flow regime throughout the main portion of the downcomer, and RELAP is adding roughly the right amount of steam to the system to produce that profile. As the downcomer pressure rise

increases, the amount of steam that RELAP adds decreases, resulting in the formation of a liquid level, and the flow regime becoming bubbly throughout the downcomer. The issue of flood-back becomes especially dangerous for the downcomer when the liquid level approaches the feedwater inlets of the downcomer model. Based on the operating pressure of the downcomer, and assuming a hydrostatic pressure rise throughout the downcomer, this would occur with a pressure rise of 2.2767.

Each power level was modeled using the B&W modified slug drag scheme to model the interphase friction, with M_{st} set to 11.8061, except for 95% power, which was also modeled at M_{st} = 5.1517.

4.4.1: 95% Power, M_{st} = 5.1517

In Figure 67, the void fraction ratio at the orifice plate is shown for various pressure rises over the downcomer, with the power level set to 95% power and the M_{st} value set to 5.1517. Figure 68 shows the corresponding void fraction ratio values at 0.1797 above the LTS. The FOAK void fraction ratio and corresponding downcomer pressure rise are also given as a point of comparison. RELAP indicated that at 95% power, the flow regime pattern for the downcomer is predominantly slug flow, with a buildup of liquid at the orifice plate changing the flow regime to bubbly flow at the orifice plate, followed by a return to slug flow below the orifice plate, as seen in Figure 33.

When the mode flow regime throughout the downcomer changes from annular-mist to slug flow, the void fraction ratio at 0.1797 above the LTS increases, but the void fraction ratio at the orifice plate decreases. This indicates that the slug flow interphase friction in the downcomer is working to distribute the vapor throughout the downcomer evenly, while letting liquid water accumulate only in the volume immediately above the orifice plate.

A small jump discontinuity in the void fraction ratio profile can be noticed within the slug-bubbly-slug flow profile at a downcomer pressure rise of 1.1637, and coincides with a flow regime change in the pipe that connects the branch connection beneath the orifice plate to the tube nest from slug flow to bubbly flow. The jump discontinuity that is observed with a downcomer pressure rise of 1.6817 coincides with the flow regime changing from slug to bubbly flow in the mixing section, indicating that the liquid level is very close to the feedwater nozzles.

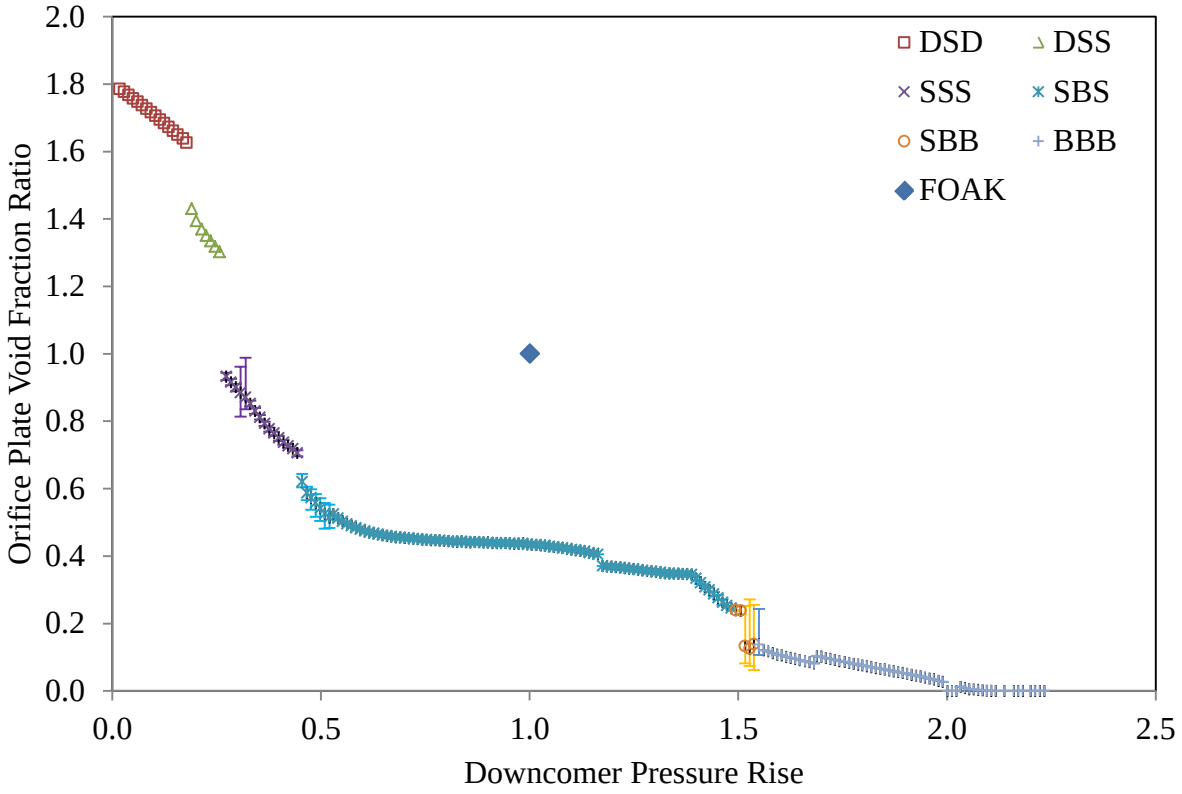

Figure 67: Orifice Plate Void Fraction Ratio for Varying Downcomer Pressure Rises at 95% Power, M_{st} = 5.1517

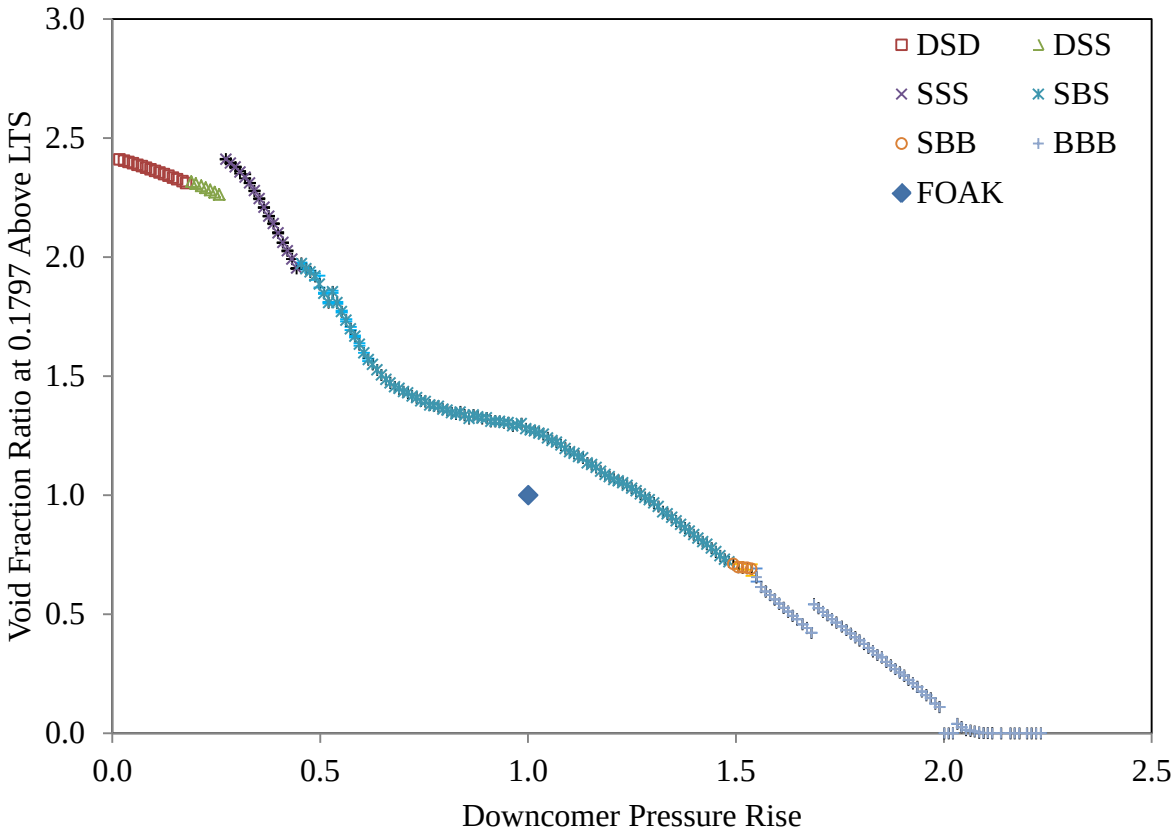

Figure 68: Void Fraction Ratio at 0.1797 Above LTS for Varying Downcomer Pressure Rises at 95% Power, M_{st} = 5.1517

4.4.2: 95% Power, M_{st} = 11.8061

When the M_{st} value is increased to 11.8061 for 95% power, the slug flow regime pattern occurs throughout the downcomer as evidenced by Figure 69 and Figure 70, as well as Figure 33. The increased interphase friction drags more vapor downward, resulting in a higher void fraction ratio at the orifice plate, while the even distribution noticed when M_{st} = 5.1517 is maintained. RELAP interprets the higher void fraction ratio at the orifice plate as being more likely to be in the slug flow regime, hence the reason why more model runs had slug flow throughout the downcomer with M_{st} = 11.8061 than with M_{st} = 5.1517. It also appears to extend the range of downcomer pressure rises for which slug flow is dominant in the main part of the downcomer because at M_{st} = 5.1517, the slug flow regime dominates the downcomer for a pressure rise as

low as 0.2731, while at M_{st} = 11.8061, a pressure rise of 0.3442 is required. Meanwhile, bubbly flow in the main part of the downcomer occurs starting at 1.6014 for M_{st} = 11.8061, but starts at 1.5497 for M_{st} = 5.1517.

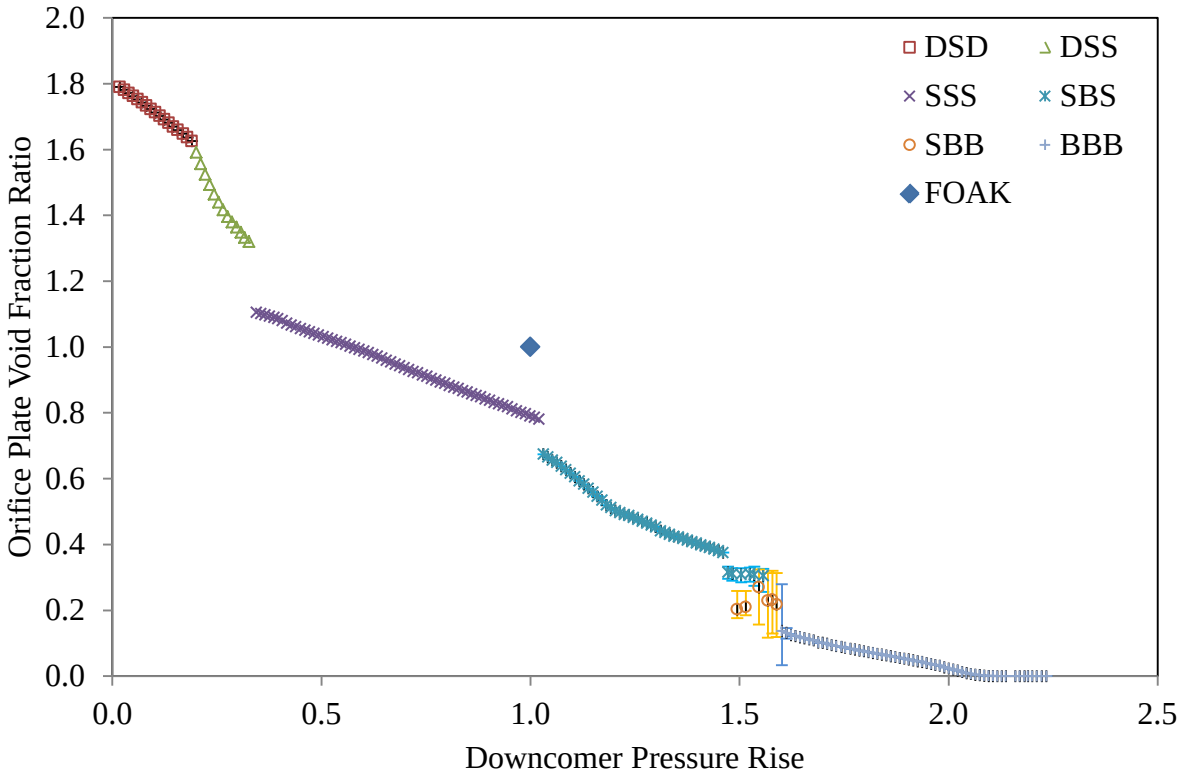

Figure 69: Orifice Plate Void Fraction Ratio for Varying Downcomer Pressure Rises at 95% Power, M_{st} = 11.8061

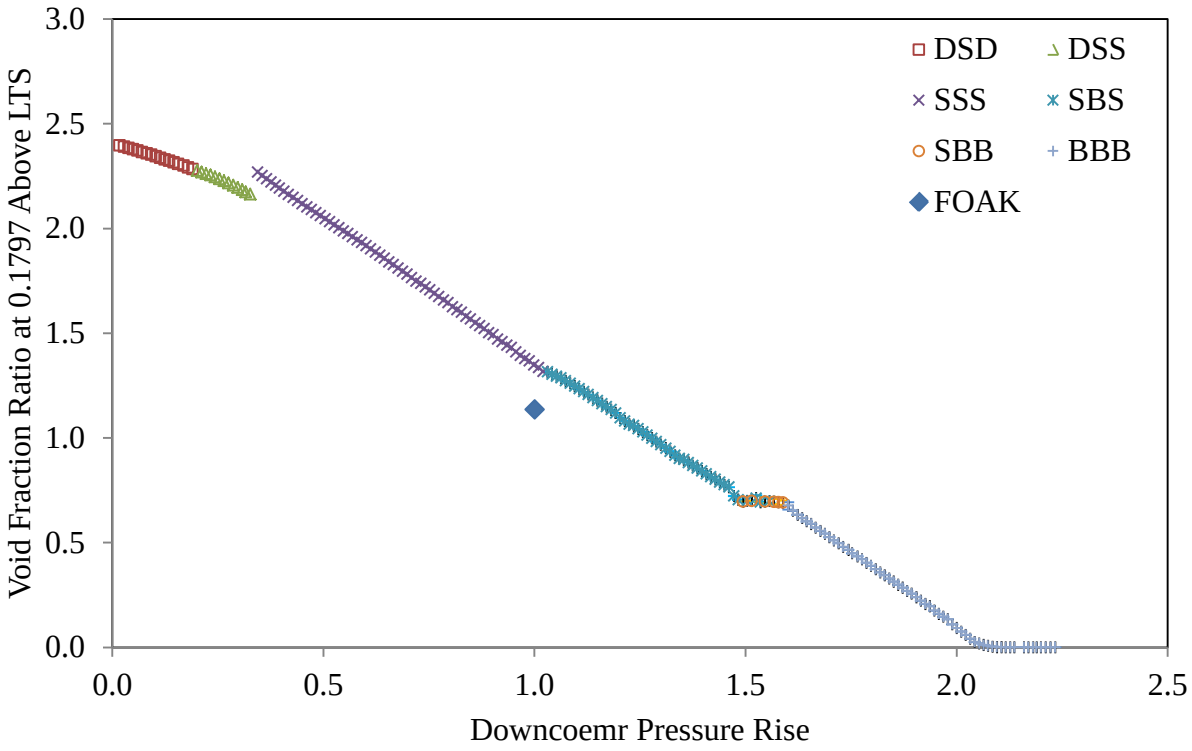

Figure 70: Void Fraction Ratio at 0.1797 Above LTS for Varying Downcomer Pressure Rises at 95% Power, M_{st} = 11.8061

4.4.3: 85% Power, M_{st} = 11.8061

At 85% power, the downcomer pressure rise indicates that the flow regime pattern is predominantly slug throughout the downcomer, and slug below the orifice plate, but immediately above the orifice plate the flow regime is bubbly flow. Figure 71 and Figure 72 show that RELAP predicts that the slug flow regime would occur throughout the main body of the downcomer for a range of downcomer pressure rises ranging from 0.3302 to 1.6116.

The discontinuity in the orifice plate void fraction ratio profile at a downcomer pressure rise of 1.2907 can be explained by the flow regime entering into the tube nest changing from slug to bubbly flow. However, the orifice plate void fraction ratio discontinuity at 0.7661 cannot be explained by a flow regime change. There is a slight drop in the liquid velocity and a slight increase in the vapor velocity in the volume above the orifice plate that occurs at the

discontinuity. This results in an increase in the velocity difference between the vapor and liquid, which increases the interphase friction force, causing more vapor to be dragged down through the orifice plate. RELAP uses different methods for determining the velocity difference between vapor and liquid within the slug flow regime, and it is likely that the circumstances caused a switch in method used to determine the velocity difference. However, the RELAP output does not provide any indication as to which method is used for a given circumstance, and determining the exact cause of the switch would require a study of the source code that is beyond the scope of this research project.

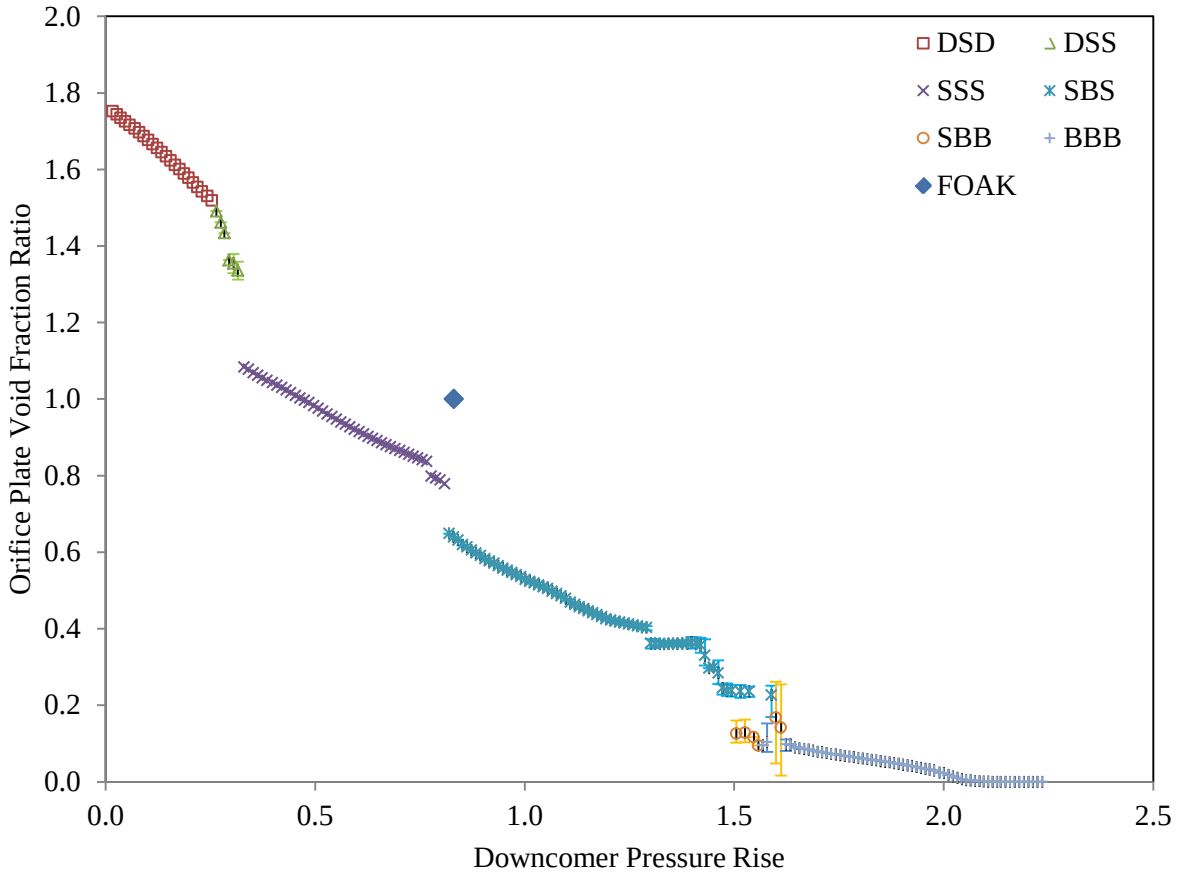

Figure 71: Orifice Plate Void Fraction Ratio for Varying Downcomer Pressure Rises at 85% Power

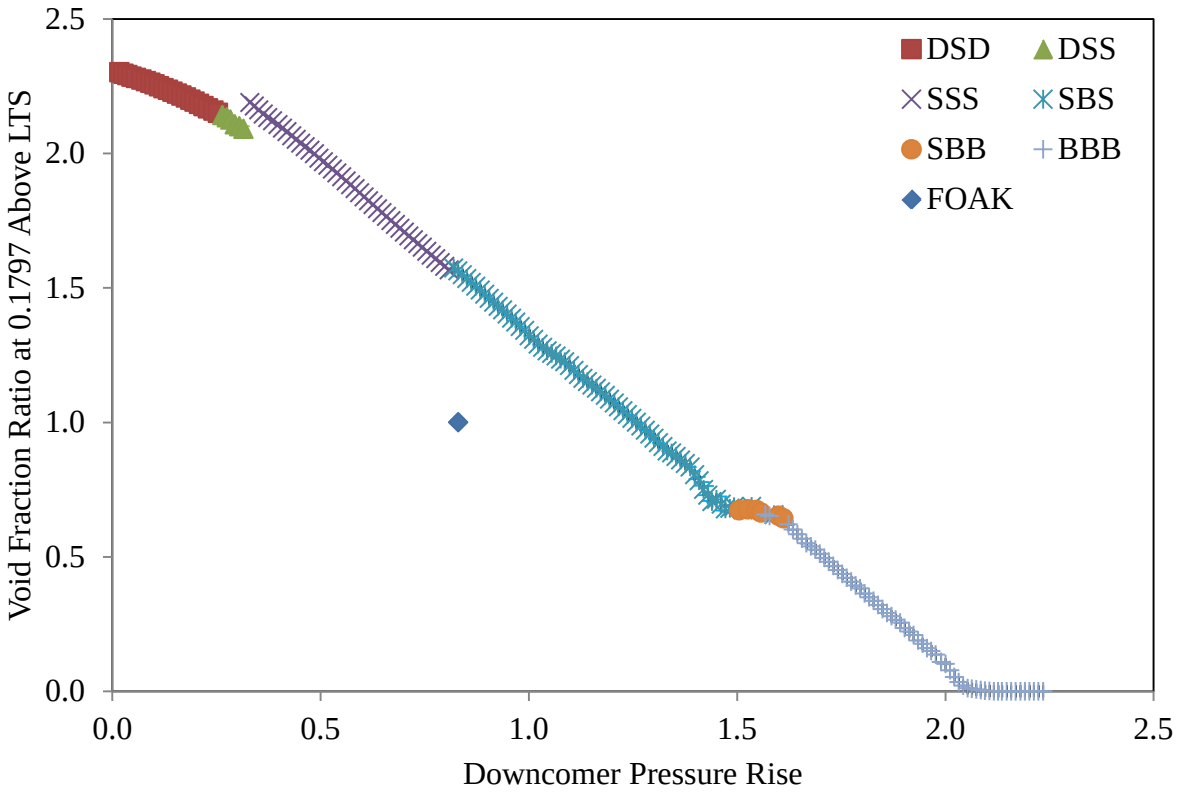

Figure 72: Void Fraction Ratio at 0.1797 Above LTS for Varying Downcomer Pressure Rises at 85% Power

4.4.4: 75% Power, M_{st} = 11.8061

At 75% power, Figure 73 and Figure 74 show how the void fraction ratio at the orifice plate and at 0.1797 above the LTS vary with increasing downcomer pressure rise, respectively. According to the data, slug flow is the predominant flow regime throughout the main part of the downcomer, with bubbly flow above the orifice plate and slug flow below the orifice plate. Slug flow throughout the downcomer starts at a pressure rise of 0.2979 and extends to as high as 1.6364. One difference between the data at 75% power and lower power levels versus the data and 85% and 95% power is the absence of the droplet-slug-slug regime, as the transition droplet to slug flow occurs simultaneously for the main body of the downcomer and the branch connection below the orifice plate.

While no major discontinuities or jumps occur in the void fraction ratio profile at 0.1797 above the orifice plate, the orifice plate void fraction ratio profile presents a change in the void fraction ratio profile pattern at 0.4436, similar to the discontinuity seen at 85% power with a downcomer pressure rise of 0.7661. The liquid and vapor velocity in the volume above the orifice plate decreases with increasing downcomer pressure rise, until 0.4436, when the vapor velocity levels off. Meanwhile the liquid velocity continues to decrease beyond the discontinuity at 0.4436. The result is a sharp increase in the velocity difference between the vapor and the liquid, increasing the interphase friction force and dragging more vapor below the orifice plate.

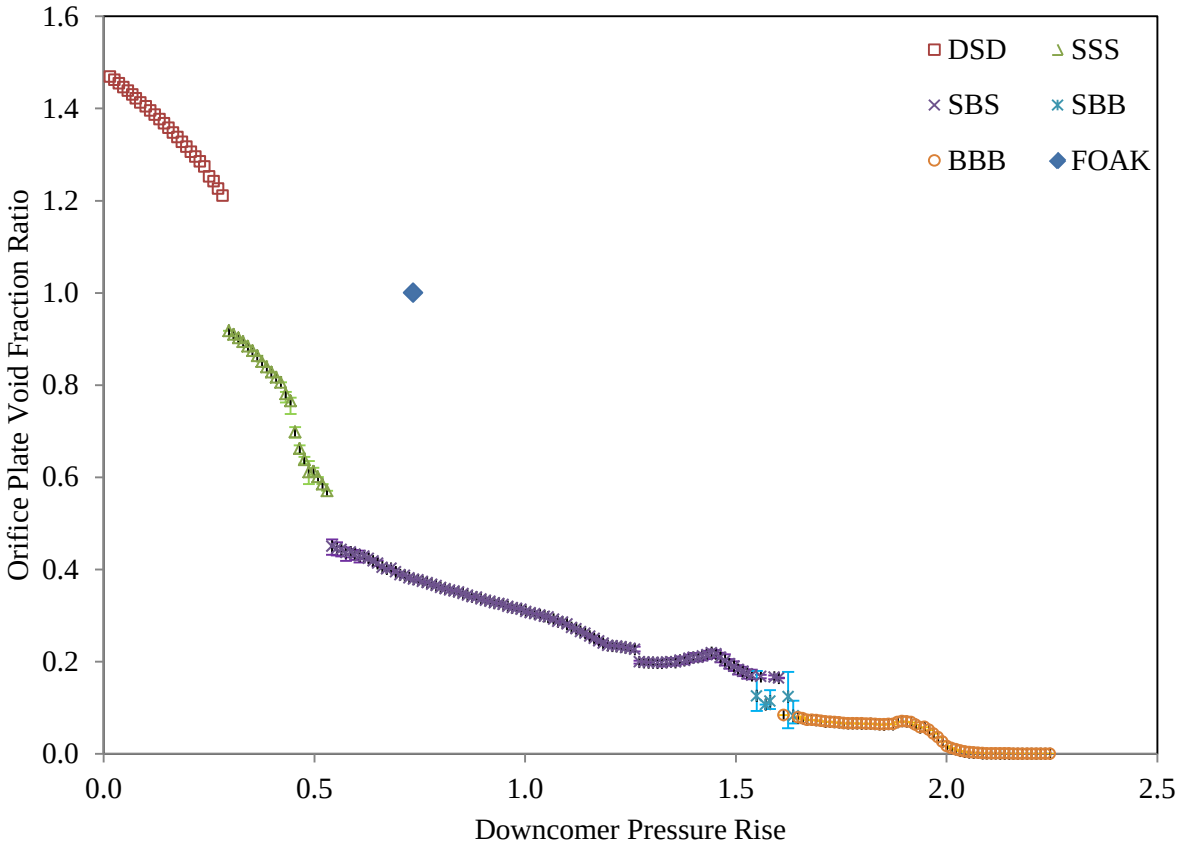

Figure 73: Orifice Plate Void Fraction Ratio for Varying Downcomer Pressure Rises at 75% Power

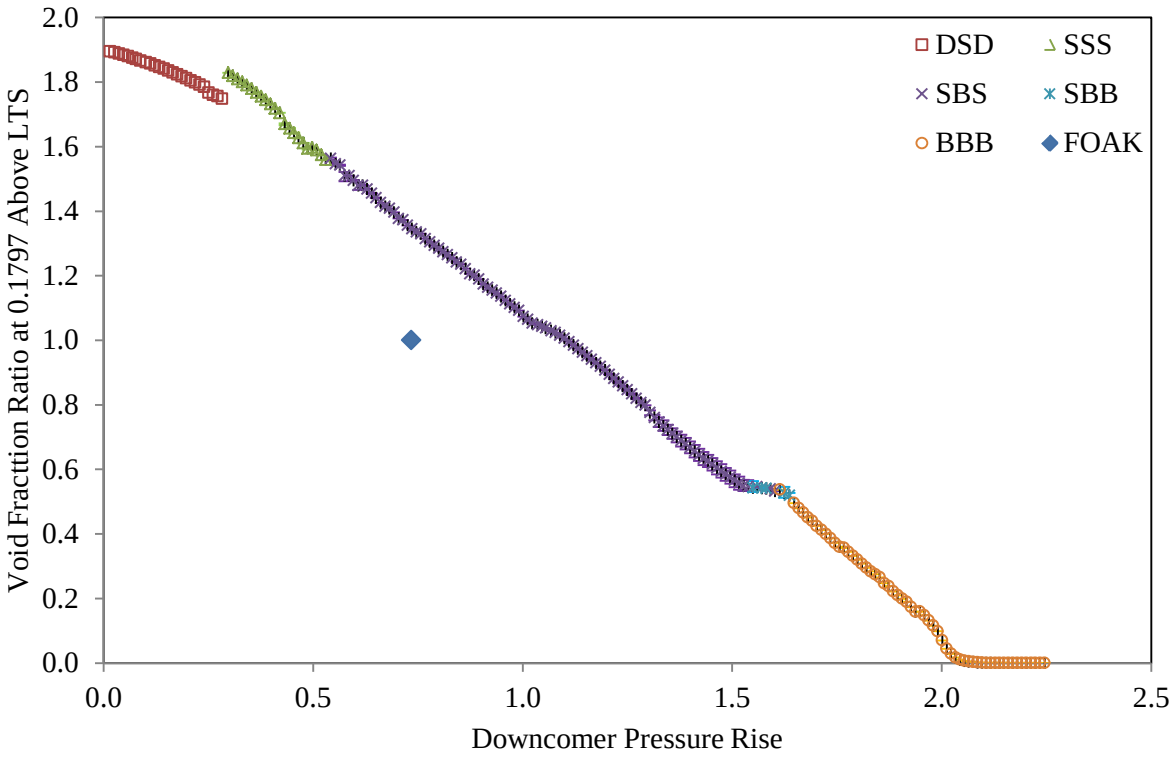

Figure 74: Void Fraction Ratio at 0.1797 Above LTS for Varying Downcomer Pressure Rises at 75% Power

4.4.5: 65% Power, M_{st} = 11.8061

Figure 75 shows the orifice plate void fraction ratio compared to the downcomer pressure rise at 65% power, while Figure 76 shows the void fraction ratio at 0.1797 above the LTS. The flow regime profile at 65% power that correlates to the FOAK data is the slug-bubbly-slug profile, with slug flow being the predominant flow regime in the main body of the downcomer ranging from a downcomer pressure rise of 0.2866 to 1.6258. Velocity data does not indicate a discontinuity within the slug-slug-slug flow regime profile as was indicated at 85% and 75% power. The discontinuity at 1.1865 does correlate to the change from slug to bubbly flow in the pipe connecting the branch below the orifice plate to the tube nest, like the discontinuities seen at higher power levels.

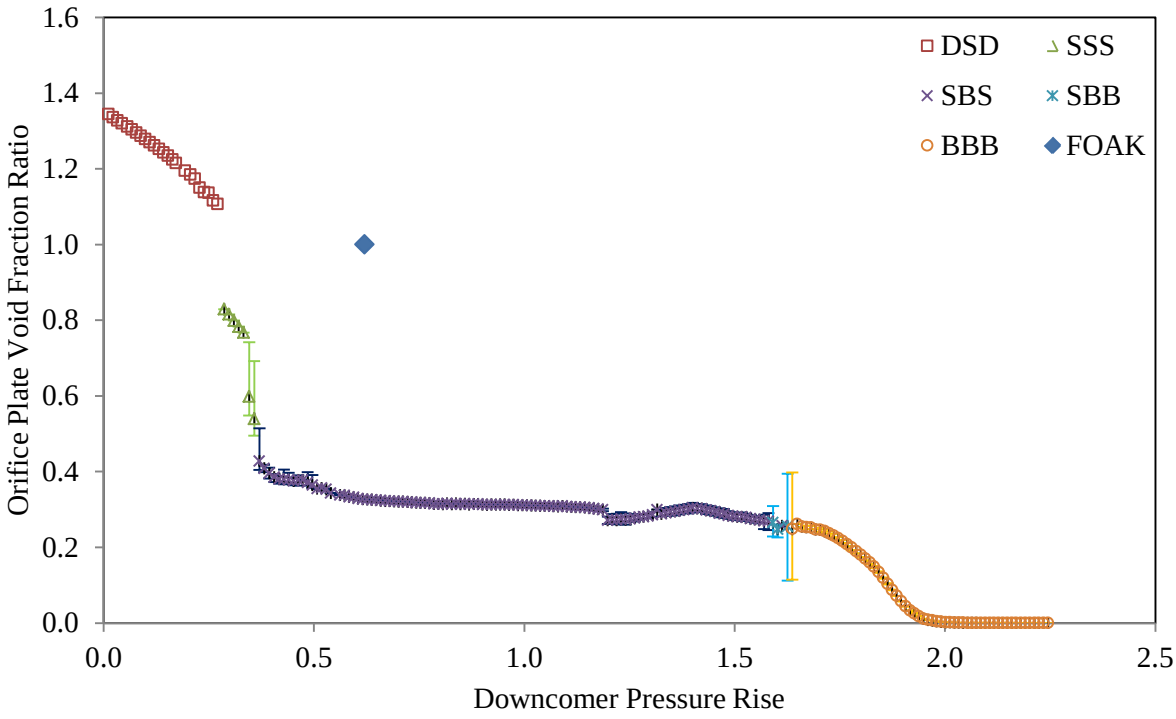

Figure 75: Orifice Plate Void Fraction Ratio for Varying Downcomer Pressure Rises at 65% Power

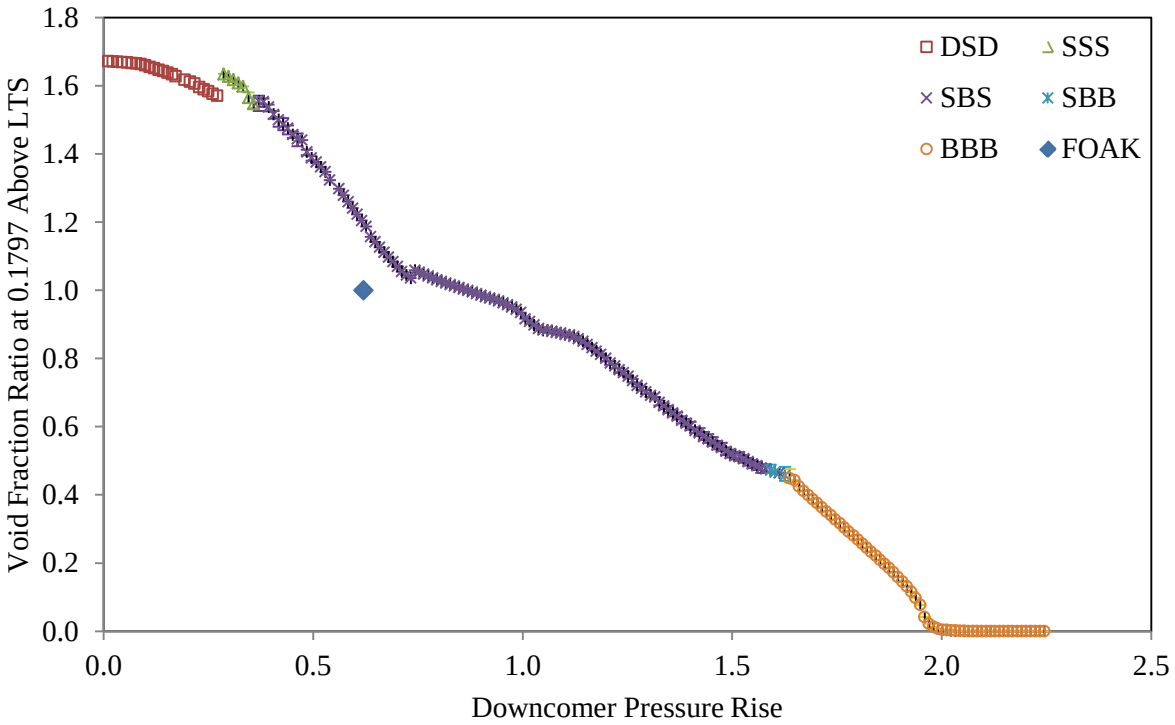

Figure 76: Void Fraction Ratio at 0.1797 Above LTS for Varying Downcomer Pressure Rises at 65% Power

4.4.6: 55% Power, M_{st} = 11.8061

At 55% power, RELAP indicates that the downcomer has a slug-slug-slug flow regime pattern, based on the void fraction ratio comparisons made to the downcomer pressure rises made in Figure 77 and Figure 78. This pattern is in contrast to the slug-bubbly-slug flow regime pattern seen at higher power levels. For downcomer pressure rise values less than 0.0766, droplet flow is present throughout the downcomer, reflecting how small the amount of liquid is that is being added to the system. Slug flow in the main part of the downcomer begins at a downcomer pressure rise of 0.2662 and ends at 1.6475.

While there are no significant discontinuities that cannot be explained by the flow regime patterns depicted, there is an oddity involving the slug-bubbly-slug flow regime pattern that occurs over two different sets of downcomer pressure rises. At all other power levels, the slug-bubbly-slug flow regime pattern only occurs at downcomer pressure rise values that are greater than those of the slug-slug-slug flow regime pattern. However, RELAP has the pattern occurring for pressure rises varying from 0.3139 to 0.3513. One possible cause is that at 0.3139, the flow regime in the mixing section also changes from droplet to slug flow, but it does not change back to droplet at 0.3513. The liquid velocity in the volume above the orifice plate experiences a jump increase at 0.3139, while vapor velocity steadily decreases throughout the interval. This indicates that the interphase friction force weakens, causing less vapor to be dragged into the volume, potentially causing the volume flow regime to switch to bubbly flow, if the orifice plate void fraction ratio dropped below 0.3737.

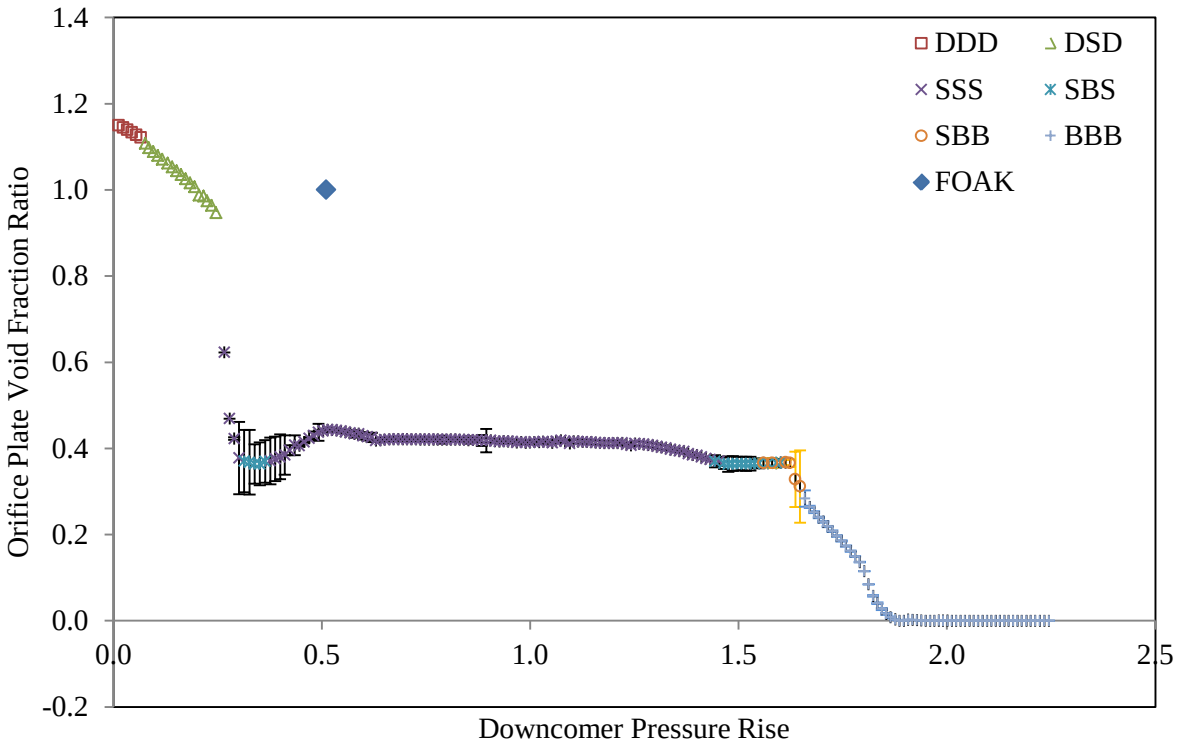

Figure 77: Orifice Plate Void Fraction Ratio for Varying Downcomer Pressure Rises at 55% Power

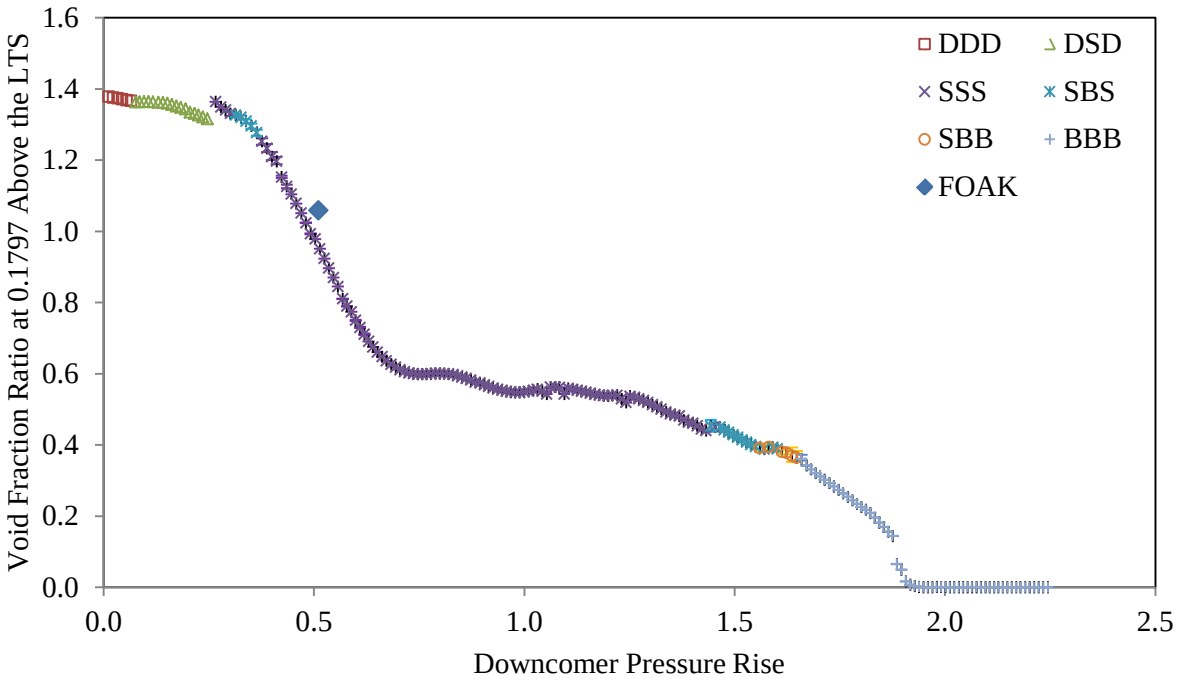

Figure 78: Void Fraction Ratio at 0.1797 Above LTS for Varying Downcomer Pressure Rises at 55% Power

4.4.7: 45% Power, M_{st} = 11.8061

Figure 79 and Figure 80 show the void fraction ratio at the orifice plate and 0.1797 above the LTS with the corresponding downcomer pressure rise at 45% power, respectively. As is the case with 55% power, the flow regime pattern for the FOAK downcomer pressure rise is slug-bubbly-slug flow. The slug flow regime in the main body of the downcomer begins at a pressure rise of 0.2408 and ends at 1.6636.

While there are no significant discontinuities, the dip in orifice plate void fraction ratio merits further study. The dip does not occur with any fluctuation in the flow regime pattern. The velocity difference between vapor and liquid is at a maximum for the dip, indicating that the interphase friction force should also be at a maximum, and that more vapor should be dragged into volume, increasing the void fraction ratio, rather than decreasing it. This anomaly is likely caused by an anomaly within the code that would require further studying beyond the scope of this project.

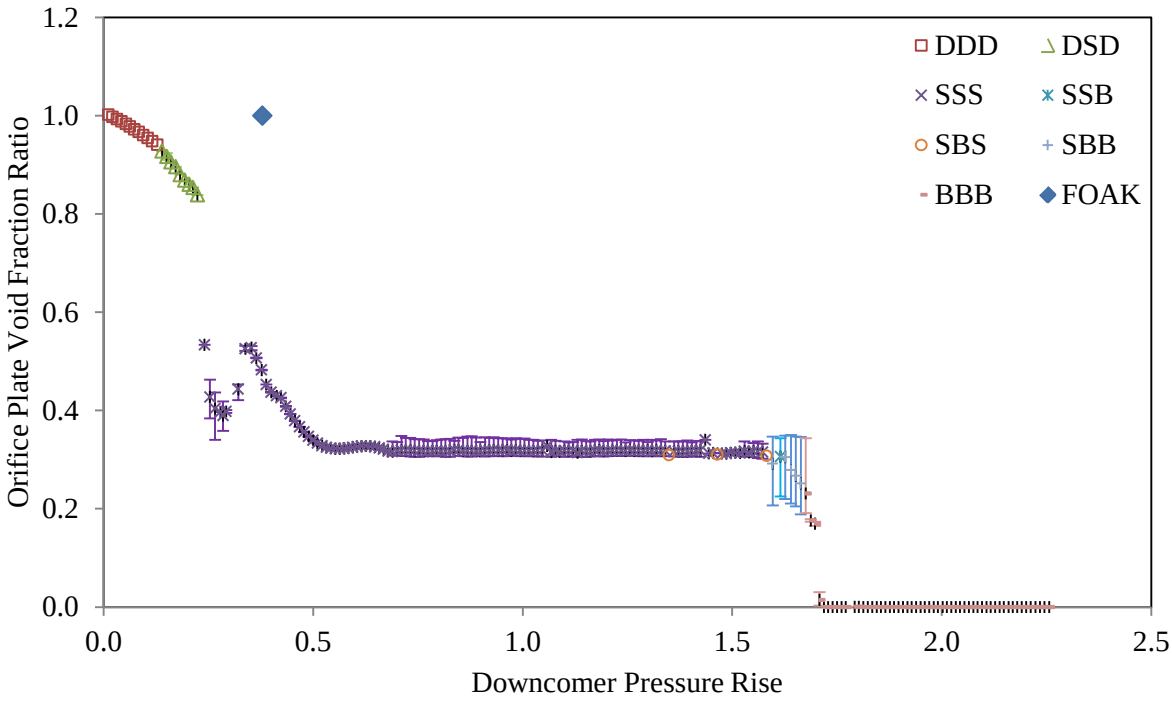

Figure 79: Orifice Plate Void Fraction Ratio for Varying Downcomer Pressure Rises at 45% Power

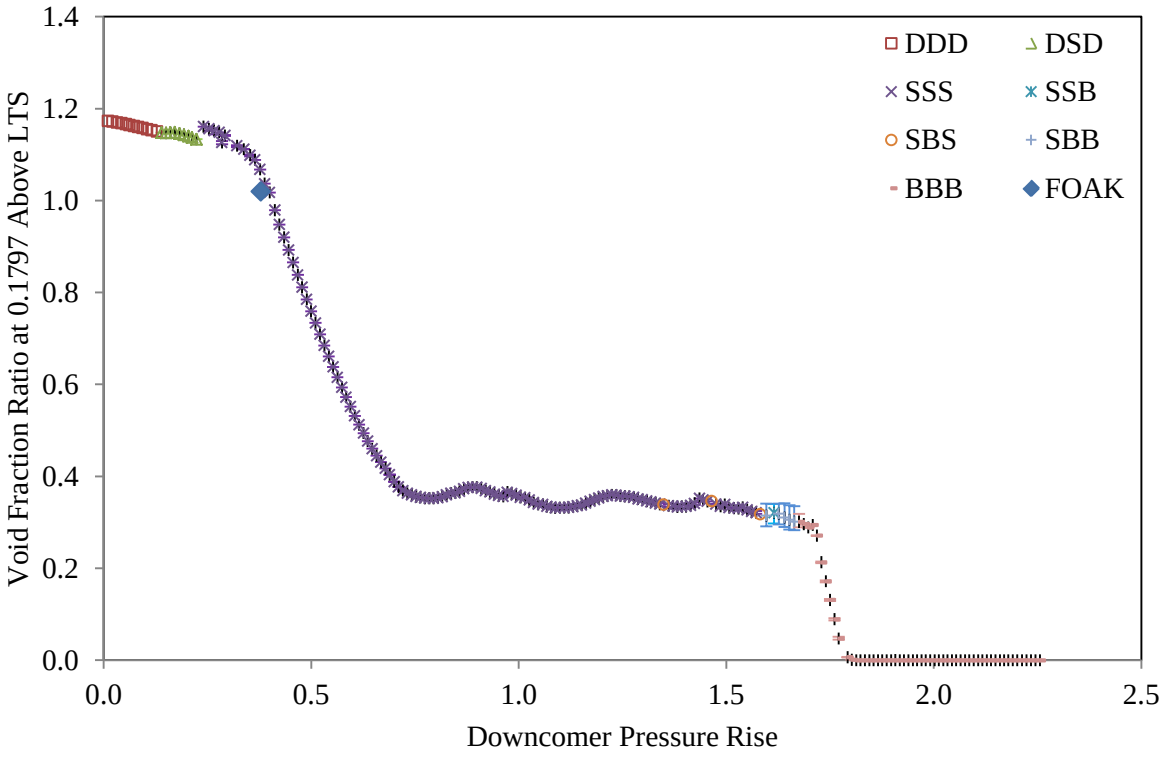

Figure 80: Void Fraction Ratio at 0.1797 Above LTS for Varying Downcomer Pressure Rises at 45% Power

By varying the downcomer pressure rise, it is shown that for the FOAK power levels, the downcomer is performing as expected, and that the downcomer is in no danger of experiencing flood-back. From the data that has been retrieved, it can be determined that flood-back would be a concern if the downcomer pressure rise were to be increased to a value of at least 1.5723, where the flow regime for the main body of the downcomer is bubbly.

4.5: Extrapolations to Higher Power Levels

While the flow regime for the main body of the downcomer is slug flow for all of the power levels that were tested in the FOAK data, there is a distinct possibility that if the power were to be raised above 100%, the downcomer pressure rise could be great enough that the bubbly flow regime would become the predominant flow regime throughout the downcomer. With power companies needing to raise their power output and the development of the E-OTSG, testing for power levels above 100% is a necessity. By running tests of the RELAP OTSG downcomer model for power levels exceeding 100%, it can be determined what power level would be the limit for which a nuclear plant could operate.

4.5.1: Extrapolating the FOAK Data

No data for higher power levels was given, but instead was extrapolated from the given FOAK data. Since several factors could affect the pressure at any given point, developing entire pressure profiles for higher power levels could not be accomplished by simple extrapolation. However, using the overall downcomer pressure rises given in Table 12, a correlation was developed relating the downcomer pressure rise to the power level. Using the equation that is included with Figure 81, downcomer pressure rises were calculated for power levels up to 145%, and have been provided in Table 13. The downcomer pressure rises have been non-

dimensionalized with respect to the 95% power pressure rise, as was the case with the FOAK power levels. As there is no FOAK void fraction data available for power levels exceeding 95%, the void fraction values shown throughout the remainder of this section have been left in their natural form.

Table 12: Downcomer Pressure Rise for Various Pressure Levels

Power Level	ΔP
45%	0.3795
55%	0.5115
65%	0.6205
75%	0.7338
85%	0.8302
95%	1.0000

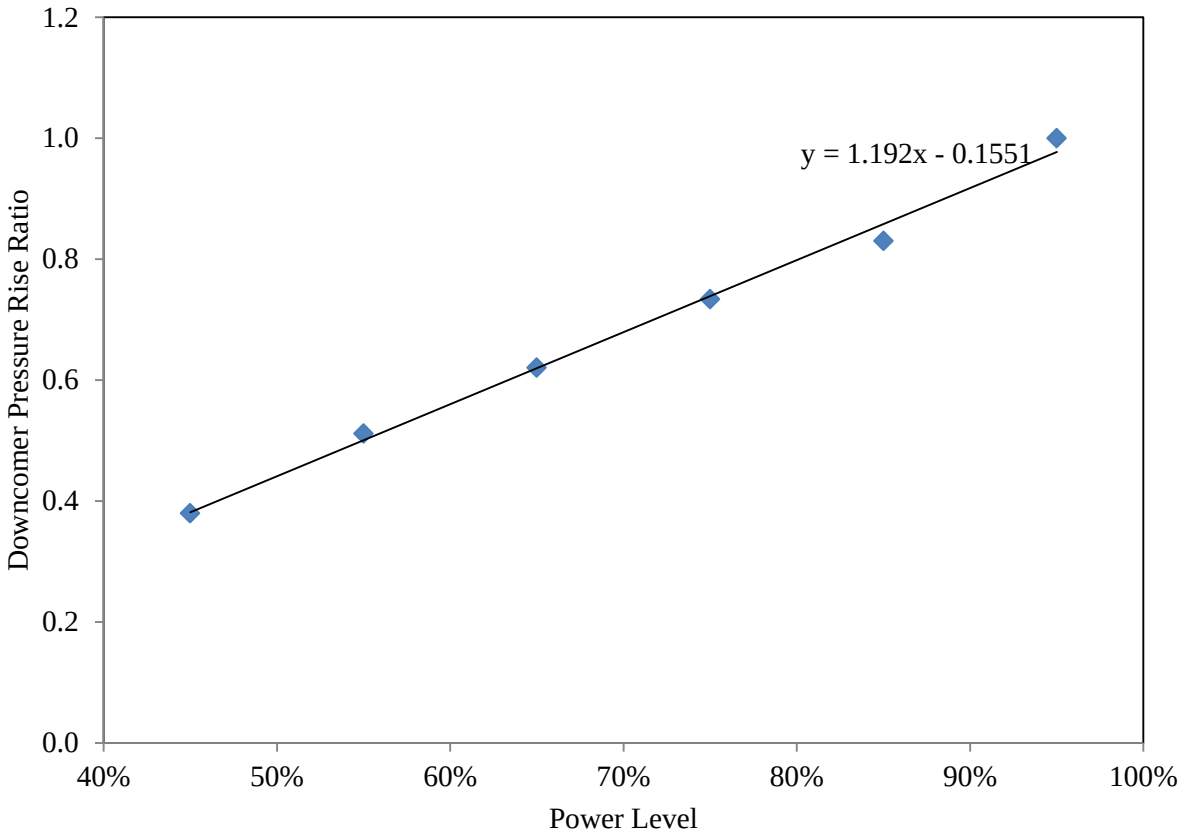

Figure 81: Downcomer Pressure Rise Ratio for Varying Power Levels

Table 13: Extrapolated Downcomer Pressure Rise for Higher Power Levels

Power Level	ΔP
105%	1.0965
115%	1.2157
125%	1.3349
135%	1.4541
145%	1.5733

4.5.2: 105% Power

At 105% power, the slug flow regime is dominant in the main body of the downcomer between a downcomer pressure rise of 0.3541 and 1.5683, which is a similar range to what has been seen in the normal operating power levels that were studied in the FOAK analysis. This is shown in Figure 82 and Figure 83. Based on the downcomer pressure rise extrapolated from the FOAK data, the flow regime pattern that can be expected would be slug flow throughout the downcomer, including immediately above and below the orifice plate, for the OTSG at 105% power.

The discontinuity in the orifice plate void fraction profile at a downcomer pressure rise of 1.2589 does not correlate with any other flow regime changes. It does coincide with a jump discontinuity increase in the vapor velocity profile, which would lead to a decrease in the magnitude of the velocity difference and a decrease in the interphase friction. A decrease in the interphase friction would result in less vapor being dragged into the volume.

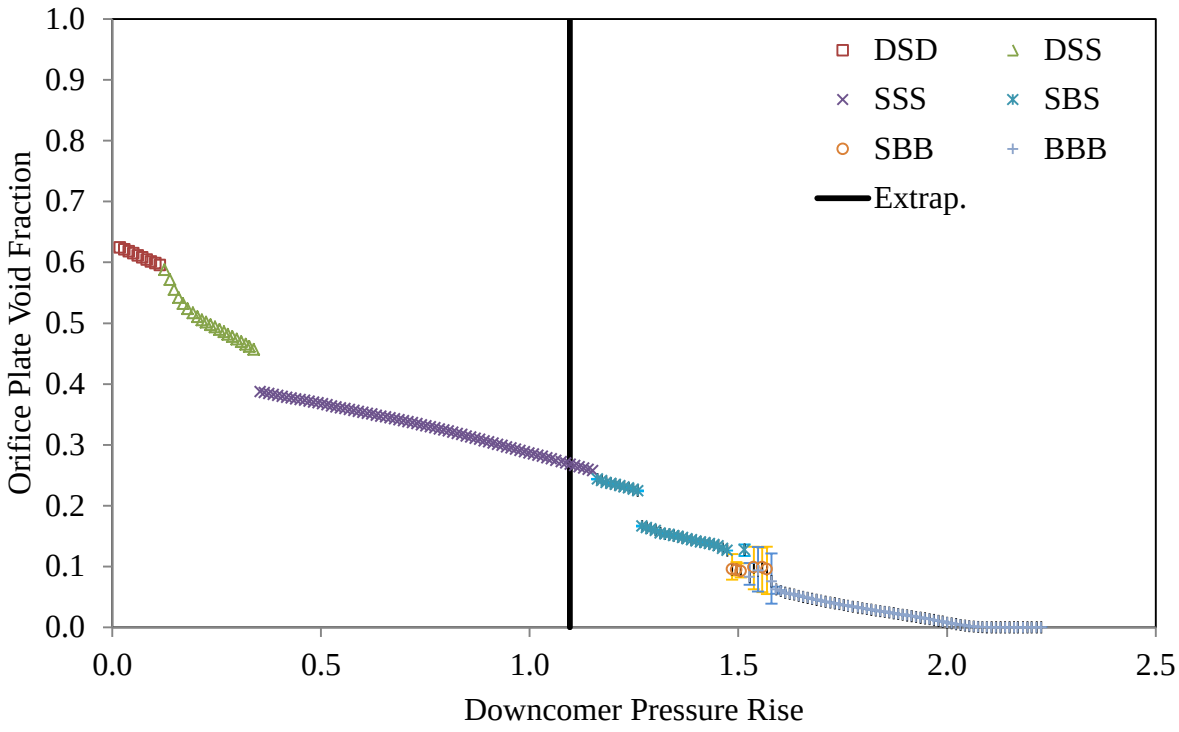

Figure 82: Orifice Plate Void Fraction for Varying Downcomer Pressure Rises at 105% Power with Extrapolated FOAK Pressure Rise

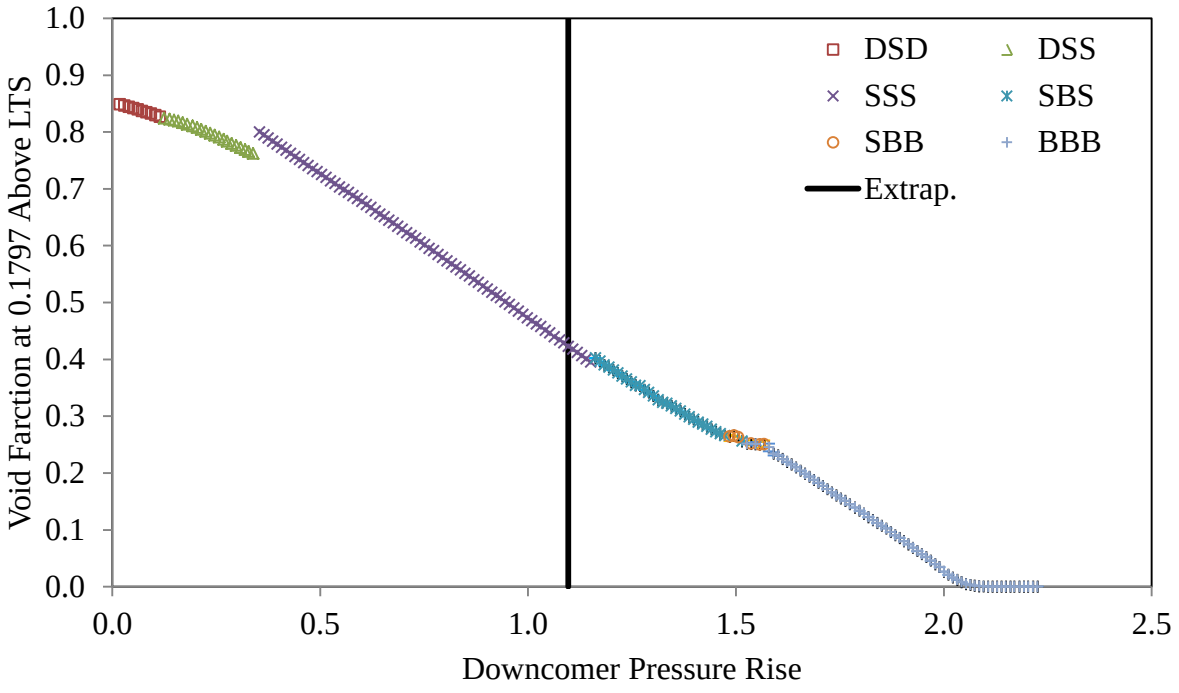

Figure 83: Void Fraction at 0.1797 Above LTS for Varying Downcomer Pressure Rises at 105% Power with Extrapolated FOAK Pressure Rise

4.5.3: 115% Power

At 115% power, Figure 84 and Figure 85 reveal that the flow regime pattern for the downcomer is slug for the main part, bubbly above the orifice plate and slug below the orifice plate. The slug flow regime is dominant in the main part of the downcomer from a downcomer pressure rise of 0.3317 to 1.5453.

A discontinuity in the void fraction profile at both the orifice plate and at 0.1797 above the orifice plate is noticeable when the downcomer pressure rise is 0.3514. This does not coincide with any flow regime changes at other points within the downcomer, although at a downcomer pressure rise of 0.3426, the flow regime in the volume at 0.8750 above the LTS switches from droplet to slug flow. There are jump discontinuities in both the vapor and liquid velocity profiles. The liquid velocity decreases in the mixing section, but increases for all volumes observed above the orifice plate. Meanwhile, the vapor velocity experiences a jump decrease over all volumes, resulting in a jump increase in the magnitude of the velocity difference for all volumes. Increasing the magnitude of the velocity difference should result in increasing the interphase friction force, which would drag more vapor through the downcomer, and should result in higher void fraction values in the lower portions of the downcomer. While this is the case at 0.1797 above the LTS, it is not the case at the orifice plate.

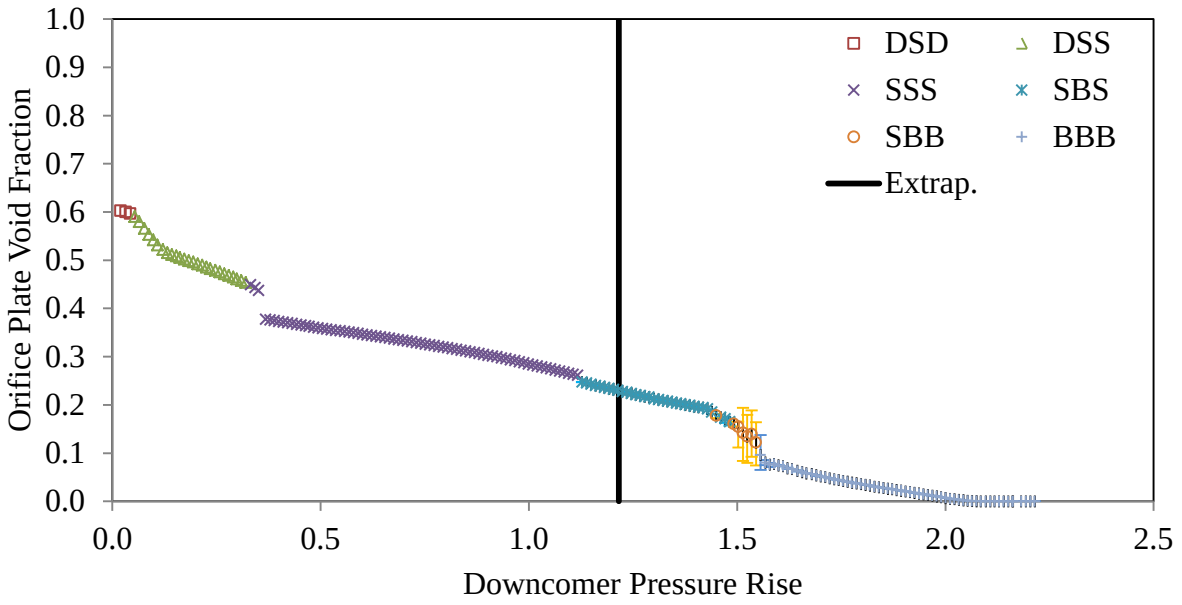

Figure 84: Orifice Plate Void Fraction for Varying Downcomer Pressure Rises at 115% Power with Extrapolated FOAK Pressure Rise

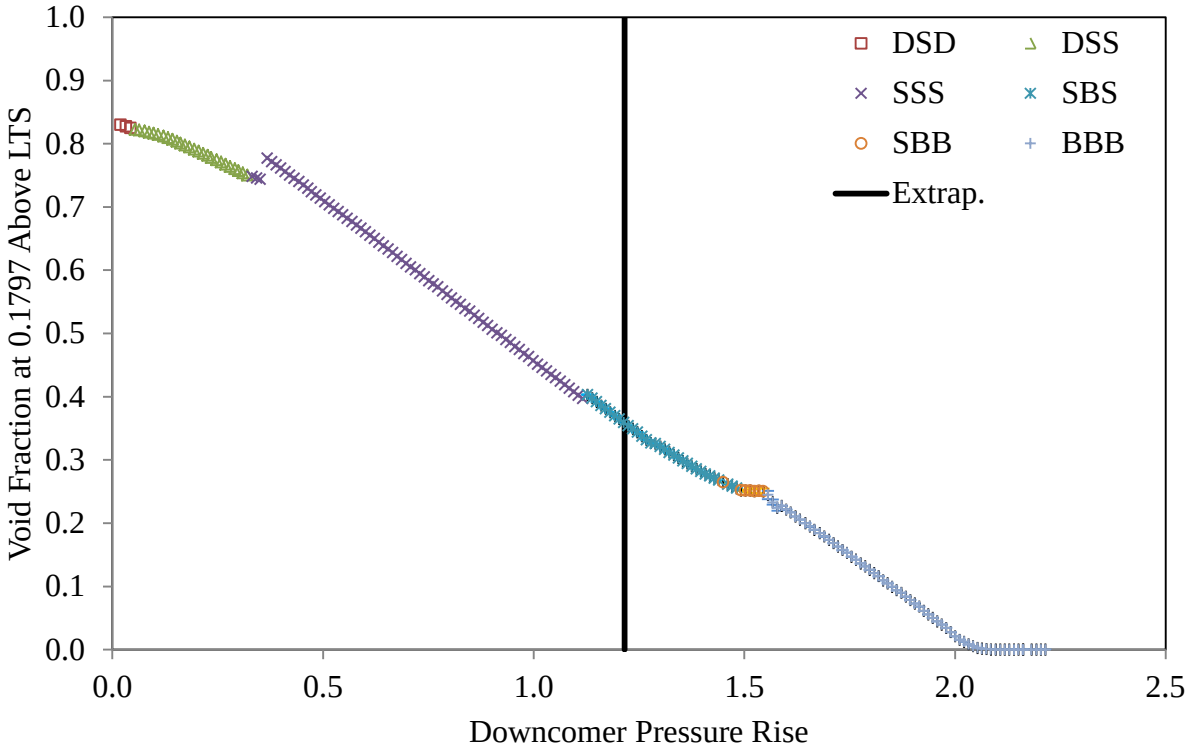

Figure 85: Void Fraction at 0.1797 Above LTS for Varying Downcomer Pressure Rises at 115% Power with Extrapolated FOAK Pressure Rise

4.5.4: 125% Power

The flow regime pattern for 125% power is slug flow for the main part of the downcomer, bubbly flow immediately above the orifice plate and slug flow below the orifice plate, as is shown in Figure 86 and Figure 87. The slug flow regime is dominant throughout the main body of the downcomer for a downcomer pressure rise as low as 0.2685 to as high as 1.5250.

The discontinuity seen in the void fraction profiles at a downcomer pressure rise of 0.3651 is similar to that seen at 115% power with a downcomer pressure rise of 0.3514. The discontinuity appears to be better reflected in the vapor velocity data, where a jump increase in the vapor velocity occurs at all observed volumes within the downcomer. This results in a jump increase in the magnitude of the velocity difference, an increase in the interphase friction force, and a greater amount of vapor being dragged down by the liquid. While this increase in vapor is evident at 0.1797 above the LTS, the opposite effect is noticed at the orifice plate.

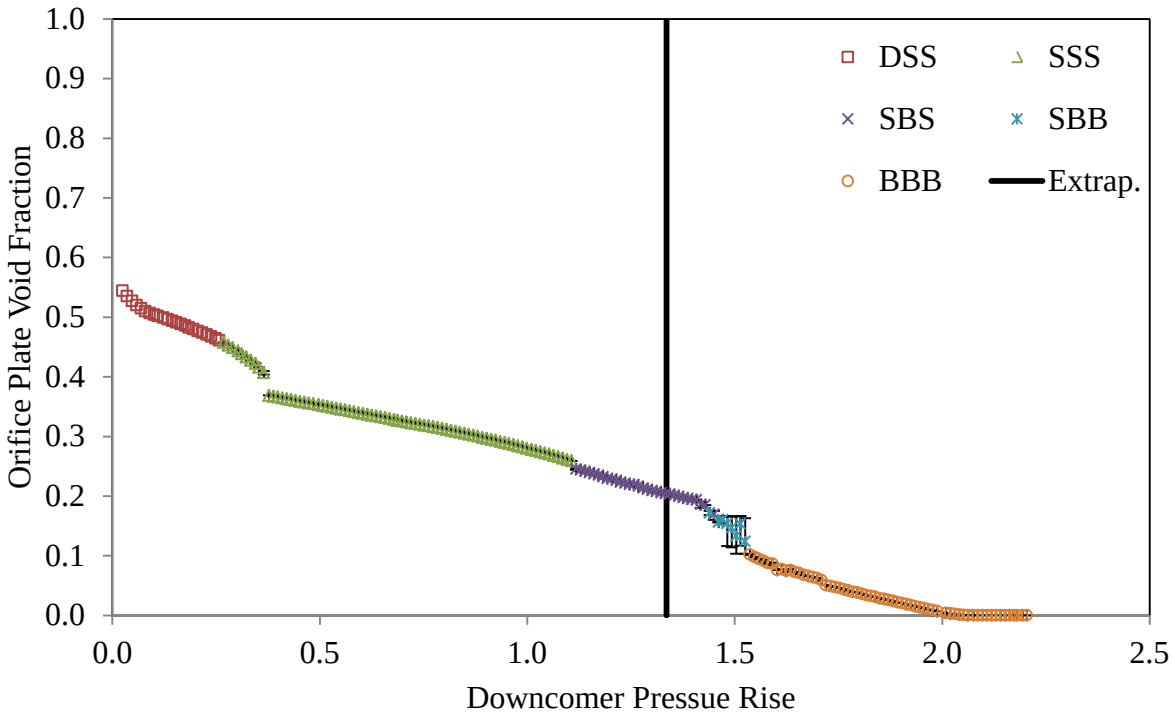

Figure 86: Orifice Plate Void Fraction for Varying Downcomer Pressure Rises at 125% Power with Extrapolated FOAK Pressure Rise

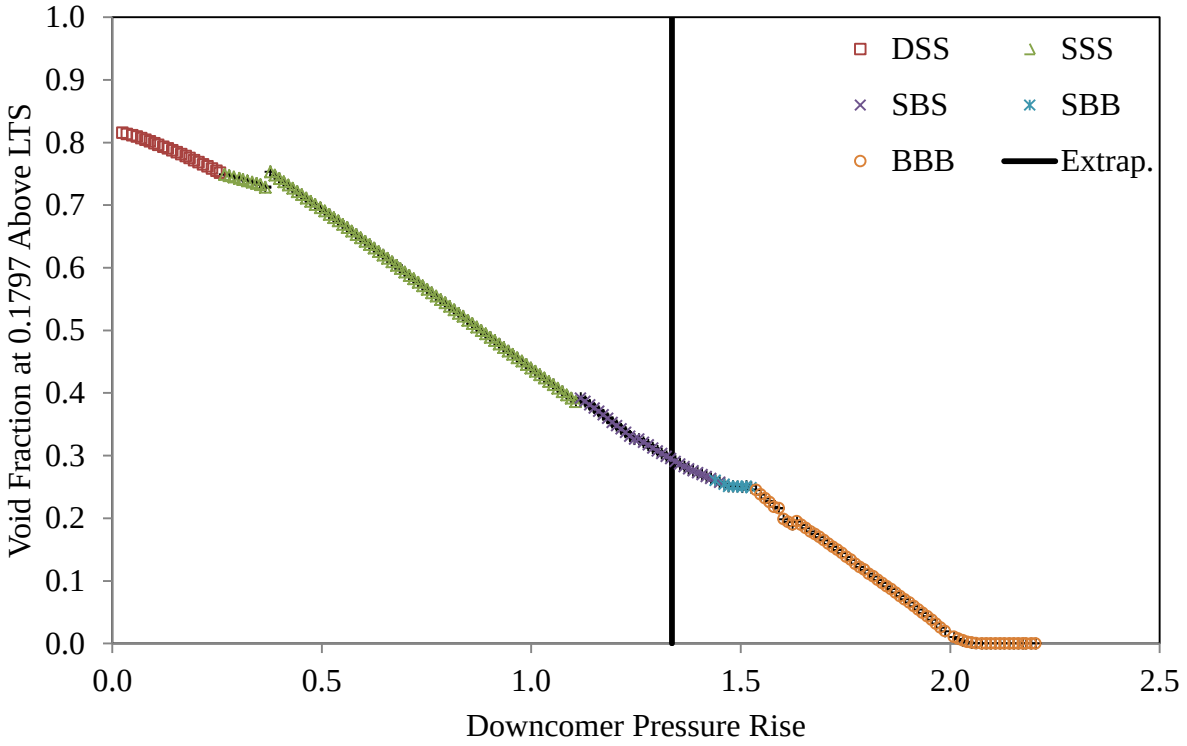

Figure 87: Void Fraction at 0.1797 Above LTS for Varying Downcomer Pressure Rises at 125% Power with Extrapolated FOAK Pressure Rise

4.5.5: 135% Power

In Figure 88 and Figure 89, the void fraction profiles with respect to downcomer pressure rise for 135% power are shown. The FOAK projection predicted that the downcomer pressure rise at 135% power should be 1.4541, which corresponds to a flow regime pattern in the downcomer of slug flow for the main body of the downcomer and bubbly flow immediately above and below the orifice plate. Slug flow is dominant throughout the main body of the downcomer for a pressure rise values ranging from 0.2075 to 1.5040. It is at this power level that the data suggests some instability in the void fraction profile, which begins the concern for flood-back. Figure 90 shows the void fraction profile for a downcomer pressure rise slightly above the FOAK extrapolation, which reveals that the void fraction is nearly constant throughout the downcomer, suggesting a liquid level very close to the mixing section of the downcomer. The void fraction is between 0.25 and 0.26 throughout the downcomer, which RELAP interprets as slug flow for each volume.

The discontinuity that has been discussed at 115% and 125% power, is also noticeable at 135% power, occurring at a pressure rise of 0.3889. A jump increase in magnitude of the velocity difference between vapor and liquid throughout the downcomer is noticed, with the increase minimized at the orifice plate. This would serve to explain why there is more vapor appearing after the discontinuity at 0.1797. above the LTS, and why the change in void fraction with increasing downcomer pressure rise decreases at the orifice plate.

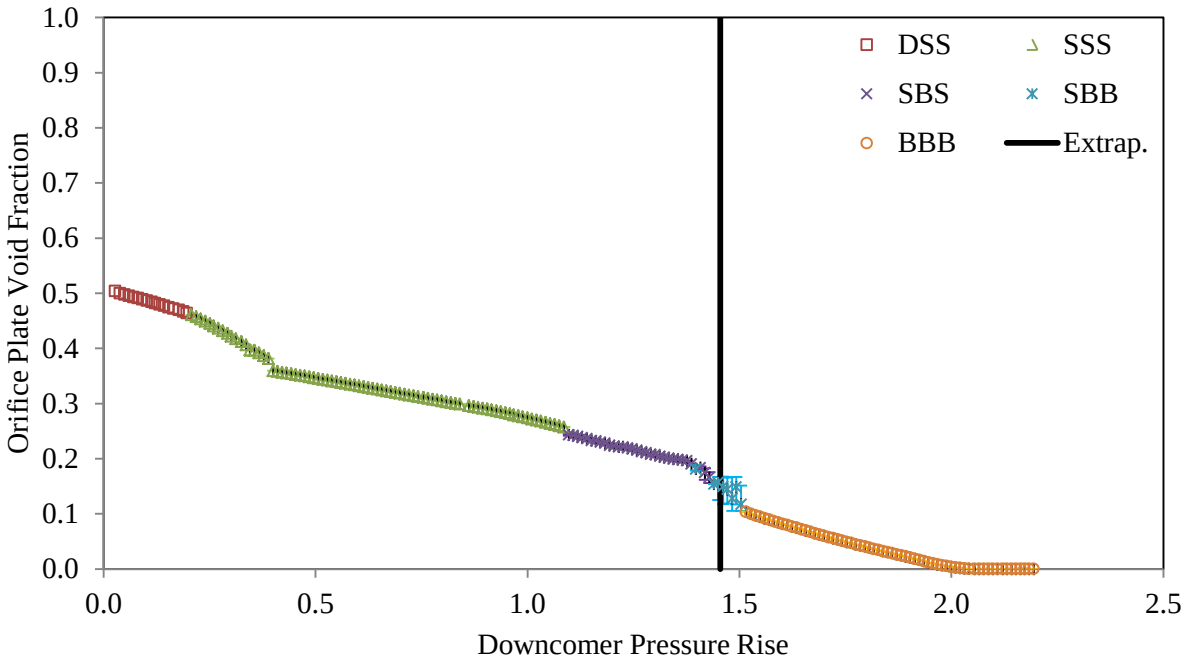

Figure 88: Orifice Plate Void Fraction for Varying Downcomer Pressure Rises at 135% Power with Extrapolated FOAK Pressure Rise

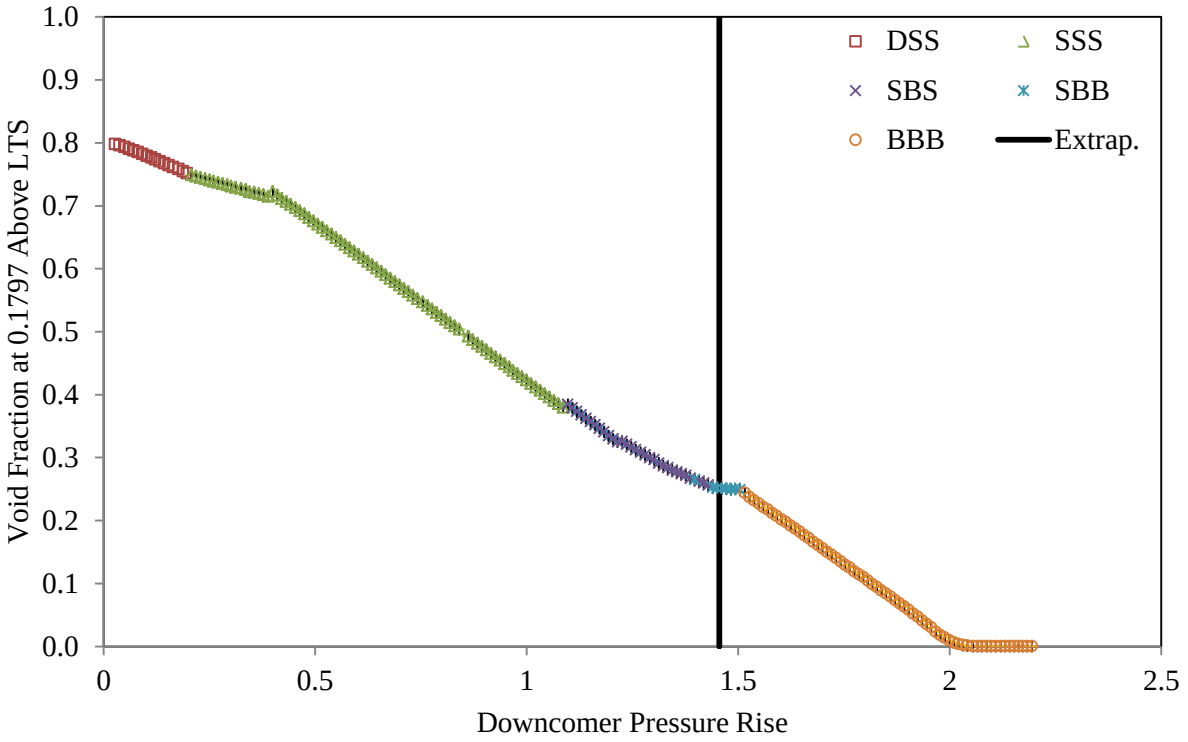

Figure 89: Void Fraction at 0.1797 Above LTS for Varying Downcomer Pressure Rises at 135% Power with Extrapolated FOAK Pressure Rise

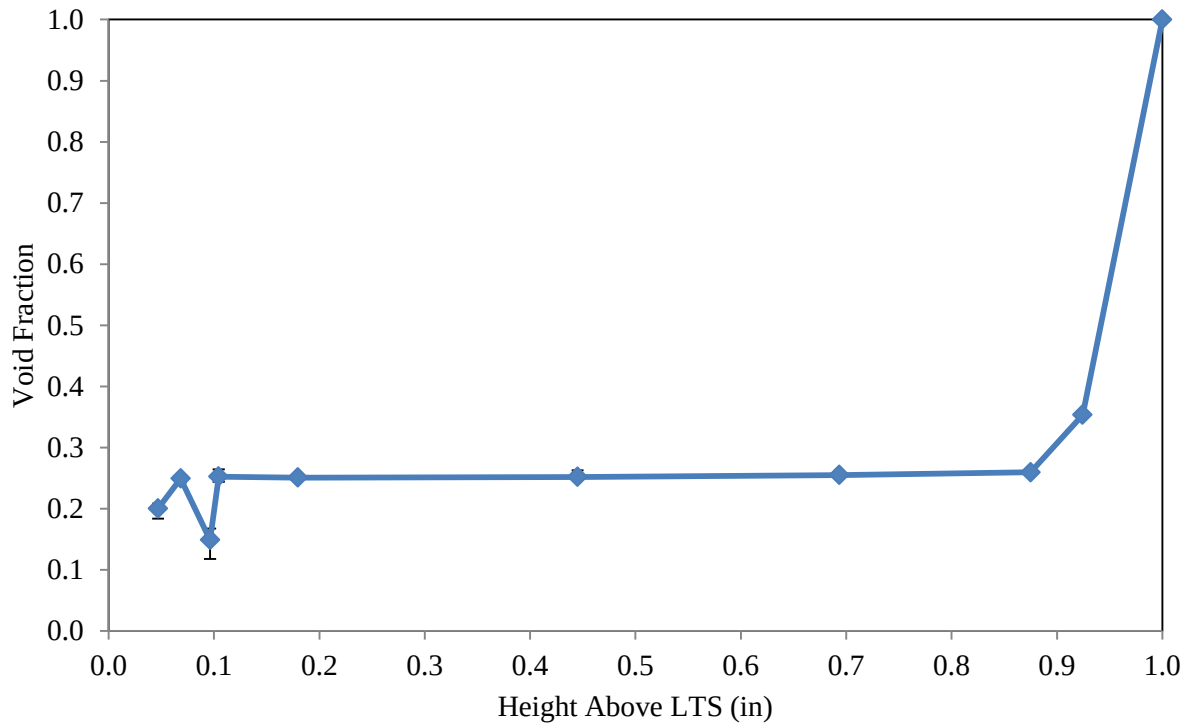

Figure 90: Void Fraction Profile for 135% Power with a Downcomer Pressure Rise of 1.4612

4.5.6: 145% Power

At 145% power, Figure 91 and Figure 92 show that the flow regime profile throughout the downcomer for a projected pressure rise of 1.5723 is bubbly throughout the downcomer. In Figure 93, the void fraction profile at 145% power with a downcomer pressure rise of 1.5807 indicates that the liquid level is within the mixing chamber, and very close to the aspirator ports, suggesting that flood-back is very likely at 145% power.

The discontinuity seen at 115%, 125% and 135% power in the void fraction profile is also noticeable at 145% power, but only as a jump discontinuity in the derivative of the void fraction profile at a pressure rise of 0.4024. Velocity data shows a small but noticeable maximum in velocity difference magnitude at 0.4024 for each volume observed within the downcomer. This should result in an increase in interphase friction force at a pressure rise of 0.4024, and an increase in the amount of vapor seen in the lower regions of the downcomer.

While the data suggests that this does occur at 0.1797 above the LTS, it does not occur at the orifice plate.

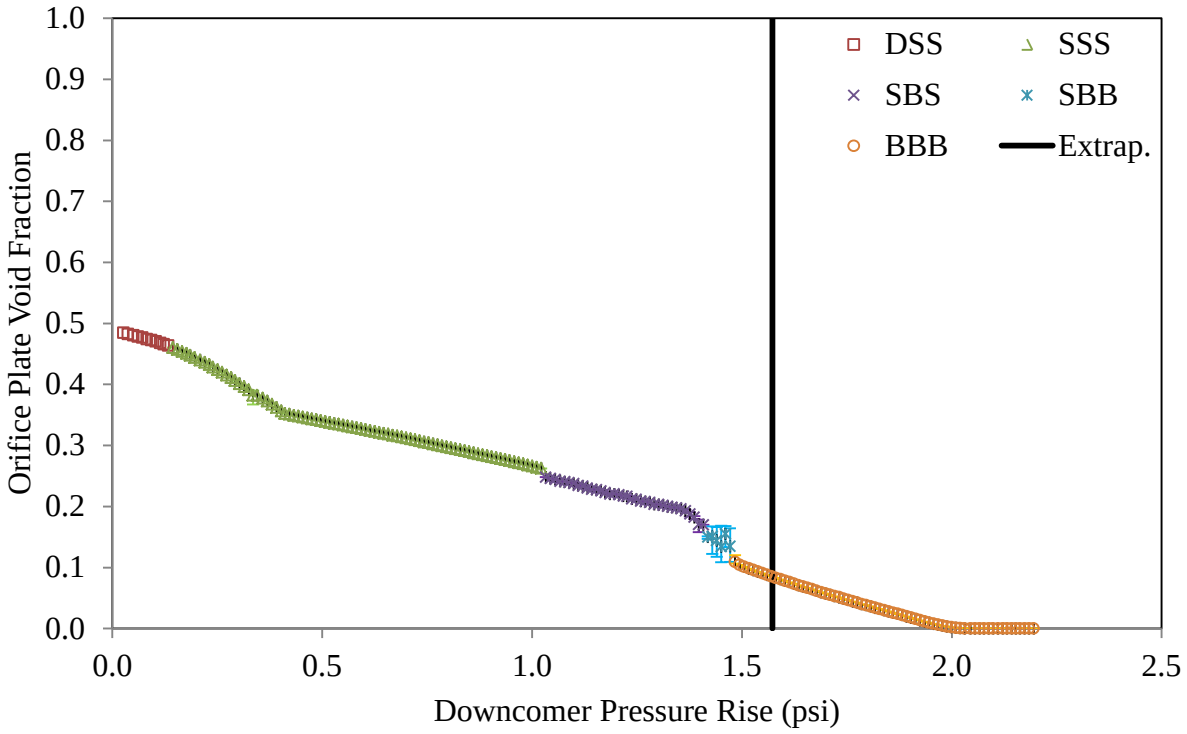

Figure 91: Orifice Plate Void Fraction for Varying Downcomer Pressure Rises at 145% Power with Extrapolated FOAK Pressure Rise

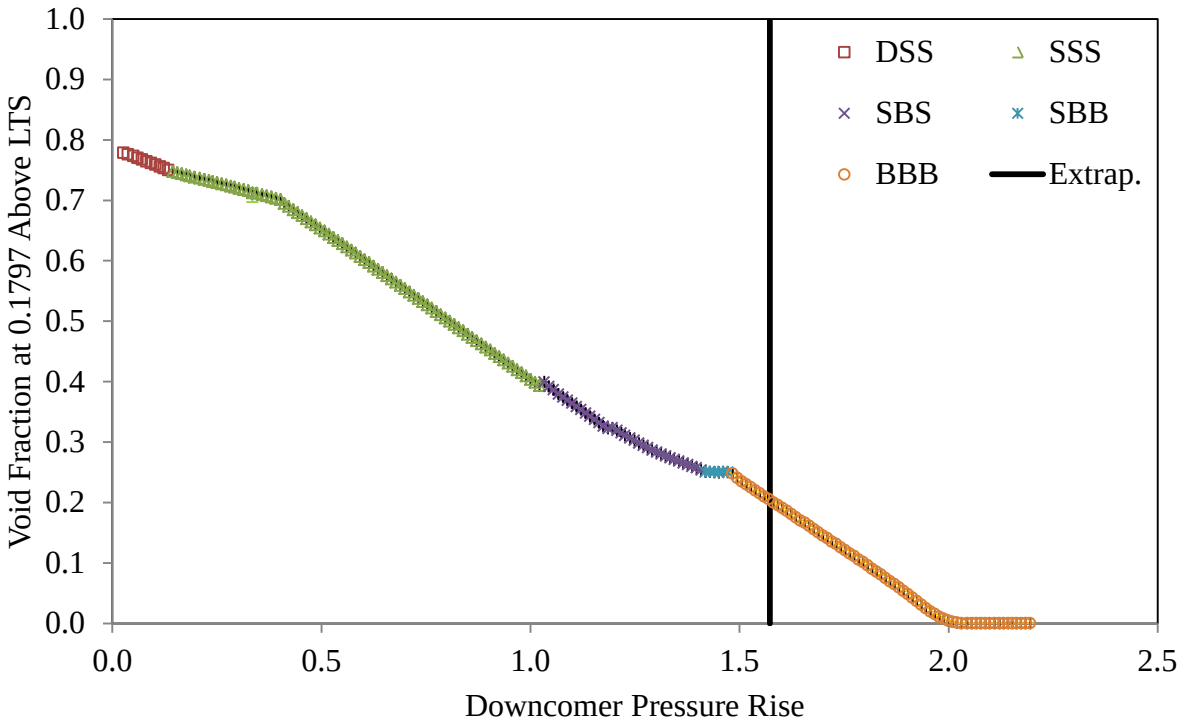

Figure 92: Void Fraction at 0.1797 Above LTS for Varying Downcomer Pressure Rises at 145% Power with Extrapolated FOAK Pressure Rise

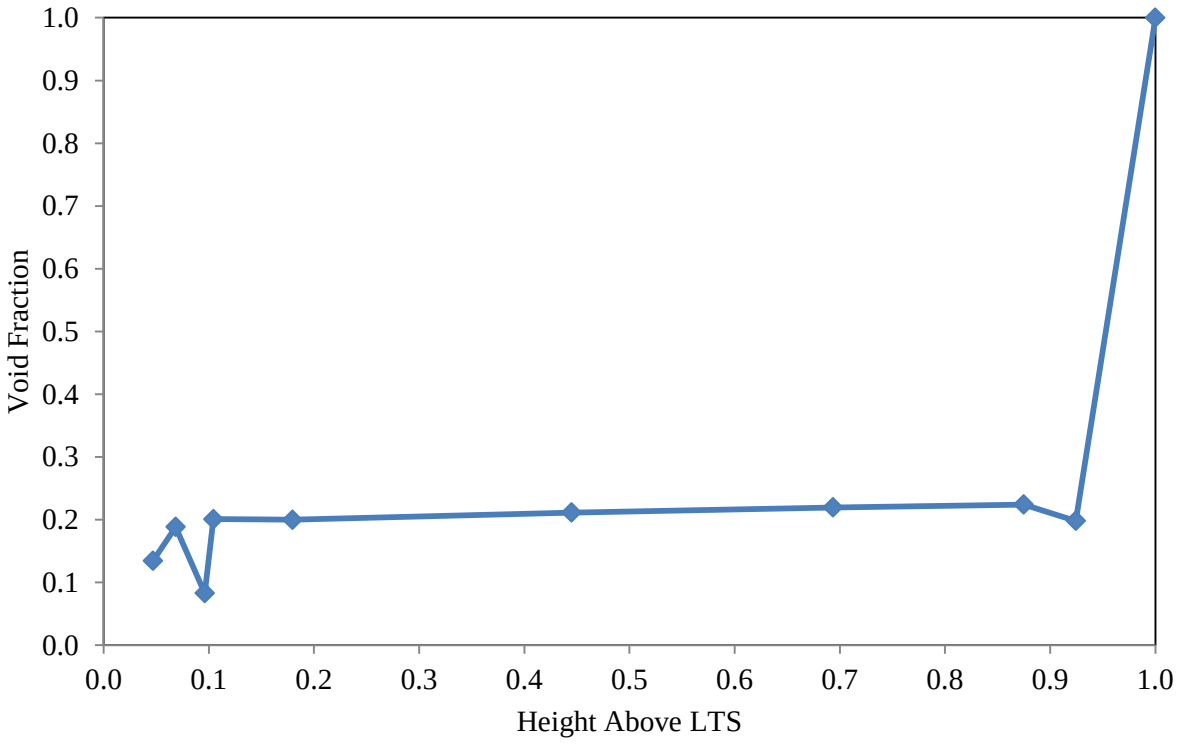

Figure 93: Void Fraction Profile for 145% Power with a Downcomer Pressure Rise of 1.5807

Since the model runs at 145% power indicate that the downcomer would be experiencing bubbly flow throughout the downcomer, it can be expected that at higher power levels, the flow regime pattern would be the same.

V. Discussion

5.1: Conclusions

An OTSG downcomer model has been developed for RELAP5/MOD2 using a FORTRAN shell program that was capable of varying numerous parameters. In this study, it was found that the interphase drag that is predicted by the default INEL slug drag model is insufficient in predicting the correct amount of vapor to be dragged downward by the feedwater moving through the downcomer. This is likely caused by the assumption in RELAP that Taylor bubbles in the slug flow regime are roughly the same diameter of the annulus.

Using a modified version of the INEL slug drag model created by B&W, this study was able to find that at the normal operating condition of 95% power, applying a multiplier of M_{st} = 5.1517 would produce the most accurate pressure profile and vapor distribution for the OTSG downcomer, based on data retrieved from the FOAK study at Oconee Unit I. This equates to an increase in interphase drag to 515% for the INEL slug drag model and 1895% for the B&W default slug drag model. For a range of power levels, it was found that the optimum multiplier was M_{st} = 11.8061, which was used for all other power levels analyzed in this study, which reflects an increase to 1181% of the interphase friction for the INEL slug drag model and 4344% for the default B&W slug drag model.

There is concern within Areva, Inc. that as the new E-OTSG becomes used in nuclear power plants that the increased power rate at which power plants are operating will cause the E-OTSG to malfunction. Of particular concern is a phenomenon known as flood-back, which occurs when a liquid level forms within the downcomer, and approaches the feedwater nozzles. In this study, RELAP showed that a liquid level would be a concern at power levels exceeding 135% power.

While there has been considerable research on two-phase flow, there has been very little research conducted that directly correlates to this study. Only a few studies on two-phase flow have examined downflow, and of the studies that examined two-phase flow in RELAP5/MOD2, none addressed two-phase vertical downflow. Studies that did research two-phase vertical downflow predominantly used air-water mixtures at atmospheric conditions, that produced greater velocity differences than seen in the operating conditions of the OTSG downcomer. Of the studies involving RELAP5/MOD2, all focused on heated steam/water rising through the tube bundle of a steam generator rather than the downcomer. In RELAP5/MOD2, two-phase downflow regimes are considered to be the same as those in two-phase upflow. The lack of relevant research to this particular problem meant that a trial-and-error approach to modeling the OTSG downcomer had to be taken in order to find the best parameters to be used, without having specific references to justify using such parameters.

5.2: Recommendations

It is the recommendation of this study that when modeling the OTSG downcomer using RELAP5/MOD2, that the physical model should resemble that which has been described in Section 3.1. The mixing section of the downcomer should be modeled using a branch connection with the forced equilibrium option turned on. At the bottom of the downcomer, the orifice plate should be modeled as a single junction, with a smooth area change that has an energy loss factor of 0.79, connected to a branch connection that represents the volume below the orifice plate. When modeling for a specific power level, the B&W slug drag model should be incorporated with the M_{st} set to the value prescribed in Table 10. However, if the user is

modeling for a power level not mentioned in Table 10, or is operating at varying power levels, the recommended M_{st} is 11.8061.

5.3: Future Research

There are several potential areas for research regarding this study that could be conducted over the next few years, and could prove to be useful across multiple branches of engineering and science.

One key area of study would be on two-phase vertical downflow, with an emphasis on steam and water interactions occurring at the operating conditions of a nuclear power plant. The development of a flow regime map for steam and water at the operating conditions of a power plant would be extremely beneficial towards understanding how the two fluids work together within a plant and would make modeling such a plant much easier.

There are several anomalies within the data shown in this study that merit further attention, mostly occurring in the form of discontinuities when comparing the void fraction profile to the downcomer pressure rise. While many of these discontinuities could be attributed to flow regime changes, several could only be correlated to changes in the velocity of one or both phases. On several occasions, the effect of the velocity changes were only partially consistent with the changes in the void fraction that was observed. There is still a mystery as to why the velocities of each phase experienced such a discontinuity, and there is no obvious reason given by that data that is output by RELAP. An in-depth study of the RELAP source code may reveal why such discontinuities occurred. One other possibility that may resolve some of the discontinuities would be to develop a RELAP5/MOD2 model of the entire OTSG.

Further research with newer codes also presents opportunities for future research. The latest version of RELAP is RELAP5-3D, which extends RELAP from being a one-dimensional

to three-dimensional. Given that the flow at the orifice plate and into the tube nest is three-dimensional rather than one-dimensional, RELAP5-3D may be better suited for modeling that feature of the downcomer. The TRAC/RELAP Advanced Computer Engine (TRACE) is also a three-dimensional model and is expected to replace all other nuclear computer modeling programs, including RELAP5-3D. However, there is very little research that has been conducted with TRACE at this point, allowing for many possibilities in the near future. Modeling two-phase downflow with TRACE and comparing the results to this study would also provide for a fitting extension of this work.

References

1. Analytis, G.T., and Richner, M. "Effect of Bubbly/Slug Interfacial Shear on Liquid Carryover Predicted by RELAP5/MOD2 During Reflood." Trans. ANS. Vol. 53. pp. 540-541. 1986.
2. Barnea, D., Shoham, and O., Taitel, Y. "Flow Pattern Transition for Vertical Downward Two Phase Flow." Chem. Engr. Sci. Vol. 37. pp. 741-744. 1982.
3. Chexal, B., and Lellouche, G. "A Full-Range Drift-Flux Correlation for Vertical Flows." EPRI NP-3989-SR. 1986
4. Chexal, B., Lellouche, G., Horowitz, J., and Heazer, J. "A Void Fraction Correlation for Generalized Applications." Prog. Nucl. En. Vol. 27. pp. 255-295. 1992
5. Coburn, J., and Coe, R. "OTSG Downcomer Performance." BWNS-21036-4. 1989.
6. Crawford, T.J., Weinberger, C.B., and Weisman, J. "Two-Phase Flow Patterns and Void Fractions in Downward Flow Part I: Steady-State Flow Patterns." Int. J. Multiphase Flow. Vol. 11. pp. 761-782. 1985.
7. Golan, L.P. and Stenning, A.H. "Two-Phase Vertical Flow Maps." Proc. Instn. Mech. Engrs. Vol. 184. pp. 108-114. 1969-1970.
8. Griffith, P. "Two-Phase Flow." Handbook of Heat Transfer Fundamentals. 2nd Edition. 1985.
9. Hassan, Y.A. "Assessment of a Modified Interfacial Drag Correlation in Two-Fluid Model Codes." Trans. ANS. Vol. 54. pp. 211-212. 1987.
10. Kataoka, I., and Ishii, M. "Drift Flux Model for Large Diameter Pipe and New Correlation for Pool Void Fraction." Int. J. Heat Mass Transfer. Vol. 30. pp. 1927-1939. 1987
11. McDonald, B., Michaud, E., and Searce, J. “Once-Through Steam Generators on the Line.” American Nuclear Society Winter Meeting. 11-15 November 1973.
12. Michaud, E. "Oconee Unit I Startup." 1973.
13. Moran, M.J., and Shapiro, H.N. "Fundamentals of Engineering Thermodynamics." 6th Edition. Wiley. 2008.
14. Munson, B.R., Young, D. R., and Okiishi, T.H., "Fundamentals of Fluid Dynamics." 5th Edition. Wiley. 2006.
15. Nithianandan, C.K., Shah, N.H., Dunn, B.M., Klingenfus, J.A., Thurston, C.G., Wissinger, G.J., Schamp, C.A., Mays, M.E. and Petris, W.J. "RELAP5/MOD2 - An Advanced Computer Program for Light Water Reactor LOCA and Non-LOCA Transient Analysis" Volume 1. Revision Z.
16. Oshinowo, T. and Charles, M.E. "Vertical Two-Phase Flow Part I. Flow Pattern Correlations." Can. J. Chem. Engr. Vol. 52. pp. 25-35. 1974.
17. Putney, J.M. "Development of a New Bubbly-Slug Interfacial Friction Model for RELAP5." Nucl. Engr. Des. Vol. 131. pp. 223-240. 1991.
18. Putney, J.M. and Preece, R.J. "Assessment of PWR Steam Generator Modelling in RELAP5/MOD2." NUREG/IA-0106. TEC/L/0471/R91. US Nuclear Regulatory Commission. 1993.
19. Ransom, V. H., Wagner, R. J., Trapp, J. A., Feinauer, L. R., Johnsen, G. W., Kiser, D. M. and Riemke, R. A., "RELAP5/MOD2 Code Manual Volume 1: Code Structure, System Models and Solution Methods." NUREG/CR-4312. EGG-2396. Idaho National Engineering Laboratory. 1985.

20. RELAP5/MOD3 Code Manual Volume I: Code Structure, System Models, and Solution Methods. NUREG/CR-5535. INEL-95/0174. (Formerly EGG-2596). Idaho National Engineering Laboratory. 1995.
21. Taitel, Y., Bornea, D., and Dukler, A.E. "Modeling Flow Pattern Transitions for Steady Upward Gas-Liquid Flow in Vertical Tubes." AIChE Journal. Vol. 26. pp. 345-354. 1980.
22. Vince, M. A. and Lahey, R.T., "On the Development of an Objective Flow Regime Indicator." Int. J. Multiphase Flow. Vol. 8. pp 93-124. 1982.
23. Wallis, G.B., "One-Dimensional Two-Phase Flow." McGraw-Hill. 1969.
24. Wilson, J.F, Grenda, R.J. and Patterson, J.F., “The Velocity of Rising Steam in a Bubbling Two-Phase Mixture.”, Trans. ANS, Vol. 5, pp. 151-2, 1962.
25. Zuber, N., and Findlay, J.A., "Average Volumetric Concentration in Two-Phase Flow Systems." J. Heat Transfer. Vol. 87. pp. 453-468. 1965.